REMOVAL OF HYDROGEN SULFIDE
BY REGENERABLE METAL OXIDE SORBENTS

A THESIS SUBMITTED TO
THE GRADUATE SCHOOL OF NATURAL AND APPLIED SCIENCES
OF
MIDDLE EAST TECHNICAL UNIVERSITY

BY

DİLEK KARAYILAN

IN PARTIAL FULFILLMENT OF THE REQUIREMENTS FOR THE DEGREE OF
MASTER OF SCIENCE
IN
CHEMICAL ENGINEERING

JUNE 2004

Approval of the Graduate School of Natural and Applied Sciences

_____

Prof. Dr. Canan Özgen

Director

I certify that this thesis satisfies all the requirements as a thesis for the degree of Master of Science.

_____

Prof. Dr. Timur Doğu

Head of Department

This is to certify that we have read this thesis and that in our opinion it is fully adequate, in scope and quality, as a thesis for the degree of Master of Science.

_____   _____

Prof. Dr. Gülşen Doğu   Prof. Dr. Timur Doğu

Co-Supervisor   Supervisor

Examining Committee Members

Prof. Dr. Serpil Takaç (Ankara Univ., CHE)   _____

Prof. Dr. Timur Doğu (METU, CHE)   _____

Prof. Dr. Suna Balcı (Gazi Univ., CHE)   _____

Assoc. Prof. Dr. Naime Sezgi (METU, CHE)   _____

Asst. Prof. Dr. Halil Kalıpçılar (METU, CHE)   _____

I hereby declare that all information in this document has been obtained and presented in accordance with academic rules and ethical conduct. I also declare that, as required by these rules and conduct, I have fully cited and referenced all material and results that are not original to this work.

Name, Last name : Dilek Karayılan

Signature :

ABSTRACT

REMOVAL OF HYDROGEN SULFIDE

BY REGENERABLE METAL OXIDE SORBENTS

Karayılan, Dilek

M.S., Department of Chemical Engineering

Supervisor   : Prof. Dr. Timur Doğu

Co-Supervisor: Prof. Dr. Gülşen Doğu

June 2004, 166 pages

High-temperature desulfurization of coal-derived fuel gases is an essential process in advanced power generation technologies. It may be accomplished by using metal oxide sorbents. Among the sorbents investigated CuO sorbent has received considerable attention. However, CuO in uncombined form is readily reduced to copper by the H_2 and CO contained in fuel gases which lowers the desulfurization efficiency. To improve the performance of CuO-based sorbents, they have been combined with other metal oxides, forming metal oxide sorbents.

Sulfidation experiments were carried out at 627 ^{o}C using a gas mixture composed of 1 % H_2S and 10 % H_2 in helium. Sorbent regeneration was carried

out in the same reactor on sulfided samples at 700 ^{o}C using 6 % O_2 in N_2. Total flow rate of gas mixture was kept at 100 ml/min in most of the experiments.

In this study, Cu-Mn-O, Cu-Mn-V-O and Cu-V-O sorbents were developed by using complexation method. Performance of prepared sorbents were investigated in a fixed-bed quartz microreactor over six sulfidation/regeneration cycles. During six cycles, sulfur retention capacity of Cu-Mn-O decreased slightly from 0.152 to 0.128 (g S)/(g of Sorbent) while some decrease from 0.110 to 0.054 (g S)/(g of Sorbent) was observed with Cu-Mn-V-O. Cu-V-O showed a very good performance in the first sulfidation and excessive thermal sintering in the first regeneration prevented further testing. Sulfur retention capacity of Cu-V-O was calculated as 0.123 (g S)/(g of Sorbent) at the end of the first sulfidation. In addition, SO_2 formation in sulfidation experiments was observed only with Cu-V-O sorbent.

Keywords: Hot Gas Desulfurization, H_2S removal, Copper Based Sorbents, Integrated Gasification Combined Cycle Systems

ÖZ

HİDROJEN SÜLFİDİN YENİLENEBİLİR METAL OKSİT SORBENTLER İLE UZAKLAŞTIRILMASI

Karayılan, Dilek

Yüksek Lisans, Kimya Mühendisliği

Tez Yöneticisi   : Prof. Dr. Timur Doğu

Ortak Tez Yöneticisi: Prof. Dr. Gülşen Doğu

Haziran 2004, 166 sayfa

Kömür türevi yakıt gazlarının yüksek sıcaklıkta desülfürizasyonu gelişmiş güç üretim teknolojileri için gerekli bir prosestir. Sıcak gaz desülfürizasyonu metal oksit sorbentler kullanılarak yapılabilir. Araştırılan sorbentler arasında bakır oksit sorbenti büyük ölçüde dikkat çekmiştir. Fakat yakıt gazları içerisinde bakır oksit tek başına, hidrojen ve CO tarafından kolaylıkla metalik bakıra indirgenmektedir buda sülfürizasyonun verimliliğini düşürmektedir. Bakır oksit bazlı sorbentlerin performansını iyileştirmek için bakır oksitler diğer metal oksitlerle birleştirilerek metal oksit karışım sorbentlerinin oluşması sağlanmaktadır.

Sülfidasyon deneyleri 627 ^{o}C' de 1 % H_2S, 10 % H_2 ve dengede helyum gaz karışımı kullanılarak yapılmıştır. Sorbent rejenerasyonu aynı reaktörde sülfitlenmiş sorbentler üzerinde 700 ^{o}C de 6% O_2 ve dengede N_2 gaz karışımı kullanılarak yapılmıştır. Çoğu deneylerde toplam gaz karışımının akış hızı 100 ml/min' de sabit tutulmuştur.

Bu çalışmada, Cu-Mn-O, Cu-Mn-V-O ve Cu-V-O sorbentleri komplexleştirme metodu kullanılarak geliştirilmiştir. Sorbentlerin performansları sabit yataklı cam reaktörde 6 sülfidasyon/rejenerasyon döngüsü boyunca incelenmiştir. 6 sülfidasyon/rejenerasyon döngüsü boyunca Cu-Mn-V-O sorbent kükürt tutma kapasitesinin 0.110'dan 0.054 (g kükürt)/(g sorbent)'e düştüğü gözlenirken, Cu-Mn-O sorbent kükürt tutma kapasitesi 0.152'den 0.128 (g kükürt)/(g sorbent)'e düşmüştür. Cu-V-O sorbenti birinci sülfidasyonda iyi performans göstermiştir ve birinci rejenerasyondaki aşırı ısısal bozulma sorbentin daha fazla test edilmesini engellemiştir. Birinci sülfidasyon sonundaki Cu-V-O kükürt tutma kapasitesi 0.123 (g kükürt)/(g sorbent) olarak hesap edilmiştir. Buna ilaveten, sülfidasyon deneyinde SO_2 oluşumu yalnız Cu-V-O sorbentiyle gözlemlenmiştir.

Anahtar Kelimeler: Yüksek Sıcaklık Desülfürizasyonu, H_2S Uzaklaştırılması, Bakır Esaslı Sorbentler, Entegre Gazlaştırma Kombine Çevrim Sistemi

To My Family,

ACKNOWLEDGEMENTS

TABLE OF CONTENTS

xiii

LIST OF TABLES

xvi

LIST OF FIGURES

xviii

NOMENCLATURE

a	Activity of the solid reactant
C_A	Outlet concentration of reactant gas, mol/cm^3
C_{Ao}	Inlet concentration of reactant gas, mol/cm^3
k_d	Deactivation rate constant, min^{-1}
k_o	Initial sorption rate constant, cm^{3}g^{-1}min^{-1}
Q	Volumetric flow rate, cm^3/min
t	Reaction time, min
W	Catalyst mass, kg

Abbreviations:

^oC	Degrees Celsius
Cu-Mn-O	Copper-Manganese-Oxide
Cu-Mn-V-O	Copper-Manganese-Vanadium-Oxide
Cu-V-O	Copper-Vanadium-Oxide
DOE	Department of Energy, United States
FTIR	Fourier Transform Infrared Spectroscopy
G	Gram
GC	Gas Chromatograph
Gtoe	Gigatone oil equivalent
IGCC	Integrated Gasification Combined Cycle System
METC	Morgantown Energy Technology Center
Ppm	Parts per million
ppmv	Parts per million by volume
SEM	Scanning Electron Microscope
XRD	X-Ray Diffraction

CHAPTER 1

INTRODUCTION

1.1   Electrical Energy Generation

Increasing world population and economic development is resulting in an ever growing global primary energy demand. This increase in demand could be seen in the consumption of various fuels as presented in Table 1.1. In the last 25 years the total energy consumption has almost doubled. For the purpose of meeting this increasing demand research is conducted both on new sources of energy and on the improvement of the present energy production technologies. On the latter the efficiency of the energy production technology becomes quite an important issue in both, i.e. the new energy sources and the improvement of the present technologies, pollution prevention becomes indispensable for the sake of sustainable development (Sage, 1996a).

This energy demand can be met by renewable and non-renewable energy sources. The renewable sources that contribute the world energy use at about 15% can be split into two categories as traditional and non-traditional sources. The traditional sources include fuel wood, crop residues and hydropower whereas

the non-traditional sources include solar, wind, geothermal and biomass (Sage, 1996a).

Table 1.1 Global Fuel Consumption in 1969 and 1994 (Sage, 1996a)

	1969 (Gtoe)	**1994 (Gtoe)**
Oil	2.1	3.2
Gas	0.9	1.8
Coal	1.5	2.2
Nuclear	Negligible	0.6
Hydroelectric	0.1	0.2
TOTAL	**4.6**	**8.0**

The renewable energy sources often require larger structures involving high material requirements and land use. Large scale developments can also have climatological or ecological impacts. These impacts are due to the diversion of a natural energy flow or intensive use of natural energy stock. Also, the world wide utilization of renewables requires high capital investments and it does not seem likely that there will be a significant increase in their development in the near future (Sage, 1996a). The non-renewable energy sources include all potentially recoverable coal, conventional oil and natural gas, unconventional oil resources (e.g. oil shale, tarsands and heavy crude) and unconventional natural gas resources (e.g. gas in pressurized acquifers and coal seams). Among the non-renewable energy sources, as seen in Table 1.2, coal reserves have the highest share in recoverable fossil fuel reserves (Sage, 1996a; Ayala, 1996a).

Thus, coal seems to have the highest potential as an energy source within the next decades.

Table 1.2 Ultimate Recoverable Fossil Fuel Reserves in World
(Ayala, 1996a)

	Reserves (Gtoe)	Percentage (%)
Coal	3400	76
Conventional Oil	200	5
Unconventional Oils		
-Heavy Crude	75	2
-Natural Bitumen	70	2
-Oil Shale	450	10
Natural Gas	220	5
TOTAL (approximately)	**4400**	**100**

Advisory Group with the data supplied from world Energy Council. The results are presented in Table 1.3. There is a vast amount of coal reserves that would last for 500 years, and coal resources that would last about 12 centuries. This is an unavoidable quantity of energy source, considering the other non-renewable sources have far less lifetimes and the renewables are not enough in quantity to supply the whole demand and their development is quite slow as well as usually being local and not uniform.

In Turkey, as it is seen in Table 1.3, hard coal and lignites have the highest reserves among the non-renewable energy sources. Here it should be noted that, as lignites are low rank coals with respect to other coal types such

bitumunous or antracite, they are classified separately. However, the Turkish lignites which posses the biggest share in fossil fuel reserves are high in sulfur, ash and moisture contents and low in calorific value as tabulated in Table 1.4. Thus, in our country, we need systems to produce energy from coal with high efficiency and low sulfur emissions.

Table 1.3 Ultimate Recoverable Fossil Fuel Reserves in Turkey
(Türkiye'de Çevre Kirlenmesi Öncelikleri Sempozyumu, 1997; Derinöz, 1998)

Fuel	Reserves (10^6 tones)
Coal	1,368
Lignites	8,374
Asphaltite	82
Bitumens	1,641
Crude Oil	39,1
Natural Gas (10^6 m^3)	14,103

At the present, mainly two major sources of energy are being utilized in Turkey, namely fossil fuels (mainly lignites) and hydro-power. As it can be seen in Table 1.4 (Atakül et al. , 1993) most of the Turkish lignites have high sulfur content, reaching a very high value of 8.40% (dry ash free basis) in the Çan reserve. Among these important Turkish lignite reserves only Soma, which constitutes about 5% of the total reserves, is said to satisfy the EPA standards as power station fuels (Atakül et al. , 1993). Although Turkish lignites give such a poor profile with low calorific values, the demand for energy will eventually force their use. In this respect, having a system that has high efficiency in

energy conversion becomes a more attractive choice. For this reason in the utilization of Turkish lignites both efficiency and sulfur retention become highly important.

Table 1.4. Characteristics of the Main Turkish Lignite Reserves (Atakül, 1993)

Name	Total Reserve (x10^6 tons)	Lower Calorific Value (kj/kg)	% Dry Ash Free				Ash Fusion Temperature (^{o}C)
			C	H	S	N	-
Zonguldak	539.20	27,839	87.30	5.10	0.50	-	-
Tunçbilek	220.30	15,215	74.50	5.50	1.40	2.95	1200
Soma	515.00	15,591	73.50	4.80	0.90	1.12	1150-1350
Çan	128.30	11,704	66.10	5.50	8.40	2.25	-
Seyitömer	228.60	13,627	70.00	5.00	2.00	-	1142
Orhaneli	58.50	11,202	69.40	5.60	3.20	-	1100
Beypazarı	222.00	10,283	70.80	5.80	7.30	2.50	-
Yatağan	535.10	10,617	-	-	3.90	-	-
Saray	143.00	8276	-	-	6.30	-	-
Kangal	176.00	5685	-	-	7.50	-	1195
Elbistan	3539.00	4680	66.20	5.50	2.70	1.40	-
Göyük	2500.00	12,720	56.00	6.75	1.45	-	-

Advanced power generation systems comprise advanced pulverized fuel technology, variants of fluidized bed combustion, integrated gasification combined cycle and hybrid systems (combination of gasification and combustion technologies) (Sage, 1996b). Electrical energy, which is one of the cleanest forms of energy, is usually produced by conventional systems such as pulverized coal-fired (PC) or stoker-fired boilers with steam turbine and generators. The

energy conversion efficiency in these systems is usually around 30-35%, which means two thirds of the heat generated is being wasted. In order to increase the efficiency in the generation of electrical energy from coal, new technologies are being developed in the United States and other industrialized countries.

Integrated Gasification Combined Cycle (IGCC) technology is receiving increased attention because of its promise of higher thermal efficiency and reduced environmental impacts compared to today's coal fired plants (Harrison, 1995).

Current IGCC plants operate with an efficiency of about 43%, compared to 35% for a conventional coal plant (Van Der Ham et al. , 1996b). With improved gas turbines and high temperature gas cleanup technology, efficiencies exceeding 52% by the end of 2010 and 60% by year 2020 are targeted (De Moss, 1997). In these systems a reduction of 99% in sulfur emissions can be accomplished compared to 90% efficiency for the conventional systems and similar reductions in NO_x and particulates are expected (Harrison, 1995).

In a coal gasifier, unlike coal combustion processes, the sulfur in the coal is released in the form of hydrogen sulfide, H_2S, rather than sulfur dioxide, SO_2. The IGCC process must employ hot gas cleanup techniques to remove sulfur and other impurities in the fuel gas stream, principally to meet the stringent governmental regulations for sulfur emissions and also to protect turbine components from the corrosive action of H_2S (Ben-Slimane and Hepworth, 1994b). Typical gasifier exhaust contains about 5000 ppmv H_2S whereas sulfur concentration limitation of approximately 150 ppmv for IGCC systems has been established. Therefore, a desulfurization system capable of reducing H_2S

6

concentration from about 5000 ppmv to 150 ppmv or lower is required (Ben-Slimane and Hepworth, 1995)

Although in IGCC systems about 30% less SO_x and NO_x are being emitted Per unit of energy generated as compared to pulverized coal plants, H_2S formed in the gasifier creates a problem (Harrison, 1995). Approximately 95% of the sulfur present in the coal is converted to H_2S in the gasifier (Watkinson et al. , 1991). If the coal has high sulfur content such as the Turkish lignites, H_2S concentrations in the coal gas could well pass the typical value of 5,000 ppm (Atımtay et al. , 1993). H_2S being a very corrosive gas, could be damaging to the mechanical parts and the construction material at high temperatures and pressures under IGCC system conditions. Also H_2S when exposed to air easily oxidizes to form SO_x which is an air pollutant. For this purpose the desulfurization is essential in IGCC systems.

Hydrogen sulfide should be removed from the product gas while it is still hot so that the gas can be used directly without losing its heat. This completely eliminates the costly, less efficient method of low temperature, liquid based, fuel gas scrubbing systems. Additionally, since the volume of the fuel gas stream is a lot similar than that of the flue gas stream, the removal of H_2S at high temperature results in considerably lower hardware costs than would be required by a conventional SO_2 scrubbing method at low temperature (Ben-Slimane and Hepworth, 1994b). This fact emphasizes the importance of "hot gas cleanup".

The high temperature desulfurization can be succesfully accomplished by using metal oxide sorbents which will react with H_2S to form the corresponding metal sulfide and which, according to thermodynamics, have the ability to reduce the H_2S concentration to the required level. In addition, the sorbent must

be stable in the coal gas atmosphere, have acceptable sulfur loading capacity, be regenerable, and maintain activity through a large number of sulfidation regeneration cycles (Harrison, 1995). All these properties could not be met by a single metal oxide. For this reason metal oxides are tried in combinations in the hope to improve thermodynamic, kinetic, and physical properties.

The purpose of this study could be stated as developing highly reactive copper-based mixed oxide sorbents, Cu-Mn-O, Cu-Mn-V-O and Cu-V-O, for hot coal gas desulfurization applications. Also, the reactivity and performance of these sorbents in 6 sulfidation/regeneration cycles were evaluated by taking into account characterization results. Characterization of the fresh sorbents was studied with the aid of Hg porosimetry, N_2 sorptometry, X-ray diffraction and Scanning electron microscopy. Beside, deactivation model was used for the prediction of breakthrough curves of H_2S in a fixed-bed reactor to confirm the experimental data and to calculate the rate parameters. Finally, sulfidation/regeneration reaction mechanisms were proposed at high temperatures.

CHAPTER 2

THEORETICAL BACKGROUND

2.1 Integrated Gasification Combined Cycle Systems

The world relies increasingly on coal as a primary energy source. All over the world most power plants burn coal to run turbines. The sulfur in coal is gasified, and every year tens of thousands of tons of sulfur are emitted into the atmosphere from the chimneys of power plants. With increasing attention being paid to environmental protection, it has become clear that sulfur emission sources must be reduced. As a main pollution source the emission of sulfur from power plants should be strictly controlled.

Integrated Gasification Combined Cycle (IGCC) technology was developed to improve the overall efficiency of powdered coal power plants. A configuration of an ideal system is shown in Figure 2.1. In such systems the coal is gasified with oxygen or steam under high pressure to produce fuel gas. After purification the fuel gas is used to drive a gas turbine and generate electricity. The exhaust gas from the gas turbine passes through a boiler to produce high pressure steam used by a steam turbine. At the exit of a typical gasifier the temperature is about 1150 K. If the fuel gas can be purified at such a high temperature, the heat efficiency of the whole IGCC system will be greatly improved.

9
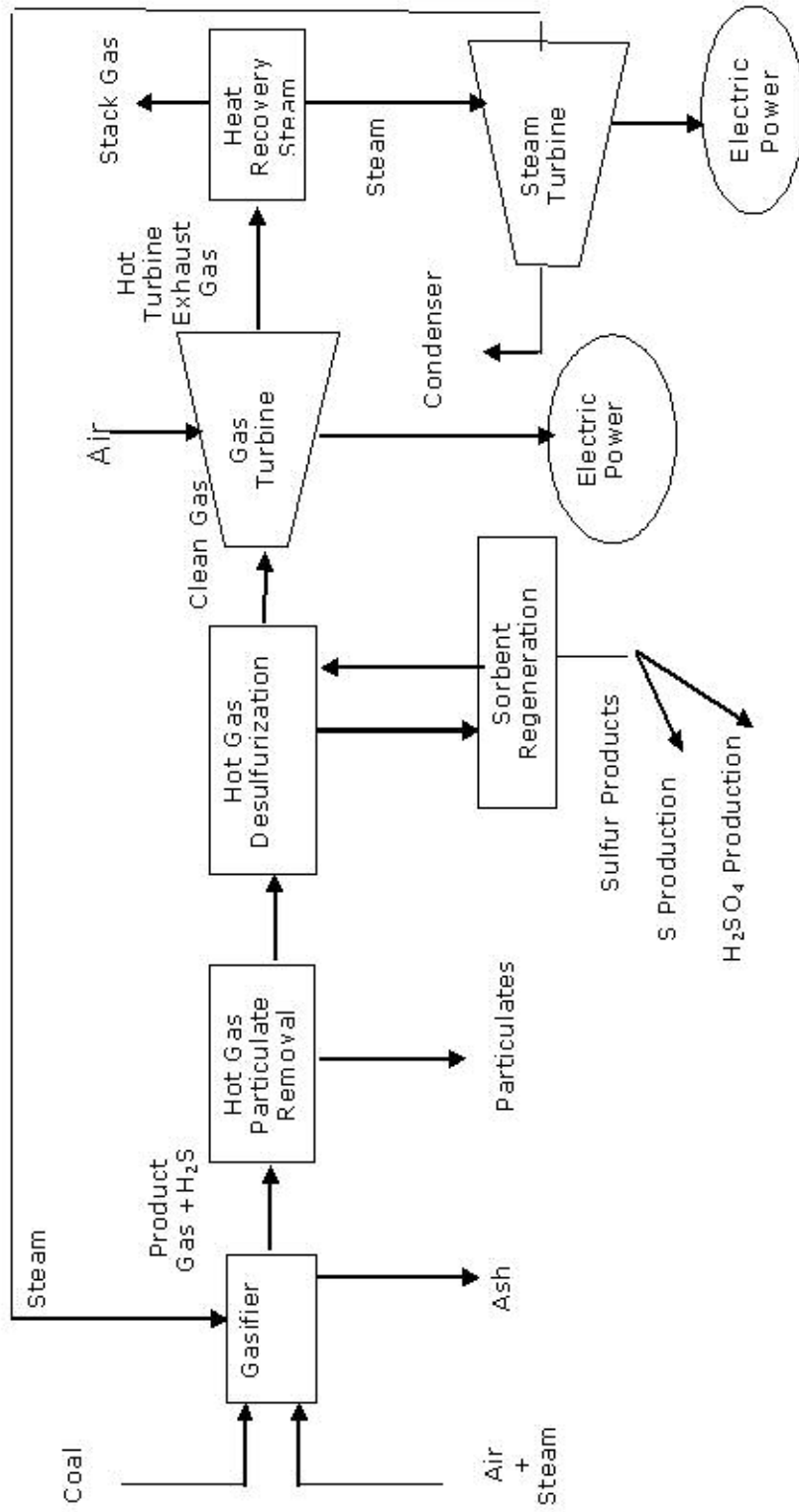
Figure 2.1. Schematic Representation of an Integrated Gasification Combined Cycle System (IGCC)

As the sources of petroleum and natural gas reduce, many chemical processes have to consider coal as their raw material. However, synthesis gas from coal contains almost all of the sulfur in coal. A typical H_2S composition is 0.1-1.5 %. Such a concentration of sulfur is fatal to most catalysts, and the synthesis gas must be desulfurised before it is used as a reactant (Liang, 1999).

By reacting the sulfur held in the desulfurization sorbents with oxygen sulfur dioxide is formed. For the removal of this sulfur dioxide, it could be turned into sulfuric acid (by such processes as Wellman-Lord process) or elementary sulfur (by such processes as Claus process). Both of these are marketable products. Sulfur dioxide produced during regeneration reaches to concentrations of 12 % by volume, which is suffcent for H_2SO_4 production (Harrison, 1996). Production of elemental sulfur could be accomplished from dilute streams as 1-2 % by volume yielding as high as 98 % S_2 or directly by the regeneration of sorbents by sustaining partial oxidation (Flytzani- Stephanopoulos, 1996c).

The advantages of IGCC systems over the pulverized coal-fired power generation systems are:

- Higher power generation efficiency,
- Lower air emissions,
- Smaller amounts of solid wastes,
- Lower water consumption,
- Simple plant configuration,
- Capability of staggered / phase construction (Ayala, 1996b).

In the IGCC system, the gasifier exit gas needs the removal of:

- Dust/particulate mater,
- Sulfur species,

11

- Amonia or NO_x,

- Alkali and halogens,

- Organica and trace elements (heavy metals),

- Greenhouse gases (CO_2, N_2O_4) (Ayala, 1996a).

Among the contaminants sulfur has received more attention than any other because it is a main precursor to acid rain and causes severe corrosion problems in most systems using coal gasification, such as power plants and synthesis gas conversion plants.

2.2 Coal Gasification

Gasification is expected to be among the most promising conversion process to produce synthesis gases. Gases produced by this process however contain H_2S and other sulfur compounds that hazardous and corrosive. Generally, almost 90 % of the sulfur is in the H_2S form. In many applications, gases are required to contain not more than a few ppm of H_2S. In IGCC system, coal gasification is integrated with combined-cycle power generation. Both gasification and power generation are high temperature processes (Atakül et al.,1996).

Gasification process consists of incomplete combustion with 1/5 to 1/3 amount of the oxygen theoretically required for complete combustion to CO_2 and H_2O. A typical gas mixture contains CO, H_2, CO_2, CH_4, N_2, H_2O, H_2S, COS, NH_3, HCl and particulate matter (Watkinson et al., 1991).

The concentration of the various species in fuel gas depends on type of coal, type of reactor used (fixed bed, fluidized bed, or entrained flow) and operating conditions (temperature, pressure, flow and equivalence ratio). As a

result gasifier operating conditions should be carefully controlled to obtain the desired fuel gas composition (Ben Slimane et al., 1994).

2.3 Hot Gas Clean up Techniques

Hot gas clean up techniques must be employed to remove sulfur and other impurities in the fuel gas stream, principally;

- To meet stringent government regulations for sulfur emissions and also to protect turbine components from the corrosive action of H_2S.

- To achieve maximum efficiency, the H_2S should be removed by purifiying the product gas while it is still hot so that the gas can be used directly without loss of heat values. This completely eliminates the more costly, less efficient method of low-temperature, liquid based, fuel gas scrubbing systems.

- Since the volume of the fuel gas stream is significantly less than that of the flue gas stream, particularly since it is usually also at elevated pressure, the removal of sulfur-bearing species at high temperature results in considerably lower hardware costs (Ben Slimane, 1994b).

The contaminants in the gasifier exit gas are:
- Sulfur species
- Dust particulate materials
- Nitrogen compounds (ammonia or NO_X)
- Alkali and halogens
- Hazardous organics
- Trace elements (heavy metals)
- Greenhouse gases (CO_2, N_2O_4) (Harrison,1995)

Following technologies can be used to remove particulate matters from hot gases:

- Inertial separators
- Electrostatic precipitators (ESP)
- Fabric and fabric filters
- Rigid barrier filters
- Granular bed filters (Ayala, 1996b)

In the gasifier, some of the nitrogen is converted to NH_3 and to trace quantities of HCN, NH_3 concentration in the coal gas may vary between 1000 and 5000 ppmv. It is required to achieve NH_3 emissions below 50 ppm. To remove NH_3, staged combustion and catalytic decomposition techniques can be used.

CHAPTER 3

HOT GAS DESULFURIZATION

High temperature desulfurization of coal derived fuel gas from the coal gasification unit is considered as one of the most promising advanced technologies to remove the sulfur components from coal so that environmental considerations are eliminated from the choice of using coal versus oil or natural gas as fuel feedstock. In addition, the method offers potential improvements on the thermal efficiency of the systems using coal gasification, such as integrated gasification combined cycle (IGCC) power plants, hydrogen fuelled solid oxide fuel cells (SOFC) and molten carbonate fuel cells (MCFC) technologies. The development of these systems depends on the ability to remove sulfur compounds, mainly H_2S, from the coal gas.

During gasification process, about %95 of the sulfur contained in the coal is turned into H_2S and rest of them are converted into SO_2 becomes precursor of acid rain extremely harmful to the ecosystem. The produced H_2S should be lowered from the typical gasifier output of 5000 ppm to the tolerable limit of 150 ppm (Atımtay et al, 1993). As indicated before H_2S being a very corrosive gas, could be damaging to the mechanical parts and the construction material at high temperatures and pressures under IGCC system conditions.

In order to have high efficiency in the IGCC system, removal of H_2S without cooling the coal gas is a very important task. These facts emphasices the importance of hot gas desulphurization. Hot gas desulfurization may be accomplished by using sorbents such as metal oxides that forms stable sulfides. Typically, these metal oxides are converted to sulfides during a sulfur-loading stage under reducing hot fuel gas conditions (Van Der Ham et al, 1996a).

$$Me_xO_y + xH_2S + (y-x)H_2 \rightarrow xMeS + yH_2O \qquad (R.3.1)$$
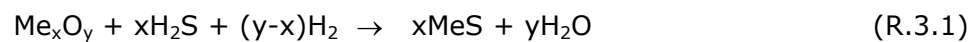
3.1   Historical Development of Regenerable Desulfurization Sorbents

Over the last two decades a number of studies have been reported on high-temperature H_2S removal, primarily using various transition metal oxides as regenerable sorbents.

The sorbent most intensively studied in the 1980's was iron oxide, which yields equilibrium H_2S concentrations in the few hundred ppm range for a composition representative of low-Btu coal derived gas and temperatures of above 500 ^{o}C. While the sulfidation kinetics of iron oxide are very good, this sorbent cannot be used for single-stage coal gas desulfurization to reduce the H_2S content of the fuel gas down to a few ppm of sulfur (Ayala et al.,1998).

Zinc oxide has been used as a non-regenerable sorbent in "guard beds" protecting catalyst beds from trace sulfur impurities. More recently, zinc oxide has also been investigated as a regenerable sorbent. The thermodynamic equilibrium for sulfidation of ZnO is quite favorable, yielding desulfurization down to a few ppm H_2S. The sulfidation kinetics of ZnO, however, are slower compared to those of pure iron oxide, and the regenerability of ZnO is restricted above

16

700°C by the loss of surface area and the formation of zinc sulfate at low regeneration temperatures.

In the late 1980's, it was shown that certain mixed oxides have superior properties compared to single oxides for hot gas cleanup. Many investigators have been conducting research to develop a superior mixed metal oxide sorbent. Mixed-metal oxide sorbents have been studied in the past both as straight zinc titanates, (e.g., Zn_2TiO_4 and $Zn_2Ti_3O_8$) or as combinations of oxides of vanadium, copper, manganese, cobalt, and others. Although zinc titanate has also shown better attrition resistance than zinc ferrite in pilot tests, this sorbent also suffers gradual loss of reactivity in long-term cyclic operation, resulting in high fresh sorbent makeup rate to maintain the desired level of desulfurization (Ayala et al.,1998).

Other mixed metal oxides such as copper-based and cobalt-based sorbents have also been investigated; however, the research has been limited to laboratory-scale equipment. Although higher temperature application offers better overall process efficiency, the stringent requirement for sulfur removal efficiency at temperatures above 538 °C (1000 °F) limits the choice of the sorbents to a few metal oxides (based on thermodynamic equilibrium). The thermodynamic equilibria of many metal oxides significantly improve as the temperature decreases, making many metal oxide sorbents suitable for hot gas cleanup application in the temperature range of 343-538 °C (650-1000 °F). Although the initial chemical reactivities of the sorbents generally decrease with decreasing temperature, the lower thermal stress incurred can lead to better sorbent reactivity after a large number of cycles, reducing the sorbent replacement cost.

In general, the benefit to be gained by lower temperature application may outweigh the slight loss of efficiency, resulting in lower overall cost of electricity. However, no extensive study has been done on the development of advanced sorbents for the lower temperature application.

3.2   Properties of Metal Oxide Sorbents for Hot Gas Desulfurization

A good sorbent will allow for a deep desulfurization to ppm levels and have good regeneration properties. This means the combination of a high affinity towards the reaction with H_2S, as well as the formation of a sulphide which can be converted back to the oxide through oxidation with air or diluted air.

Next to the residual H_2S level, sorbent durabilty is the critical issue. For economical operation, a good sorbent has to maintain a large fraction of its desulphurisation properties for a large number of sulfidation-regeneration cycles, requiring excellent sorbent stability.

As summary, in order for a metal oxide to be considered suitable for high-temperature desulfurization, the material must exhibit desirable properties in the following areas:

- Ability to remove reduced sulfur compounds such as hydrogen sulfide and carbonyl sulfide to less than 100 ppmv,
- Good sulfur loading capacity to reduce the operational cost and reactor size,
- Good regenerability,
- Mechanical strength measured as either crush strength or attrition resistance,

- Retaining its capacity over an extended period of time without undergoing drastic changes in its physical and chemical properties in order to minimize frequent replenishments,

- Environmental affinity.

3.3   Selection of Metal Oxide Sorbents for Hot Gas Desulfurization

Westmoreland and Harrison (1976) screened the high-temperature desulfurization potential of twenty-eight (28) solids, primarily metal oxides. They concluded that eleven candidate solids based upon the metals Fe, Zn, Mo, Mn, V, Ca, Sr, Ba, Co, Cu, and W showed thermodynamic feasibility for high-temperature desulfurization.

Westmoreland et al. (1976) also determined the initial rates for the reaction between H_2S and MnO, CaO, ZnO, and V_2O_3 over a temperature range of 300 to 800 $^{\circ}$C, in a thermobalance reactor. The relative magnitude of reaction rates decreased in the order MnO > CaO $\approx$ ZnO > V_2O_3. They concluded that MnO possessed favorable properties for a high-temperature desulfurization process and highly recommended that further studies be carried out. Fractional desulfurization results are summarized in Figure 3.1. From Figure 3.1, it is obvious that manganese, for example, satisfies the 95% desulfurization criterion at all temperatures below 1060 $^{\circ}$C. Figure 3.2 summarizes solid stability results. As an example, consider barium. At low temperature, $BaCO_3$ is the stable solid form. Sulfiding of the carbonate begins at approximately 800 $^{\circ}$C, and, from that point to the 1200 $^{\circ}$C melting temperature of BaS, simultaneous existance of solids BaS and $BaCO_3$ is predicted.
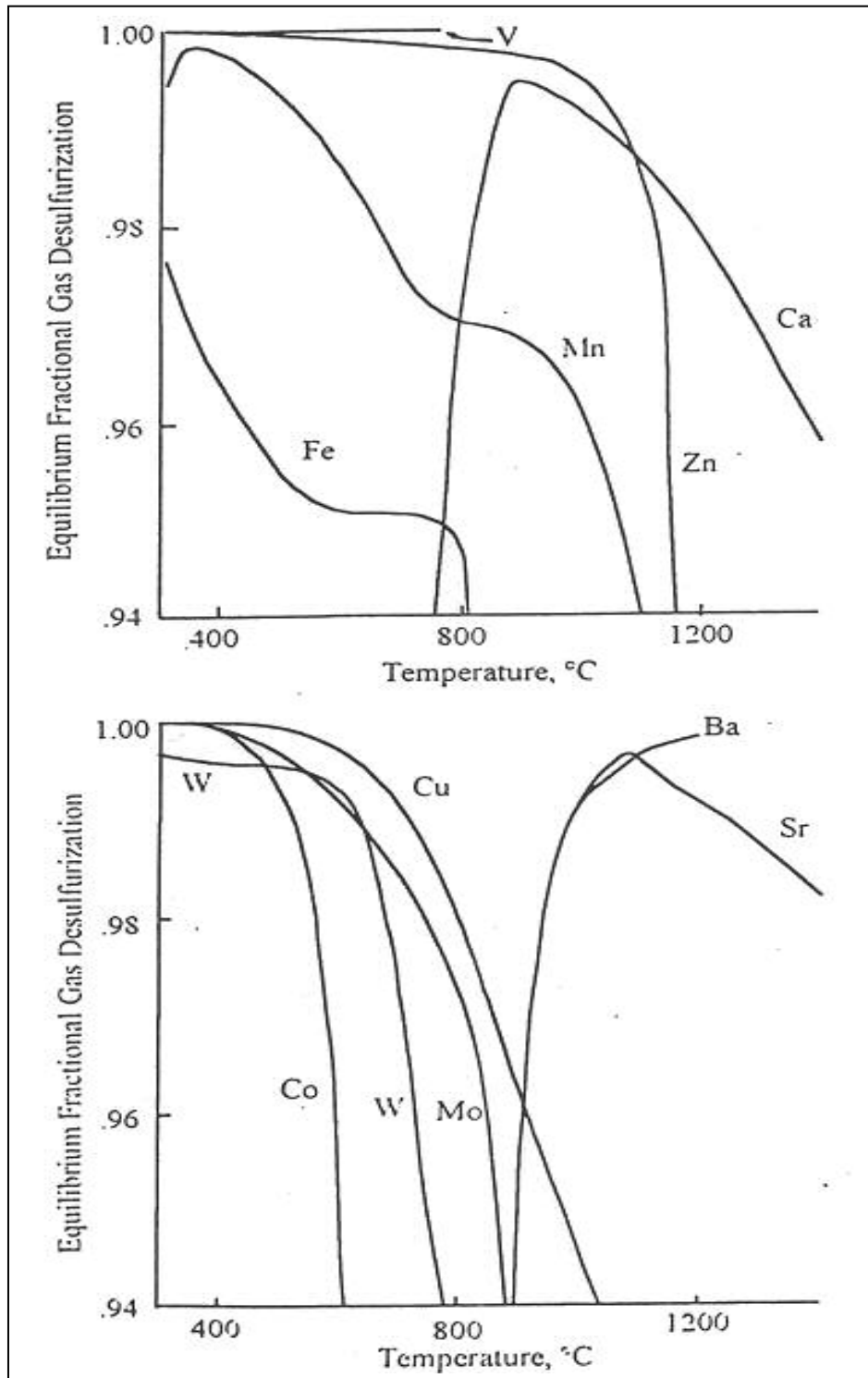
Figure 3.1. Desulfurization Potential of Canditate Solids

(Westmoreland and Harrison, 1976)
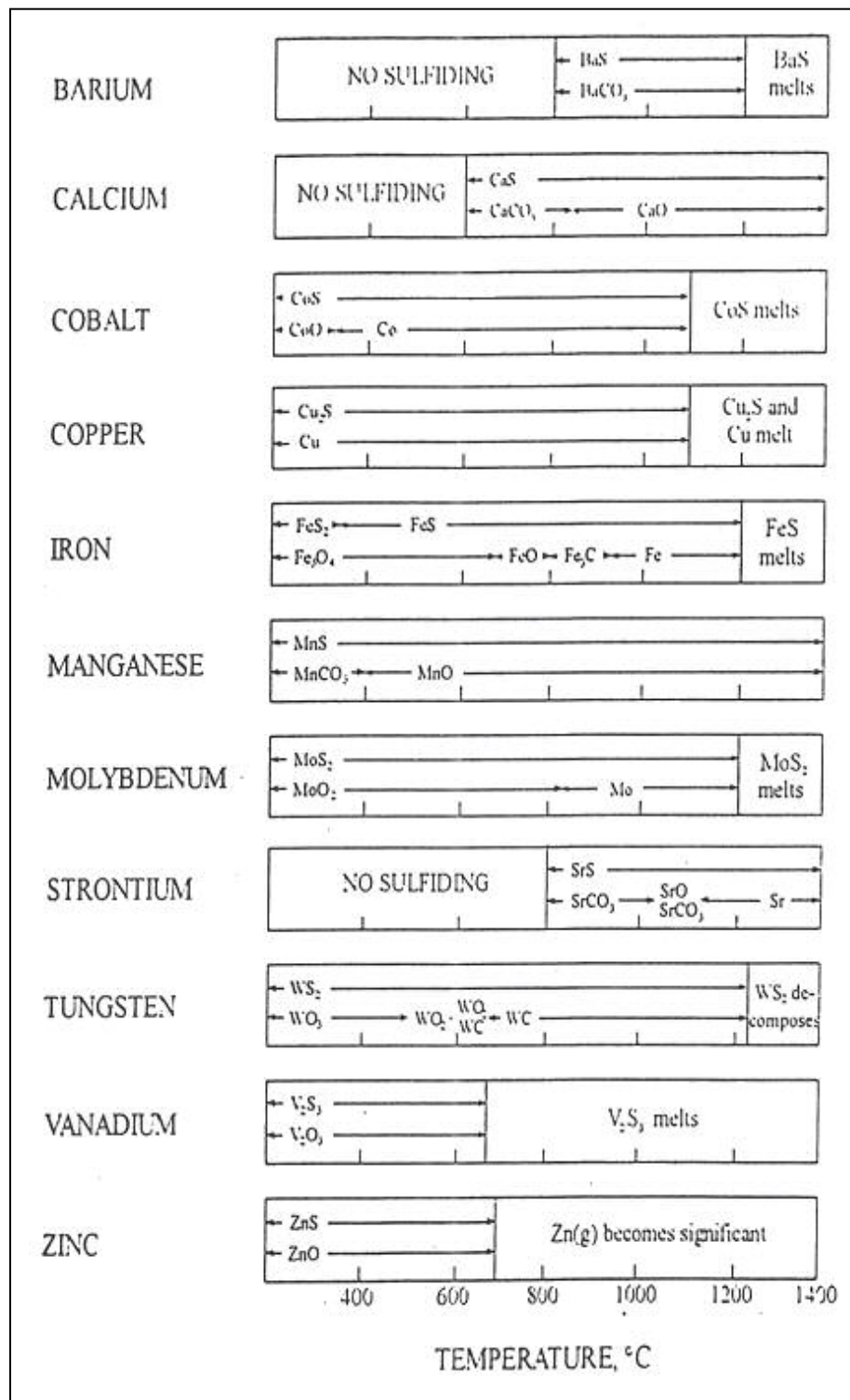
Figure 3.2. Stable Solid Phases of Canditate Solids

(Westmoreland and Harrison, 1976)

By properly combining information from Figures 3.1-3.2, the desulfurization potential of several canditate can be established. These results are summarized in the following pharagraphs.

Cobalt: Cobalt satisfies desulfurization criterion to a maximum temperature of 600 $^{\circ}$C with CoS the sulfided product. In the reducing atmosphere of coal gas, excess cobalt would be present as the metal at temperatures in excess of 300 $^{\circ}$C.

Copper: The behaviour of copper and cobalt is similar, although copper maintains 95% desulfurization capability to a temperature in excess of 900 $^{\circ}$C. In the reducing atmosphere, excess copper would be present in metallic form over the entire temperature range.

Iron: Iron is a suitable desulfurizing material at temperatures up to 700°C. At these temperatures, Fe_3O_4 is the stable form of excess iron. The rapid decrease in fractional desulfurization near 700 $^{\circ}$C corresponds to Fe_3O_4 reduction to FeO.

Manganese: Oxide stability and high fractional desulfurization are predicted to temperatures in excess of 1000 $^{\circ}$C. Below 400 $^{\circ}$C, MnO is stable. Importantly, manganese shows desulfurization potential in the temperature range of 600-700 $^{\circ}$C where metal oxides currently known to be reactive with H_2S are unsatisfactory.

Vanadium: In the reducing atmosphere, V_2O_3 is the stable form of the excess metal. Essentially 100% desulfurization, with V_2S_3 as the sulfided product, is predicted up to the melting temperature of V_2S_3 near 650 $^{\circ}$C.

Zinc: On the basis of fractional desulfurization, zinc is acceptable to 1150°C with ZnS as the sulfided form and ZnO as the stable form of excess zinc.

However, zinc is limited to a maximum temperature of approximately 700 ^{o}C because of the formation of zinc vapor. Experimental observations in this laboratory have confirmed the formation of zinc vapor in similar atmospheres at temperatures in excess of 700 ^{o}C.

From the initial screening of metals, the following metals should be ruled out immediately: Ba, Ca, Sr, and V. The main reason was the lack of sulfidation of their oxide forms in the desired range of 340-550°C (~650-1000 °F) or incompatibility with turbine operation (i.e., high-temperature corrosion by vanadium compounds).

The process of selection of metal oxides for desulfurization identified the following metals as being potentially useful for desulfurization study: Zn, Cu, Co, Fe, Ce, Mo, Mn, Sn, W, Ni. It was agreed that many of these metals have weaknesses when considered as pure metal oxides, but become useful when used in combination with others (e.g., Cu-Mo, and Zn-Mo systems). Zn, Cu, Fe, Ce, and Mo were ranked as being the most useful, hence worth further evaluation. Both molybdenum and tungsten oxides have good desulfurization potential; however, they are temperature limited because of possible carbide formation (Elseviers and Verelst, 1999). More information on thermodynamic properties is needed on the W system to proceed forward with an evaluation. Cobalt exhibits similar behavior to that of copper in its tendency to reduce to the metallic form in fuel gas atmospheres. However, compared to copper oxide, desulfurization with cobalt oxide is more temperature limited and becomes less efficient with increasing temperature. In addition, cobalt sulfide requires significantly higher temperatures for regeneration than copper sulfide (Slimane and Abbasian, 2000). Sn and Ni were ranked as being less desirable than the others and probably will not be considered before the others. Sn has one of the

23

highest H$_2$S vapor pressures and its sintering temperatures are relatively low, which may affect the regeneration process conditions, typically done from 500 to 700 °C.

The next step was consideration of the relative compositions in formulations. The metals still considered as useful at that point were divided into three functional groups:

- Main components for desulfurization
- Secondary components for desulfurization, chemical stability, or porosity modifier
- Structural component to maintain mechanical durability

Up to this point, the selection of metal oxides is a general method that is equally applicable to any desulfurization process configuration operating in the prescribed temperature regime.

Zn, Fe, Ce, Mn and Cu were selected to be the next generation of most promising metals for use as main components. Secondary components will be added to the main components to satisfy most of the evaluation criteria and a structural component will be needed to maintain morphological and mechanical durability.

All these properties could not be met by a single metal oxide. For this reason metal oxides are tried in combinations in the hope to improve thermodynamic, kinetic, and physical properties. By mixing, it may be possible to,

- improve sulfur removal efficiency,
- prevent or slow the reduction to elemental metal,

- prevent sulfate formation,

- improve dispersion and modify porosity and pore size, and

- impart structural strength and stability (Akyurtlu, A., 1996).

The stability of the sorbent is an important property as the sorbent should withstand highly reducuble atmospheres and high temperature range of 400-800 $^{\circ}$C without reducing into elemental metal form or vaporize (Westmoreland and Harrison, 1976; Akyurtlu et al., 1996).

Another sorbent property is sulfur loading capacity or sulfur adsorption capacity which is defined as the ratio of sulfur adsorbed to initial sorbent by weight (Van Der Ham et al., 1996b ; Stephanopoulos, 1996).

$$\text{Sulfur Loading Capacity} = \frac{\text{theoretical amount of sulfur adsorbed by the sorbent (g)}}{\text{total weight of sorbent (g)}}$$

The conversion of H$_2$S and the selectivity to sulfur are defined as follows:

$$\text{Conversion of H}_2\text{S (\%)} = \frac{[H_2S]_{inlet} - [H_2S]_{outlet}}{[H_2S]_{inlet}} \times 100$$

$$\text{Selectivity to sulfur (\%)} = \frac{[H_2S]_{inlet} - [H_2S]_{outlet} - [SO_2]_{outlet}}{[H_2S]_{inlet} - [H_2S]_{outlet}} \times 100$$

$[H_2S]_{inlet}$ = inlet H$_2$S concentration

$[H_2S]_{outlet}$ = outlet H$_2$S concentration

$[SO_2]_{outlet}$ = outlet SO$_2$ concentration

The cost of purchasing raw materials was also considered in the evaluation of the relative merit of the various metal oxides. Costs were kept in mind when developing formulations, but it was considered too early to make

25

decisions whether to use or not to use an oxide just because of its price, since the relative amounts of secondary components may be too small (e.g.,<1%) to have a significant impact on the cost of the sorbent and yet have a tremendous impact on the durability of the material.

3.4   Sorbent Regeneration

Regeneration is considered essential to the commercialization of sulfur sorbents since it improves overall process economics and also reduces the amount of solid waste generated and ultimately landfilled. The regeneration step is a highly exothermic oxidation process requiring careful temperature control. Too high temperature (above 800 ^{o}C) sinters and destroys the sorbent structure and reduces its ability to absorb sulfur in consecutive absorption steps. Low temperature, high SO_2 and O_2 result in sulfate formation and a lower sulfur removal efficiency.

Metal sulfides are regenerated to oxides and byproduct SO_2 containing stream by steam, oxygen or SO_2 gases.

$$MeS + H_2O \rightarrow MeO + H_2S \tag{R.3.2}$$

$$xMeS + (y/2) SO_2 \rightarrow Me_xO_y + (x+y/2) S \tag{R.3.3}$$

$$xMeS + (x+y/2) O_2 \rightarrow Me_xO_y + x SO_2 \tag{R.3.4}$$
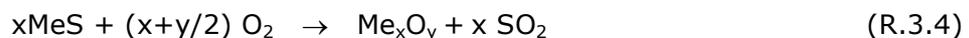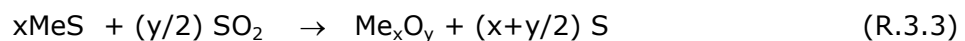
An unwanted reaction side-reaction is the formation of sulphates:

$$MeS + 2O_2 \leftrightarrow MeSO_4 \tag{R.3.5}$$
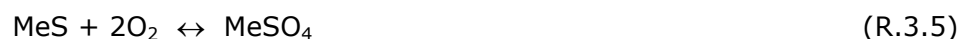
Because the formed sulphate is inert with respect to the desulphurisation and thus there is a loss of active material. Consequently, it is important to know

at which conditions this reaction (R.3.5) preceeds the desired regeneration reaction (R.3.4).

For the process to be economical, the sorbent must be regenerable and must maintain activity through many sulfidation-regeneration cycles. Most regeneration studies to date have used total oxidation in which the metal sulfide is reacted with oxygen to regenerate the metal oxide and liberate the sulfur as SO_2. In addition to the problem of controlling SO_2 in the regenerator off-gas, the highly exothermic total oxidation reaction creates reactor temperature control problems which may accelerate the deteriorating of the high surface area, porous sorbent. Decreasing the oxygen concentration of the regeneration gas to assist in temperature control reduces the SO_2 concentration in the regeneration product and complicates the SO_2 control.

Direct production of elemental sulfur during sorbent regeneration would alleviate both problems. Elemental sulfur is a marketable byproduct which can be separated by condensation and safely stored and transported.

Three possible elemental sulfur production concepts were identified from the literature. The general chemistry of each as well as a brief summary of the literature is presented below.

3.4.1 Reaction With SO_2

The generic reaction between metal sulfide and SO_2 to yield elemental sulfur is:

$$MeS\ (s) + 0.5\ SO_2\ (g) \leftrightarrow MeO\ (s) + 0.75\ S_2\ (g) \qquad (R.3.6)$$
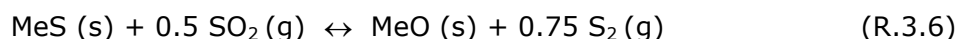
Copeland et al. (1994) have studied the regeneration of SnS (s) while Anderson and Berry (1987) have reported on the regeneration of a sulfided cobalt titanate sorbent. Several studies (Schrodt et al., 1978; Tseng et al., 1981; Patrick et al., 1993) have examined the regeneration of sulfided iron oxide. Primary questions concern the rate of reaction between metal sulfide and SO_2 and thermodynamic limitations on the maximum partial pressure of $S_2(g)$ in the regeneration product.

3.4.2 Partial Oxidation

The formation of elemental sulfur when metal sulfide is reacted with oxygen and steam under "O_2-starved" conditions is referred to as partial oxidation. The general stoichiometric reaction is:

$$MeS\ (s) + 0.5\ O_2\ (g)\ \rightarrow\ MeO\ (s) + 0.5\ S_2\ (g) \tag{R.3.7}$$
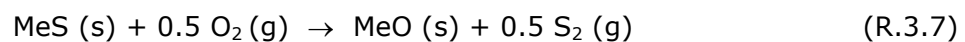
In reality, this stoichiometry represents the net result of a number of simultaneous reactions. In the presence of excess oxygen, total oxidation would occur with MeO(s) and $SO_2(g)$ as the primary products.

Several references suggest that partial oxidation to produce elemental sulfur may be possible. Joshi et al. (1979), Grindley and Steinfeld (1981), and Van der Waal (1987) have studied the partial oxidation of sulfided iron-based sorbents. As much as 75 % of the sulfur released during regeneration was in elemental form, with most of the remainder as H_2S. Kay and Wilson (1989) and Kay et al. (1993) have reported that elemental sulfur is formed during the regeneration of cerium oxysulfide, Ce_2O_2S, at conditions similar to those used for FeS regeneration.

28

3.4.3 Reaction With H_2O/Claus

By reversing the primary desulfurization reaction, regeneration to H_2S is possible according to the generic reaction:

$$MeS \text{ (s)} + H_2O \text{ (g)} \rightarrow MeO \text{ (s)} + H_2S \text{ (g)} \qquad \text{(R.3.8)}$$
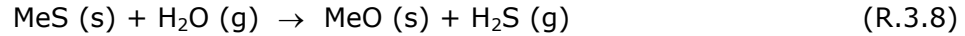
Although elemental sulfur is not a direct product, H_2S may be converted to elemental sulfur by the Claus reaction if the H_2S concentration is sufficiently high. Since regeneration with steam is the reverse of the desulfurization reaction, it is obvious that sorbents having the greatest affinity for H_2S will be the most difficult to regenerate.

The Claus process consists of two steps: thermal oxidation and catalytic reaction.

Step (I) $2H_2S + 3O_2 \rightarrow 2SO_2 + 2H_2O$ (thermal oxidation) (R.3.9)

Step (II) $2H_2S + SO_2 \leftrightarrow (3/n)S_n + 2H_2O$ (catalytic reaction) (R.3.10)
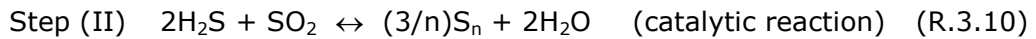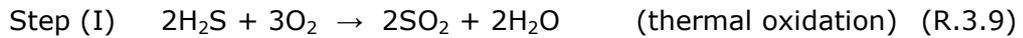
Nielsen et al. (1991) report H_2S mol fractions in the regeneration product as high as 0.25 when SnS (s) was reacted with H_2O. H_2 is also produced by this reaction and a separation step is also required to recover H_2S from the excess steam and H_2 by-product. Tamhankar et al. (1985) and Wakker et al. (1993) have studied the regeneration of sulfided iron-based sorbents with steam while Sohn and Kim (1987) have studied the steam regeneration of ZnS.

CHAPTER 4

LITERATURE SURVEY

Preliminary to the preparation of mixed-metal oxide sorbents under this study, a review of the literature was done to identify pure metal oxides and combinations of metal oxides that had been evaluated in the past for high-temperature desulfurization of coal gases.

4.1 Copper-based Sorbents

Tamhankar and Stephanopoulos (1986) widely investigated several pure and mixed oxides. ZnO, CuO, ZnO-Fe_2O_3, CuO-Fe_2O_3, CuO-Al_2O_3, and CuO-Fe_2O_3-Al_2O_3 were investigated as regenerable sorbents for the removal of H_2S at high temperatures. A special technique was used to prepare the sorbents in highly porous form. The sorbents were subjected to successive sulfidation-regeneration cycles in a packed –bed microreactor. Sulfidation was carried out at 538-650 ^{o}C with H_2S-H_2O-H_2-N_2 mixtures, regeneration with O_2-N_2-H_2O mixtures. The performance of the sorbents CuO-Fe_2O_3, CuO-Al_2O_3, and CuO-Fe_2O_3-Al_2O_3 was discussed in terms of changes in the oxidation state of copper during sulfidation. The sorbent CuO-Fe_2O_3-Al_2O_3 was found to be superior to either CuO-Fe_2O_3, CuO-Al_2O_3, yielding stable conversion and sub-equilibrium H_2S levels (with respect to metallic copper sulfidation) at temperatures as high as 650°C. Several

of these sorbents appear promising for high temperature desulfurization applications.

Copper based sorbents research results showed that they could reduce H_2S from several thousand ppm to sub-ppm levels (Tamhankar et al., 1986; Flytzani et al., 1989; Li et al., 1997; Lee et al., 2001). However, copper oxides in uncombined form are readily reduced to metallic copper by the H_2 and CO contained in fuel gases, which lowers the desulfurization efficiency because the sulfidation equilibrium constant of CuO is about 10 orders of magnitude higher than that of Cu. Various combinations of CuO with MnO_2, MoO_3 were made to prepare sorbents by using a simple mixing method. CuO was used as main active material, MnO_2 and MoO_3 as additives and SiO_2 as support material. TGA screening and GC/microreactor multi-cycle reactions were carried out to characterize reactivities of sorbents. Sulfidation temperature was 500 ^oC and regeneration temperature ranged 500~700 ^oC. Sulfidation was carried out after reduction was completely finished with H_2/N_2 gas. Without considering the effects of additives such as MoO_3 and MnO_2, they inferred that CuO be converted into Cu by H_2 and Cu into Cu_2S by H_2S. If Cu was fully converted into Cu_2S, the weight recovery during reduction would reach to twice of the weight loss during the sulfidation.

Reduction $\qquad$ $CuO + H_2 \;\rightarrow\; Cu + H_2O$ $\qquad\qquad$ (R.4.1)

Sulfidation $\qquad$ $2Cu + H_2S \;\rightarrow\; Cu_2S + H_2$ $\qquad\qquad$ (R.4.2)

Regeneration $\qquad$ $2Cu_2S + 4O_2 \;\rightarrow\; CuSO_4 + 2CuO + SO_2$ $\;\;$ (R.4.3)

Reduction $\qquad$ $H_2 + CuO \;\rightarrow\; Cu + H_2O$ $\qquad\qquad$ (R.4.4)

$\qquad\qquad\qquad$ $CuSO_4 + 2H_2 \;\rightarrow\; Cu + SO_2 + 2H_2O$ $\qquad$ (R.4.5)
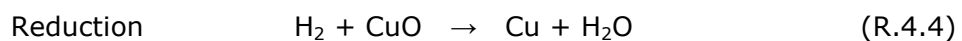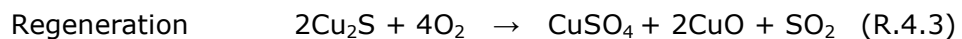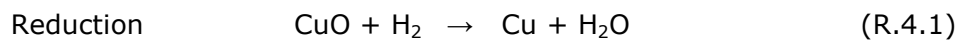
Through the TGA test, promising sorbents were chosen and tested in GC/microreactor up to the 19th cycle. Sulfur loading was most affected by the ratio of CuO, MoO_3 and MnO_2. Sorbent containing additives of MoO_3 and MnO_2 was fully stabilized after the 19th cycle and showed best sulfur loading of 15 %.

Binary Cu-Cr-O and Cu-Ce-O oxides were studied as regenerable sorbents for high temperature fuel gas desulfurization by Li and Stephanopoulos (1997). CuO-Cr_2O_3 and CuO-CeO_2 sorbents can remove H_2S from simulated coal-derived fuel gas to less than 5-10 ppmv in the temperature range of 650-850°C. The presence of stable $CuCr_2O_4$ in CuO-Cr_2O_3 solids retains some copper in the Cu^{+2} or Cu^{+1} oxidation state, which can account for the high H_2S removal efficiency. In CuO-CeO_2 sorbents, however, CuO is easily reduced to copper metal. Participation of reduced cerium oxide in sulfidation can explain the observed high desulfurization efficiency. The TGA tests and XRD analysis indicate that sulfidation proceeds through partial initial reduction of the CuO-Cr_2O_3 sorbents: $CuO \rightarrow Cu/Cu_2O \rightarrow Cu_xS$ (x<2). A simulated coal gas mixture containing H_2S, H_2, H_2O and N_2 was used in sulfidation. Regeneration was carried out by air diluted with N_2.

Flytzani-Stephanopoulos et al. (1987) and Patrick et al. (1990) studied various bulk CuO based sorbent systems, such as Cu-Fe-O, Cu-Al-O, Cu-Fe-Al-O, and Cu-Mo-Al-O. In metal oxide compounds, such as $CuFe_2O_4$ or $CuAl_2O_4$, the reduction of CuO to Cu by H_2 or CO was much slower than that of pure CuO. This is due both to the thermodynamic stability of these spinels and to slow kinetics. The slow reduction of CuO in these mixtures retained a portion of copper in +2 and/or +1 oxidation state and, therefore, achieved sub-ppm H_2S breakthrough levels at temperatures as high as 650-700°C depending on the fuel gas composition.

The sorbents consisted of various combinations of copper, molybdenum, and/or manganese oxides supported on high silica-containing zeolite were studied by Gasper-Galvin et al. (1998). These sorbents were tested in a fixed-bed reactor with simulated coal gas at 205 kPa (15psig). The combination of all three metal oxides displayed synergism in enhancing efficiency for H_2S removal and improved the crush strength on the pellets. Copper oxide was the most active component for reaction with H_2S, while molybdenum and manganese oxides appeared to act as catalyst/promoters. There were some difficulties encountered with volatilization of the Mo oxide; however, the presence of Cu and Mn oxides appeared to reduce its volatility. During multicycle testing, this ternary metal oxide sorbent retained its reactivity and mechanical strength.

Yasyerli et al. (2001) studied activities of copper oxide, Cu-V and Cu-Mo mixed oxides for high temperature removal of H_2S from industrial gases in the presence and in the absence of hydrogen. Experiments were carried out in the temperature range between 300 and 700 ^oC. In the absence of hydrogen, SO_2 formation was detected in experiments conducted with CuO sorbent. This result and larger amounts of H_2O formation in the presence of hydrogen showed the the partial reduction of CuO by hydrogen prior to reaction with H_2S. SO_2 formation was detected with Cu-V and Cu-Mo mixed oxide sorbents even in the presence of hydrogen. Additionally, H_2S sorption rate parameters found with Cu-V and Cu-Mo mixed oxide sorbents were found to be smaller than the corresponding values obtained with CuO. Finally, deactivation model was proposed for sorption reactions and this model gave excellent predictions of the H_2S breakthrough curves.

4.2   Manganese-based Sorbents

Zhang et al. (2003) studied a series of MnO-Fe_2O_3 sorbents supported upon γ-Al_2O3 prepared in order to investigate the effects of different molar ratios of Mn:Fe on the performance of Mn-Fe/γ-Al_2O_3 sorbents. Desulfurization was performed in the temperature range of 500-650 ^oC. The regeneration reaction was performed at 700 ^oC. The primary results of the sorbent desulfurization reaction were reported at fixed regeneration conditions.

Garcia et al. (2000) studied Cu and Mn mixed oxides as regenerable sorbents for hot coal gas desulfurization. Taking into account the characterization results of the fresh, reduced, sulfided and regenerated sorbents, the reactivity and performance in multicycle sulfidation-regeneration tests of manganese-based sorbents prepared by using different concentrations of copper oxides were studied. Copper was not stabilized by manganese oxides, but its presence in the fresh sorbent was completely necessary because it increases the sorbent reactivity and keeps the H_2S concentration in the outlet gas from a reactor below 50 ppmv. The gas for sulfidation was composed of H_2S, H_2 and N_2 while regeneration gases were O_2 and N_2.

Abbasian and Slimane (2000) studied with copper, iron, manganese and zinc oxides as bases for developing regenerable sorbents. Only sorbents based on copper oxide have been found to posses the best combination of high attrition resistance and sulfidation reactivity, sulfur removal efficiency, and pre-breakthrough conversion in the moderate temperature 350-550^oC. Encouraging results were also obtained with sorbents based on manganese oxide; however, their regeneration necessitates very high temperatures that cannot be accommodated by current desulfurization systems requiring regeneration ignition

temperatures of approximately 550 °C. No sorbent based on iron was found to have sufficient reactivity in the moderate temperature range.

Turkdogan and Olsson (1978) studied the practical feasibility of using manganese oxide pellets to desulfurize hot reducing gases. The results of this investigation substantiated the practical feasibility of desulfurizing hot reducing gases with manganese oxide pellets in a regenerative cyclic process with SO_2-enriched exhaust gas as a by-product. It was found that MnO-Al_2O_3 pellets were much beter than calcined dolomite in enduring this regenerative cyclic process. The best results were obtained with pellets made from a mixture of 75 parts of finely ground high-grade Comilog ore and 25 parts of alumina powder, sintered in air at 1200 °C. The pellets in a packed bed can be sulfided and regenerated almost completely at relatively high speeds and recycled without loss of reactivity or strength.

The regeneration is done readily by one of several methods of oxidative calcination using air, O_2-SO_2, or CO_2-H_2O-O_2 mixtures. The MnO-Al_2O_3 pellets maintained their reactivity and stregth in this regenerative cyclic process much better than the calcined dolomite.

4.3   Vanadium based Sorbents

Al-Shamma et al. (1989) had studied V_2O_5 / γ–Al_2O_3 in the reaction of H_2S decomposition in the interval of temperatures 500-600 ºC and proposed, that H_2S is consumed in a result of two processes:

- Reaction of H_2S interaction with vanadium oxide, which can be written as

$$5H_2S + V_2O_5 \quad \rightarrow \quad V_2S_3 + 5H_2O + 2S^0 \qquad\qquad \text{(R.4.6)}$$
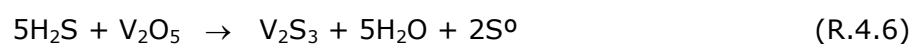
- As the surface of V_2O_5 transforms into V_2S_3, the latter plays the role of a catalyst in the reaction of hydrogen sulfide decomposition and V_2S_3 as an active center takes part in the reaction:

$$V_2S_3 + 5H_2S \rightarrow V_2S_4 + 5H_2 \quad\quad\quad (R.4.7)$$

$$V_2S_4 \rightarrow V_2S_3 + 5S^o \quad\quad\quad (R.4.8)$$

$$H_2S \rightarrow H_2 + S^o \quad\quad\quad (R.4.9)$$
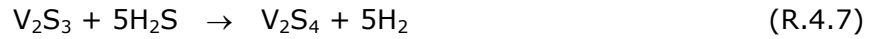
It was shown also, that %5 V_2O_5/$\gamma-Al_2O_3$ exhibits higher catalytic activity, than specially prepared %5 V_2S_3 /$\gamma-Al_2O_3$. For supported vanadia catalyst the authors proposed first order of reaction by hydrogen sulfide concentration and calculated the activation energy as E_a= 33.98 kj/mol.

Flytzani-Stephanopoulos and co-workers (1985) had shown that sorbents formed by supporting a eutectic mixture of ZnO and V_2O_5 on alumina or zirconia exhibited a stable conversion at breakthrough of about 0.65 over five cycles. The pre-breakthrough H_2S levels were always less than 1 ppm. No surface area loss took place, and the zinc was stabilized by vanadium in the alumina support suppressing the evaporative loss of metallic zinc. Although vanadium did not form any bulk vanadium sulfide, it was able to capture up to 0.20 mol H_2S /mol V_2O_5 through chemisorption which is substantially higher than that observed with titanium (0.0014 mol H_2S/mol TiO_2). This capacity, however, is impaired by the presence of high concentrations of H_2O in the coal gas. It was found that H_2O/H_2S ratios up to 10/1 might be allowed before a drastic inhibition of H_2S chemisorption occurs.

The reactions for the $ZnO-V_2O_5$ system may be summarized as follows:

Sulfidation

$$ZnO.V_2O_5 + H_2S + (5-x)H_2 \leftrightarrow ZnS + V_2O_x + (6-x) H_2O \qquad (R.4.10)$$

Chemisorption

$$V_2O_x + H_2S \leftrightarrow V_2O_x.H_2S \qquad (R.4.11)$$

$$3 V_2O_5 + (5-x)H_2S \leftrightarrow 3 V_2O_x + (5-x) SO_2 + (5-x) H_2O \qquad (R.4.12)$$

Regeneration

$$V_2O_x.H_2S \leftrightarrow V_2O_x + (1-y)H_2S + yH_2 + (y/2)S_2 \qquad (R.4.13)$$

$$ZnS + V_2O_x + (3+w-x/2)O_2 \leftrightarrow ZnO.V_2O_5 + wSO_2 \qquad (R.4.14)$$
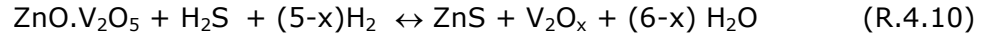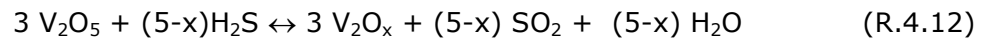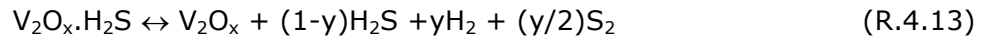
Akyurtlu et al. (1995) investigated the performance of zinc ferrite promoted with V_2O_5 as a hot gas desulfurization sorbent. The sorbents were prepared by the incipient impregnation technique, and the vanadium loading and the calcination temperature were varied. The sorbents were tested in a packed-bed microreactor set-up for five sulfidation-regeneration cycles to investigate their breakthrough behaviour. Sulfidation was performed at 873-973 K with H_2S-H_2-H_2O-N_2 mixtures, while regeneration was carried out at 923-973 K with O_2-N_2 mixtures. The fresh, sulfided, and regenerated sorbents were characterized by atomic absorption spectroscopy, X-ray diffraction, surface area and porosity measurements.

The results of the investigation indicated that the sorbents exhibited a more stable cyclic performance with higher vanadium loading, all vanadium-promoted sorbents reduced the H_2S content of the gas to levels below the equilibrium level for zinc oxide, some H_2S was chemisorbed by vanadium, and two-step calcination imparted structural stability to the sorbents.

4.4   Other Metal Oxide Sorbents

Tamhankar and coworkers (1981) widely investigated ferrite sorbents for H_2S removal efficiency and regenerability. They showed that the high temperature thermochemistry of the iron oxide-H_2S reaction prevents desulfurization at the low partial pressures required for IGCC or fuelcell application.

Flytzani and coworkers (1985) widely investigated zinc sorbents efficiency and regenerability for removal of H_2S at high temperature. They showed that the reaction of H_2S with ZnO was favorable at 500-700 ºC. However, they also proved the formation of elemental zinc because of zinc evaporation during the desulfurization process above 650 ºC, which could lower its reactivity for removal of H_2S.

The behaviour of different mixed oxides, including zinc titanates (ZT) and zinc ferrites modified with CuO (ZFC) or TiO_2 (ZFT), as hot gas desulfurizing sorbents were investigated by Garcia et al. (1997). The sorbents were prepared by calcination at 650ºC. Kinetic studies of the sulfidation reaction were carried out in a thermobalance in the temperature range of 550-650ºC. The study shows that the addition of TiO_2 or CuO to zinc ferrite based sorbents calcined at 650ºC has little effect on the stability against reduction but markedly influences their textural properties. The stabilizing effect of Ti is observed in samples calcined at higher temperature or in non-iron-containing sorbents. The calculated kinetic constants indicate that the Zn content and the incorporation of Cu have an enhancing effect on the kinetics of the sulfidation process. Including H_2 in the feed gas decreases the reactivity and increases the activation energy. Extrudated sorbents showed a good performance as desulfurizing agents and

maintained the H_2S concentration in the outlet gas below 20 ppm. ZT sorbent exhibit a poor efficiency, which makes the addition of Ti questionable.

Tamhankar et al. (1986) investigated several pure and mixed oxides, ZnO, CuO, ZnO-Fe_2O_3, CuO-Fe_2O_3, CuO-Al_2O_3 and CuO-Fe_2O_3-Al_2O_3, as regenerable sorbents for the removal of H_2S at high temperatures. These sorbents had been found to improved performance for hot gas cleanup applications over conventional H_2S sorbents. This is displayed by sharp H_2S breakthrough curves, indicating rapid reaction and diffusion rates and minimal pore plugging, which all result in high absorption capacity, stability and regenerability of sorbents.

Jun et al. (2001) investigated the role of a cobalt additive and proposed sulfidation/regeneration kinetics. For this purpose, the reactivities of Zn-Ti-based sorbents with/without a cobalt additive were studied in a fixed bed reactor over multiple sulfidation/regeneration cycles at high and middle temperature conditions. The composition of mixed gases for sulfidation was H_2S, H_2, CO and CO_2. N_2 gas mixed with oxygen was introduced to regenerate the sulfided sorbents. Compared to conventional ZT based sorbents, cobalt containing zinc titanate sorbents have shown an excellent sulfur removing capacity and no deactivation even after 10 cycles of sulfidation/regeneration in a fixed bed reactor at both high and middle temperatures. Also, the cobalt additive increased the regeneration capacity of Zn-based sorbents because it played an important role as the catalyst for oxidation.

CHAPTER 5

EXPERIMENTAL METHOD

In this study, hot coal gas desulfurization applications were carried out with copper-manganese, copper-vanadium and copper-manganese-vanadium mixed oxide sorbents in a packed bed quartz microreactor over 6 sulfidation/ regeneration cycles.

Experimental section can be divided into three as follows.

- Sorbent Preparation
- Sorbent Characterization
- Multicycle Tests
    - Sulfidation of Sorbent
    - Sorbent Regeneration

5.1   Sorbent Preparation

Several methods are described in the literature for synthesizing highly dispersed mixed oxides. Early attempts to form high surface area metal oxide sorbents by precipitating mixed carbonates from homogeneous salt solutions followed by drying and calcining resulted in materials of low surface area. The bulk sorbents either in single or mixed form were then prepared by a technique

that resulted in high pore volume and surface area. Following a general procedure suggested in the literature (Marcilly et al., 1970), an aqueous solution of metal salts in the desired proportion and an organic polyfunctional acid containing at least one hydroxyl- and at least one carboxylic function is rapidly dehydrated under vacuum at a temperature of 70°C. An amorphous solid foam forms which is calcined at an elevated temperature above 300 ^{o}C, usually 500 ^{o}C to 600 ^{o}C, to form a mixed oxide phase. The crystallized mixed oxides thus formed are homogeneous and highly porous.

The complexation method, originally described by Marcilly et al., (1970), was used to prepare the mixed oxides given below:

- Copper-Manganese-Oxide : Cu-Mn-O
- Copper-Vanadium-Oxide : Cu-V-O
- Copper-Manganese-Vanadium-Oxide : Cu-Mn-V-O

Materials were prepared as dispersed microcrystalline solids with high porosity.

5.1.1 Complexation Method

In this method, equimolar amounts of citric acid (complexation agent) and the salt of the metal were mixed in solution. In the preparation of the mixed metal oxide sorbents, $Cu(NO_3)_2.3H_2O$ (copper nitrate trihydrate), H_4NO_3V (ammonium vandate) and $C_4H_6MnO_4.4H_2O$ (manganese II acetat tetrahydrate) salts were used as source of copper, vanadium and manganese respectively. For these mixed oxide sorbents, equimolar quantities of copper and manganese (or vanadium) were used. The steps of the complexation method are explained below:

First Step : The solution of citric acid and the metal salt was evaporated at 70°C for about 24 h, with continuous stirring until its viscosity had noticeably increased.

Second Step : Dehydration was compleated in an oven at 70 ^{o}C by placing the viscous solution as a thin layer in a glass dish upto a viscous liquid endpoint to form a porous solid foam. Care should be taken in the citrate method to avoid any explosion.

Third Step : The solid foam produced by this procedure was then calcined at 550 ^{o}C for 8 h. After calcinations, the solid was crushed and sieved to the desired size. The crystallized mixed oxides thus formed are homogenous and highly porous.

The sorbent preparation conditions and raw materials used are summarized in Table 5.1. The schematic representation of complexation method is also given in Figure 5.1.

Table 5.1. Sorbent Preparation Conditions

Sorbent	Raw Material	I.Step	II.Step	III.Step
Cu-Mn-O (mol_{Cu} : mol_{Mn} =1)	$Cu(NO_3)_2.3H_2O$, $C_4H_6MnO_4.4H_2O$	65°C, 35 h	70°C, 36 h	550°C, 8 h
Cu-V-O (mol_{Cu} : mol_V =1)	$Cu(NO_3)_2.3H_2O$ H_4NO_3V	65°C, 24 h	70°C, 49 h	550°C, 8 h
Cu-Mn-V-O (mol_{Cu} : mol_{Mn} : mol_V =1)	$Cu(NO_3)_2.3H_2O$, $C_4H_6MnO_4.4H_2O$, H_4NO_3V	65°C, 26 h	70°C, 46 h	550°C, 8 h

1 M Metal Salt + H_2O 1 M $C_6H_8O_7 \cdot H_2O$ + H_2O

Metal Salt Solution

Citric Acid Solution

H_2O CO_2 H_2O CO_2

Q

T=70 °C

(1. Step)
(Heating, Stirring)

Citric acid-Metal ion complex formation

H_2O CO_2 H_2O CO_2

Q

(2.Step)
(Dehydration)

T=70 °C

$MeCO_3$ formation

CO_2 CO_2 CO_2 CO_2

Q

(3.Step)
(Calcination)

T=550 °C

MeO formation
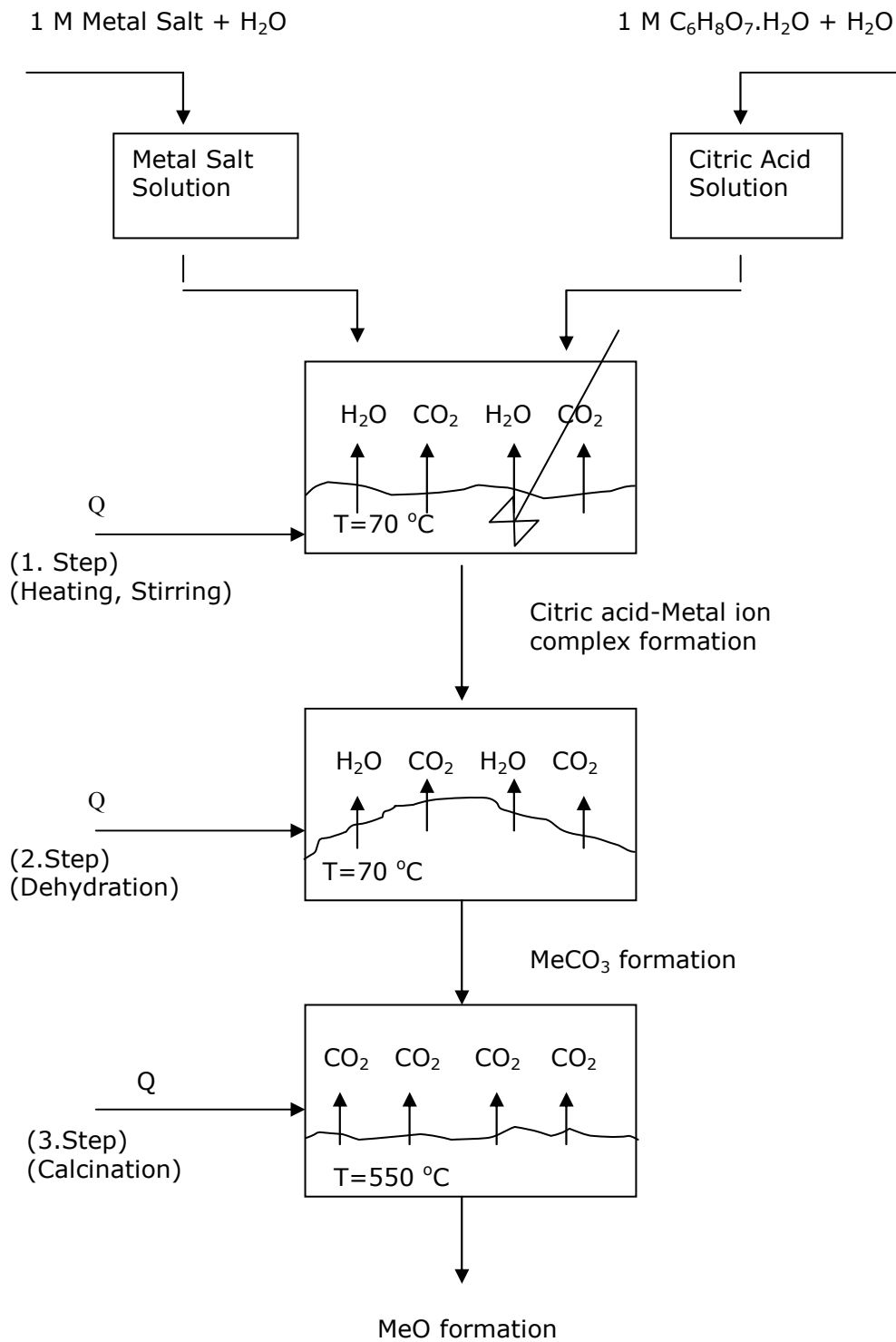
Figure 5.1. Schematic Representation of Complexation Method

(Yasyerli et al., 2001)

5.2   Sorbent Characterization

The complexation method was used to prepare the mixed oxides Cu-Mn-O, Cu-Mn-V-O and Cu-V-O. All these materials were prepared as dispersed microcrystalline solids with high porosity.

Detailed study of caracterization of the prepared sorbents was investigated with the aid of N_2 sorptometry, Hg porosimetry, X-ray difraction and Scanning electron microscopy.

5.2.1 Determination of Surface Area with N_2-Sorptometer

The surface areas were measured in a Quantachrome Monosorb model BET apparatus. The theoretical information about this analysis method is discussed somewhere else (Balcı et al., 1992).

5.2.2 Porosity Analyses with Mercury Porosimetry

Quantachrome Autoscan 60000 psig mercury porosimetry was used to measure pore volumes and obtain the pore size distribution of prepared sorbents.

As stated by Efthimiadis et al. (1992), both methods, N_2 sorptometry and Hg porosimetry, provide structural information about mesopores, where as Hg porosimetry is unreliable in the micropore region and the same is valid for N_2 adsorbtion in the macropore region.

5.2.3 X-Ray Diffraction (XRD) Analysis

The crystalline phases present on the sorbents were determined by Philips PW 1840 X-Ray Diffractometer employing a Cu-Kα radiation source (λ=1.5418) of the Department of Chemical Engineering.

The interplanar distance of the crystal (d) and strength (% I) values were calculated by using Bragg's Law ($n\lambda = 2dSin\theta$). The calculated values were compared with the literature ones given in Appendix E to determine the crystalline phases present on the sorbents.

5.2.4 SEM Analysis

The distribution of the metal oxides on the unreacted sorbent was determined by the application mapping conducted with the Scanning Electron Microscope (SEM) in the Turkish Cement Manufacturers' Assotiation (LEO 435 VP). In other words, scanning electron microscopy (SEM) is used to observe the porous surface of the sorbents.

5.3 Multicycle Tests

From the practical point of view, the Cu-Mn-O, Cu-Mn-V-O and Cu-V-O sorbents should possess regenerability in cyclic operation. This was shown to be good in microreactor tests. In this work, to determine the sorbent regenerability, six cycles of consecutive sulfidation-regeneration were performed with prepared sorbents. The reactor was purged for 30 min by N_2 after each sulfidation and regeneration experiments. Exit compositions of H_2S and SO_2 were evaluated with breakthrough curves.

5.3.1 Sulfidation of Sorbent

In this study, sorption experiments were carried out with copper-manganese, copper-vanadium and copper-manganese-vanadium mixed oxide sorbents in a packed bed quartz microreactor. Sorption experiments were carried out in the presence of the reducing gas hydrogen. Experiments were carried out at 627 ^{o}C using a gas mixture composed of 1 vol % H_2S and 10 vol % H_2 in

helium for about 80 min The total flow rate of the gas mixture (100 ml/min-measured at 25°C) and the gas composition were kept constant in most of the experiments. The schematic representation and photographs of the experimental setup was given in Figure 5.2 and Figure 5.3 respectively. The system constitutes from the following main parts:

- Tubular furnace,
- Packed bed quartz microreactor,
- Computer interface with FTIR,
- Computer interface with GC,
- Gas cylinders and rotameters,
- Energy supply.

An FTIR spectrometer and a gas chromatography equipped with a thermal conductivity detector (TCD) connected to the exit stream of the reactor allowed for an on-line chemical analysis of H_2S, SO_2 and H_2O. The column used in the analysis was a 1/8 in. Stainless Steel tube packed with Propak T. Preparation and testing of Porapak-T gas chromatograph adsorption column is given in Appendix D. FTIR calibration graphs for H_2S, SO_2 and H_2O gases are given in Figure A.1, A.2 and Figure B.1 respectively. GC calibration graph for H_2S is also given in Appendix C. Typical IR absorption bands of FTIR spectrometer observed at 1050 and 1232 cm^{-1} indicate the presence of SO_2. Multiple bands observed between 1414 and 1972 cm^{-1} correspond to H_2O and the bands observed between 2614 and 2772 cm^{-1} correspond to H_2S. H_2S also gives IR bands between 3398 and 4039 cm^{-1}, but these absorption bands coincide with the bands of H_2O. Additional chemical analysis of the solid product obtained after the sulfidation/regeneration cycle experiments allowed the sulfur balance around the reactor to be verified. For this purpose, a Leco SC 132 sulfur analyzer was used.
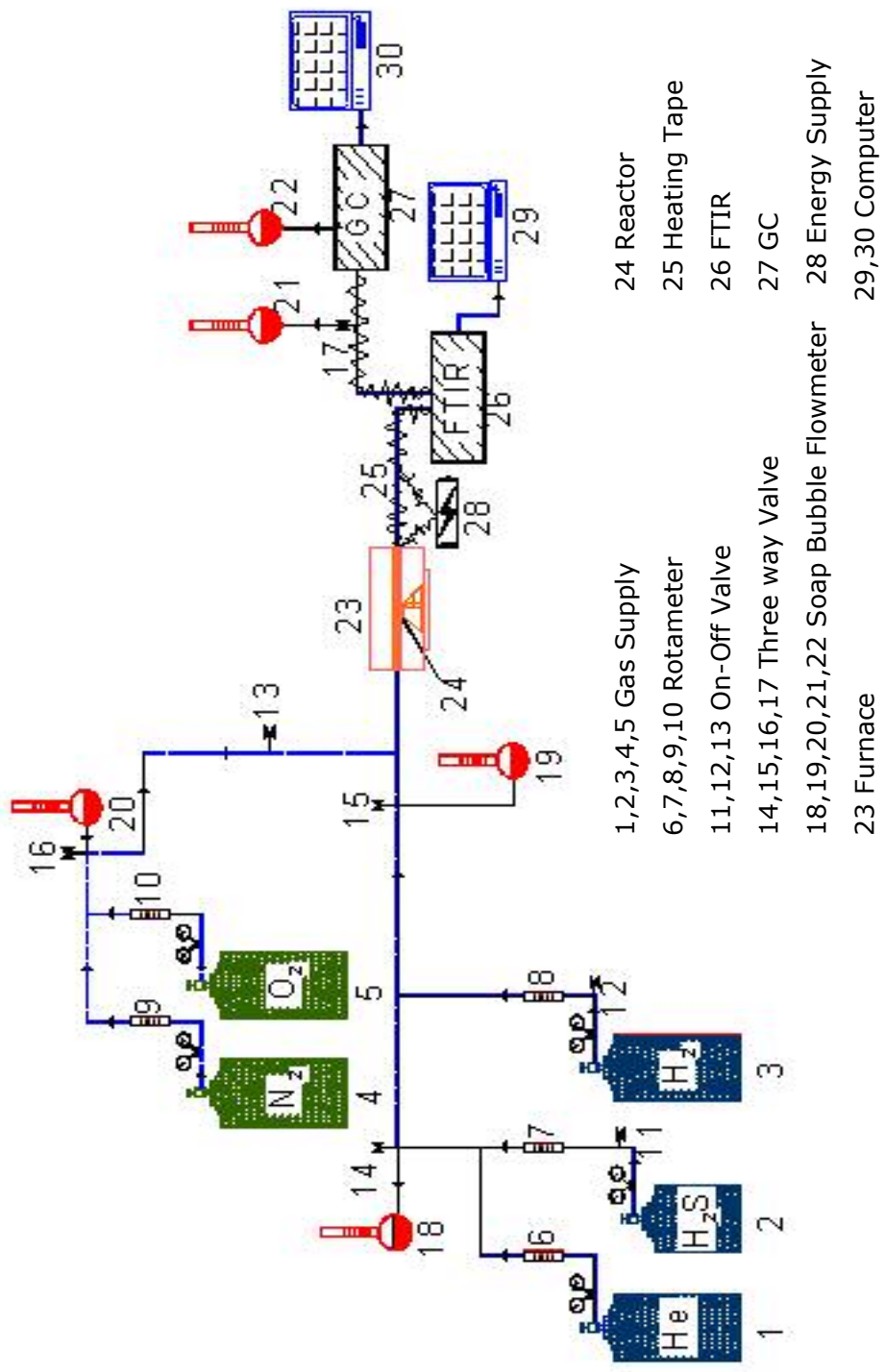
Figure 5.2. Schematic Representation of Sorbent Sulfidation/Regeneration Experimental Setup

1,2,3,4,5 Gas Supply   24 Reactor

6,7,8,9,10 Rotameter   25 Heating Tape

11,12,13 On-Off Valve   26 FTIR

14,15,16,17 Three way Valve   27 GC

18,19,20,21,22 Soap Bubble Flowmeter   28 Energy Supply

23 Furnace   29,30 Computer

47

(a)

Figure 5.3. Photographs of The Experimental Setup, (a), (b), (c)

(b)

(c)

Figure 5.3. (continued)

In all experiments, 0.2 g of sorbent was placed into a 0.6-cm-diameter quartz reactor. Sorbent particles were supported by quartz wool from both sides. The quartz reactor was placed into a tubular furnace equipped with a temperature controller which was used to set the temperature of the furnace. All the piping, joints and valves between the flowmeter and the reactor were made of stainless steel to prevent corrosion due to H_2S. For this reason, all the connections from H_2S cylinder to the flowmeter were chosen specially stainless steel to prevent corrosion. Other tubings were made of copper or plastic. The length of the packed sorbent section of the bed was in the range of 0.8-1.5 cm for different sorbents. No temperature profiles were observed within this section. All of the flow lines between the reactor, FT-IR spectrometer and Gas Chromatograph were heated to eliminate any condensation. Three-way valves placed before and after the reactor allowed for flow of the gas mixture through the bypass line during flow rate adjustments. Composition of the inlet stream was also checked by the analysis of the stream flowing through the bypass line, at the start of the experiments.

5.3.2 Sorbent Regeneration

The regeneration experiments were also performed in the same packed-bed microreactor set-up on sulfided samples. Sulfided solids were purged in nitrogen for about 30 min and then regenerated with a 6 % O_2 and balance N_2 mixture for about 30 min at 700 ^{o}C. The total flow rate of the gas mixture (100 ml/min-measured at 25°C) and the gas composition were kept constant in most of the experiments. The exit gas from regeneration runs was analysed for H_2S and SO_2 by FTIR. The standard regeneration procedure was conducted as follows.

After the sulfidation experiment, the reactor temperature was raised to 700°C under flowing nitrogen to desorb any H_2S chemisorbed on the sorbent; this procedure was terminated when the H_2S concentrations in the off-gas fell to about zero. Then, the regeneration gas was switched to the (6% O_2 + 94% N_2) mixture at 700° C. The regeneration gas was continued until the SO_2 content of the off-gas was reduced to approximately zero; the oxygen was then turned off. The sorbent was treated with nitrogen at 700 °C to dissociate any sulfate that might have been formed on the sorbent. This procedure was continued until the SO_2 content of the off-gas reduced to about zero.

Selected samples of the regenerated sorbents were characterized structurally and chemically by the methods cited in Sorbent Characterization.

CHAPTER 6

DEACTIVATION MODEL FOR BREAKTHROUGH ANALYSIS

Sorption experiments were carried out with copper-manganese, copper-vanadium and copper-manganese-vanadium mixed oxide sorbents in a packed bed quartz microreactor. Experimental results were evaluated with breakthrough curves obtained for exit composition of H_2S data taken with time. The deactivation rate constant, k_d, and the initial sorption rate constant, k_o, were calculated by using deactivation model.

The formation of a dense product layer over the solid reactant creates an additional diffusion resistance and is expected to cause a drop in the reaction rate. It also causes significant changes in the pore structure, active surface area and activity per unit area of solid reactant with reaction extent. All of these changes cause a decrease of activity of the solid reactant with time. For such gas-solid reactions the deactivation model works well. In this model, the effects of all of these factors on the diminishing rate of sulfur fixation were combined in a deactivation rate term. The schematic representation of reaction between gas-solid was shown in Figure 6.1 (Yasyerli et al., 2001).
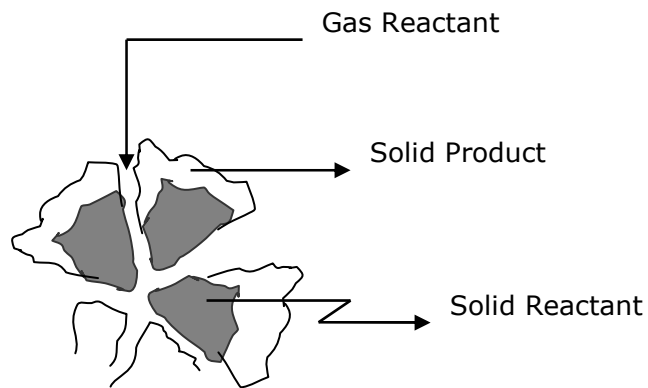
Figure 6.1. Schematic drawing of the sorbent

Factors effecting the observed rate in gas-solid noncatalytic reactions can be summarized as below.

- Pore diffusion resistance,

- Product layer diffusion resistance,

- Pore mouth closure,

- Active surface area variations,

- Porosity and pore size distribution variations.

The schematic illustration of packed bed reactor is presented in Figure 6.2 where Q, C_{Ao} and C_A are total volumetric flow rate, inlet and outlet concentration of H_2S respectively (Yasyerli et al., 2001).
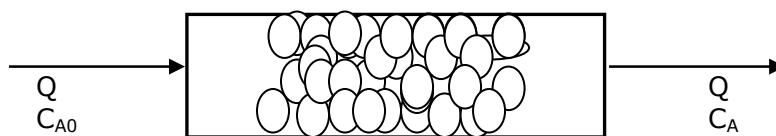
Figure 6.2. Schematic representation of packed bed reactor.

With the pseudo-steady-state assumption the isothermal species conservation equation for the reactant gas H_2S in the packed column is

$$-Q\frac{dC_A}{dW} - k_o C_A a = 0 \qquad \text{(E.6.1)}$$

In this equation, axial dispersion in the packed column and any mass transfer resistances were assumed to be negligible.

According to the proposed deactivation model the rate of change of the activity of the solid reactant (a) was expressed as

$$-\frac{da}{dt} = k_d C_A^n a^m \qquad \text{(E.6.2)}$$

where k_d is the deactivation rate constant.

6.1   The Zeroth Solution of The Deactivation Model

The zeroth solution of the deactivation model is obtained by taking n=0, m=1 and the initial activity of the solid as unity. The solution steps are as follows (Yasyerli and Doğu, 2001).

$$-\frac{da}{dt} = k_d \; C_A^0 \; a \qquad \text{(E.6.3)}$$

By the assumption of $C_A = C_{A0}$,

$$a = \exp\left[-k_d C_A^0 t\right] \qquad \text{(E.6.4)}$$

By defining $k_d' = k_d \; C_A^0$, the change of activity with time is given in Eqn.6.5.

$$a = \exp\left[-k_d' t\right] \qquad \text{(E.6.5)}$$

We can write Eqn.6.5 into Eqn.6.1 to obtain Eqn.6.6.

$$-Q\frac{dC_A}{dW} - k_0 C_A \exp\left[-k_d' t\right] = 0 \qquad \text{(E.6.6)}$$

The zeroth solution of the deactivation model (Eqn. 6.7) is obtained by integrating Eqn.6.6 from $C_{A,0}$ to C_A for concentration and 0 to W for weight.

$$\frac{C_A}{C_{A,0}} = \exp\left[-\frac{k_0 W}{Q}\exp(-k_d' t)\right] \qquad \text{(E.6.7)}$$

This solution is equivalent to the breakthrough equation proposed by Suyadal et al. (2000) and assumes a fluid phase concentration that is independent of deactivation on processes along the reactor.

Realistically, the deactivation rate is expected to be concentration dependent and accordingly, axial-position-dependent in the packed bed.

6.2   First Correction for Deactivation Model

To obtain analytical solutions of Eqns. 6.1 and 6.2 by taking n=m=1, an iterative procedure is applied (Yasyerli and Doğu, 2001)

The conservation Eqn. for the reactant gas H_2S in packed column is

$$-Q\frac{dC_A}{dW} - k_0 C_A a = 0 \qquad \text{(E.6.1)}$$

and the rate of change of activity of the solid reactant is

$$-\frac{da}{dt} = k_d C_A^n a^m \qquad \text{(E.6.2)}$$

By taking n=m=1, Eqn. 6.8 for deactivation rate is obtained.

$$-\frac{da}{dt} = k_d C_A a$$

(E.6.8)

The zeroth solution (Eqn. 6.7) was substituted into Eqn. 6.8 and first correction for the activity is obtained (Eqn.6.18) by the integration of this equation.

$$-\frac{da}{dt} = k_d a C_{A0} \exp[-\frac{k_0 W}{Q} \exp(k_d' t)]$$

(E.6.9)

$$-\int_1^0 \frac{da}{a} = \int_0^t \{k_d C_{A0} \exp[-\frac{k_0 W}{Q} \exp(-k_d' t)]\} dt$$

(E.6.10)

$$u = \exp[-\frac{k_0 W}{Q} \exp(-k_d' t)]$$

(E.6.11)

$$udt = \frac{du}{[\frac{k_0 W}{Q} k_d' \exp(-k_d' t)]}$$

(E.6.12)

$$-\ln a = k_d C_{A0} \int_0^1 udt$$

(E.6.13)

Eqn.6.14 is obtained by solving Eqn.6.11 and Eqn.6.13 together.

$$\ln a = \int \frac{du}{\ln u} = \ln(\ln u) + \ln u + \frac{(\ln u)^2}{4} + \ldots\ldots$$

(E.6.14)

By taking the first two term of the Eqn.6.14 the corrected activity (a)

expression is obtained.

$$a = \exp(-k'_d t) \exp\left[\frac{k_0 W}{Q}(1 - \exp(-k'_d t))\right] \qquad \text{(E.6.15)}$$

Then, the corrected activity (a) expression was substituted into Eqn.6.1 and integration of this equation gave the first corrected solution for the breakthrough curve.

$$-Q\frac{dC_A}{dW} = k_0 C_A \exp(-k'_d t) \exp\left[\frac{k_0 W}{Q}(1 - \exp(-k'_d t))\right] \qquad \text{(E.6.16)}$$

$$-\int_{C_{A0}}^{C_A} \frac{dC_A}{C_A} = \int_0^W \frac{k_0}{Q} \exp(-k'_d t) \exp\left[\frac{k_0 W}{Q}(1 - \exp(-k'_d t))\right] dW \qquad \text{(E.6.17)}$$

$$\frac{C_A}{C_{A0}} = \exp\left[\frac{[1 - \exp(\frac{k_0 W}{Q}(1 - \exp(-k_d t)))]}{[1 - \exp(-k_d t)]} \exp(-k_d t)\right] \qquad \text{(E.6.18)}$$

This iterative procedure can be repeated for further improvement of the solution. In this procedure, higher order terms in the series solutions of the integrals were neglected .

The breakthrough equation derived above (Eqn.6.18) was applied for the nonlinear regression analysis of the experimental breakthrough data obtained for H_2S sorption on sorbent. Then, rate parameters were calculated from the breakthrough data.

CHAPTER 7

RESULTS AND DISCUSSION

In this study, copper based sorbents, Cu-Mn-O, Cu-Mn-V-O and Cu-V-O, were developed using complexation method and the performance of prepared sorbents were investigated in a fixed-bed quartz microreactor over six sulfidation/regeneration cycles. In addition, detailed study of caracterization of the fresh sorbents was investigated with the aid of Hg porosimetry, N_2 sorptometry, X-ray diffraction, and Scanning electron microscopy. The change of crystallographic form of regenerated Cu-Mn-O and Cu-Mn-V-O sorbents from the sixth cycle were followed by the powder X-ray diffraction method. Additionally, deactivation model was used for the prediction of breakthrough curves of H_2S in a fixed–bed reactor to confirm the experimental data and to calculate the rate parameters for each cycle. Experimental results were divided into two as given below.

- Sorbent Preparation and Characterization
- Multicycle Tests
    - Sorption of H_2S on Sorbents
    - Regeneration of Sorbents

7.1   Sorbent Preparation and Characterization

The complexation method was used to prepare the mixed oxides, Cu-Mn-O, Cu-Mn-V-O and Cu-V-O. All these sorbents were prepared as dispersed microcrystalline solids with high porosity.

7.1.1 Identification of The Crystalline Phases in Sorbents

The crystalline phases present on the fresh sorbents were determined by Philips PW 1840 X-Ray Diffractometer employing a Cu-Kα radiation source (λ=1.5418) of the Department of Chemical Engineering.

The interplanar distance of the crystal (d) and strength (% I) values were calculated by using Bragg's Law ($n\lambda$ = 2dSinθ). The comparison of calculated XRD data with literature values are given in Table E.1 and Table E.2 for Cu-V-O and Cu-Mn-O sorbents respectively.

The crystalline phases identified by XRD in the fresh sorbents are shown in Table 7.1.

Table 7.1. Crystalline Phases identified by XRD in Fresh Sorbents

Sorbent	XRD Identification
Cu-Mn-O	$CuMn_2O_4$,$Cu_{1.5}Mn_{1.5}O_4$,CuO and an amorphous phase
Cu-Mn-V-O	An amorphous phase
Cu-V-O	β-$Cu_2V_2O_7$

XRD patterns obtained showed that the crystal structures of the Cu-Mn-O sorbent are consistent with $Cu_{1.5}Mn_{1.5}O_4$, $CuMn_2O_4$, CuO and an amorphous phase. The Cu-Mn-V-O sorbent consists of an amorphous phase while β-$Cu_2V_2O_7$ is the only detected phase in the Cu-V-O sorbent.

The XRD patterns of the fresh sorbents Cu-Mn-O, Cu-Mn-V-O and Cu-V-O are shown in Figure 7.1 (a), (b), and (c) and also in Figure K.1 (a), (b), (c) respectively.
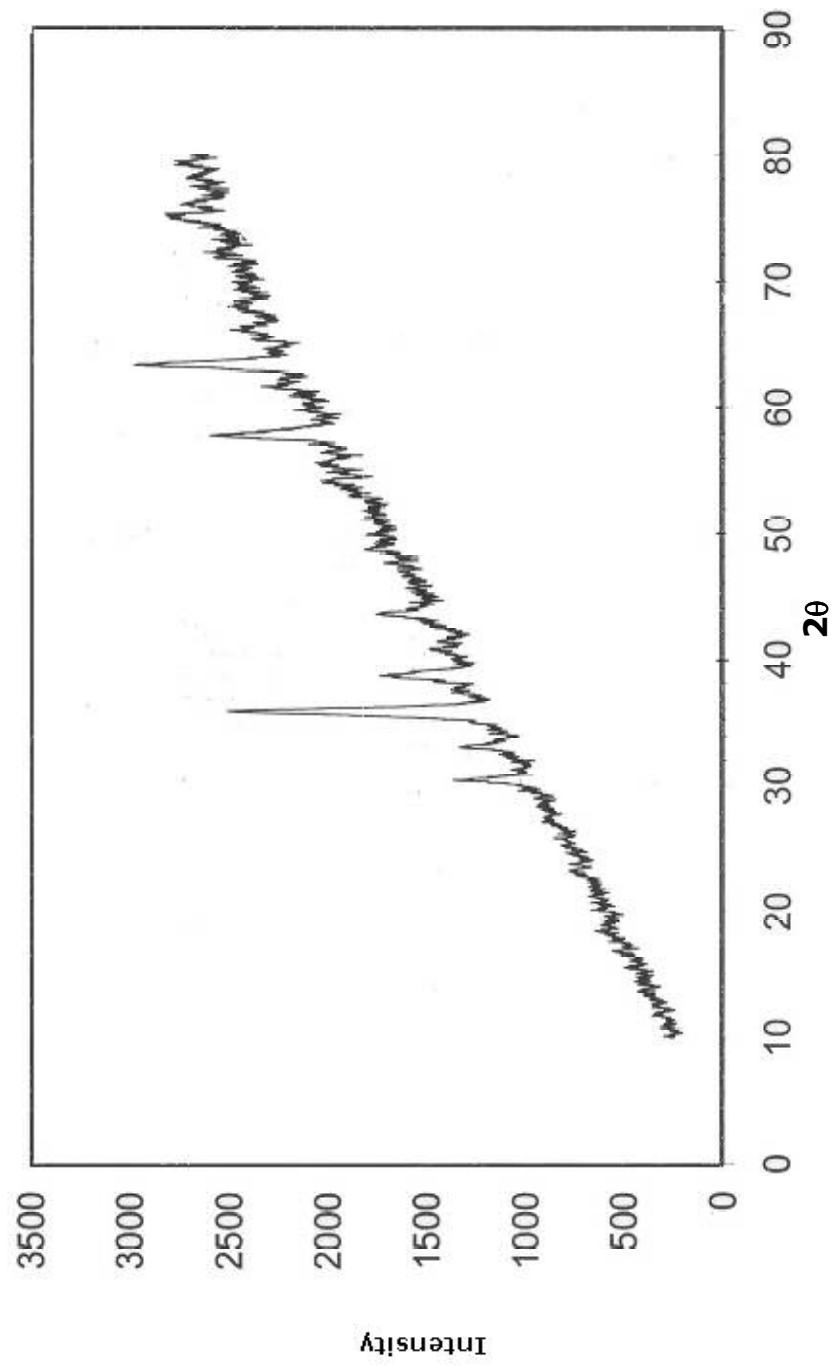
(a) Cu-Mn-O

Figure 7.1. XRD Patterns of the fresh sorbents (a) Cu-Mn-O, (b) Cu-Mn-V-O, (c) Cu-V-O
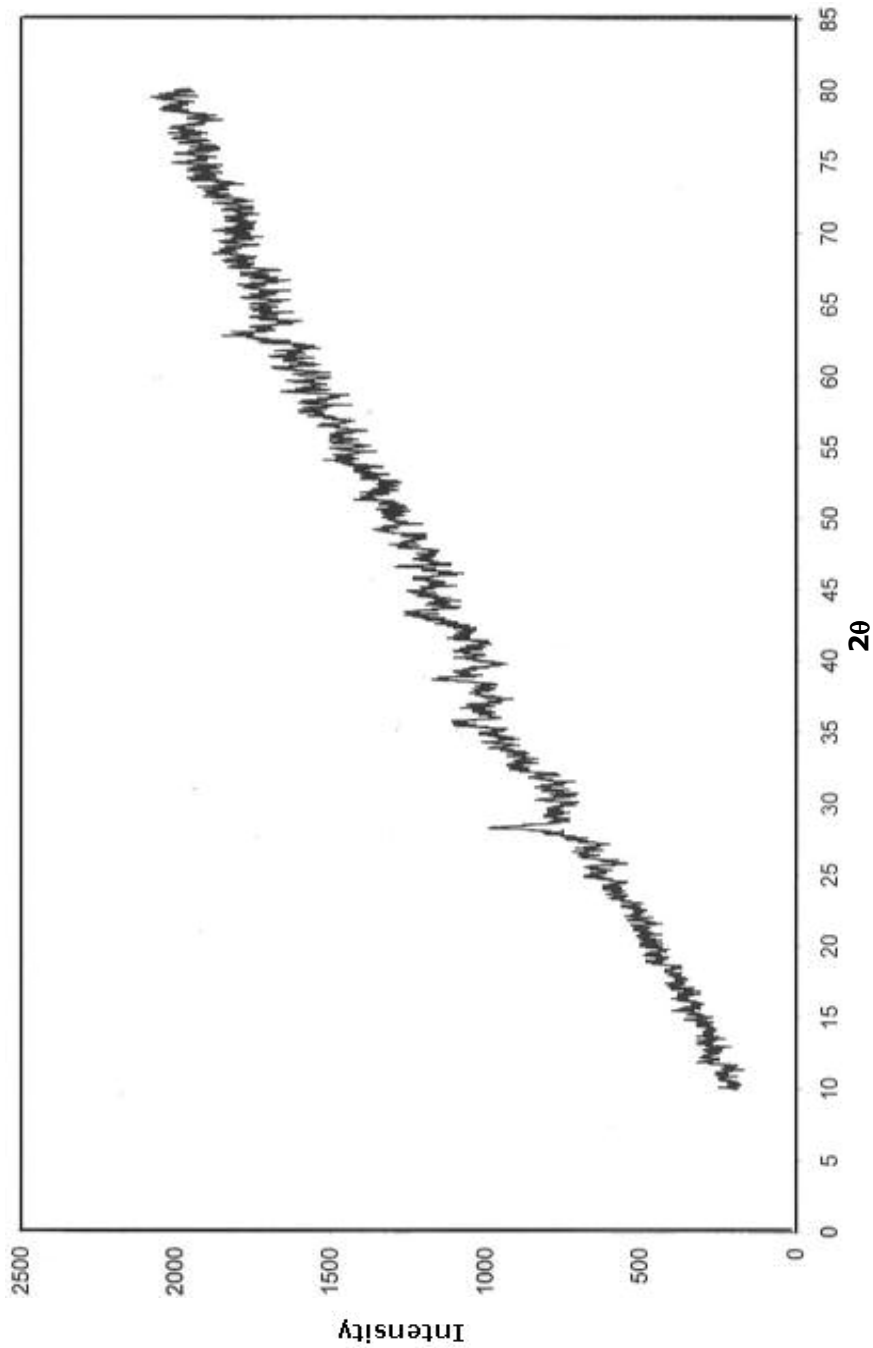
(b) Cu-Mn-V-O

Figure 7.1. (continued)
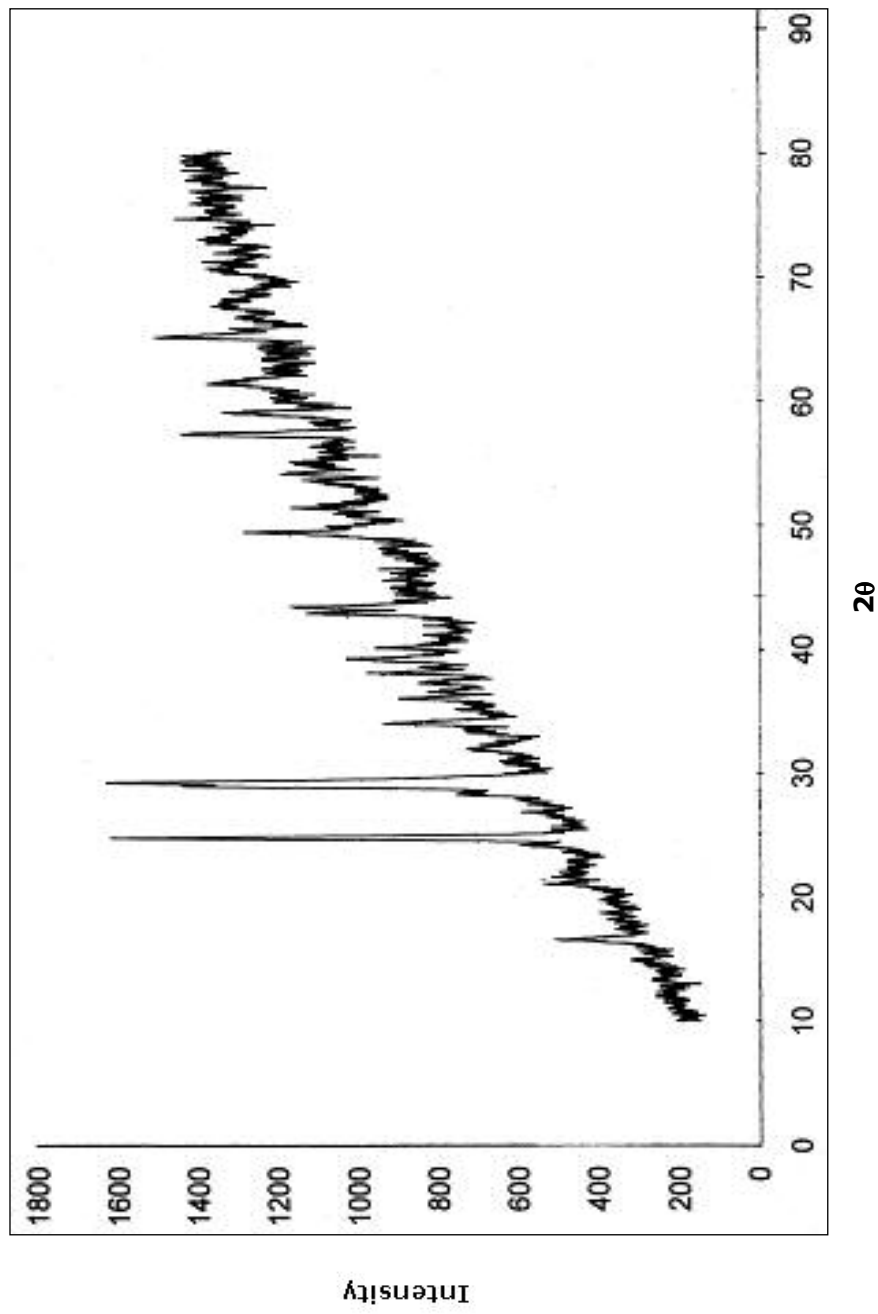
(b) Cu-V-O

Figure 7.1. (continued)

7.1.2 Physical Properties of Sorbents

As mentioned above, a chemical and structural characterization of the sorbents used in this study were investigated with the aid of Hg porosimetry, N_2 sorptometry, and Scanning electron microscopy. Table 7.2 lists the physical characteristics of the fresh sorbents prepared in this work. The values of average pore radius were evaluated from Pore volume vs. Radius data obtained from mercury porosimetry. The original Hg porosimetry data and calculated average pore radius values are given in Appendix F.

Table 7.2. Physical Properties of Fresh Sorbents Used in Sulfidation Experiments

Sorbents	BET Surface Area (m^2/g)	Hg Porosimetry Surface Area (m^2/g)	Porosity	Average Pore Radius (nm)
Cu-Mn-O	45	9	0.77	814
Cu-V-O	44	16	0.51	698
Cu-Mn-V-O	57	30	0.70	399

The difference between BET surface area and Hg Porosimeter surface area values of fresh metal oxide sorbents can be explained by the formation of micro pore structure. As can be seen from Table 7.2, BET surface area values are higher than Hg porosimetry surface area values that indicates the existing of micropore structure in sorbents. As stated by Efthimiadis et al. (1992), both methods provide structural information about mesopores, where as Hg porosimetry is unreliable in the micropore region and the same is valid for N_2 adsorbtion in the macropore region.

The surface areas were measured in a Quantachrome Monosorb model BET apparatus. N_2-sorptometer experimental data and BET surface area calculation of sorbents are given in Appendix G.

Quantachrome Autoscan 60000 psig mercury porosimetry was used to measure pore volumes and obtain the pore size distribution of prepared sorbents. According to results of the Hg porosimetry, pore radius versus Surface Area graphics of the sorbents were obtained. These graphics are given in Appendix F.

The distribution of the metal oxides on the unreacted sorbent was determined by the application mapping conducted with the Scanning Electron Microscope (SEM) in the Turkish Cement Manufacturers' Assotiation (LEO 435 VP). In other words, scanning electron microscopy (SEM) is used to observe the porous surface of the sorbents. SEM micrographs of the fresh metal oxide sorbents Cu-Mn-O, Cu-Mn-V-O and Cu-V-O are given in Figure 7.2 (a), (b), and (c) respectively.
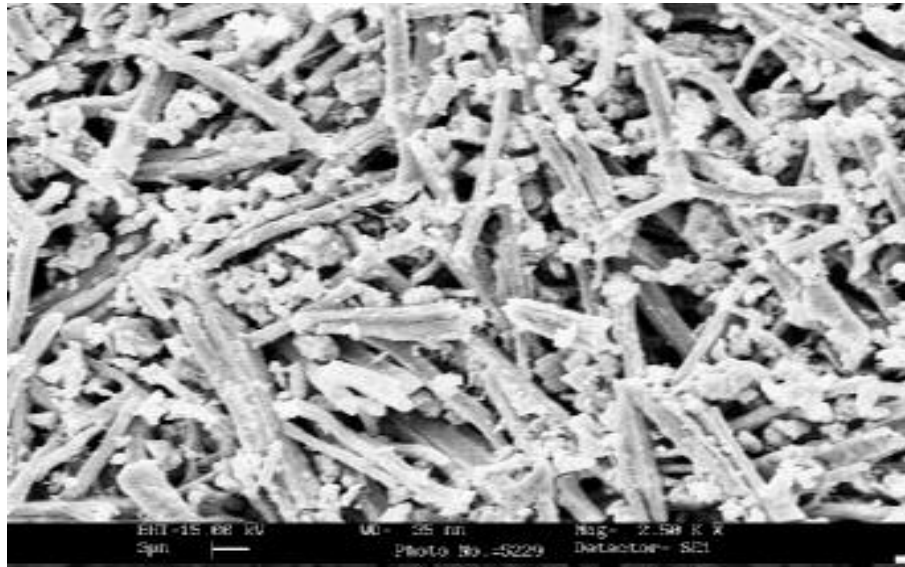
(a1) (Enlarge x 5000)
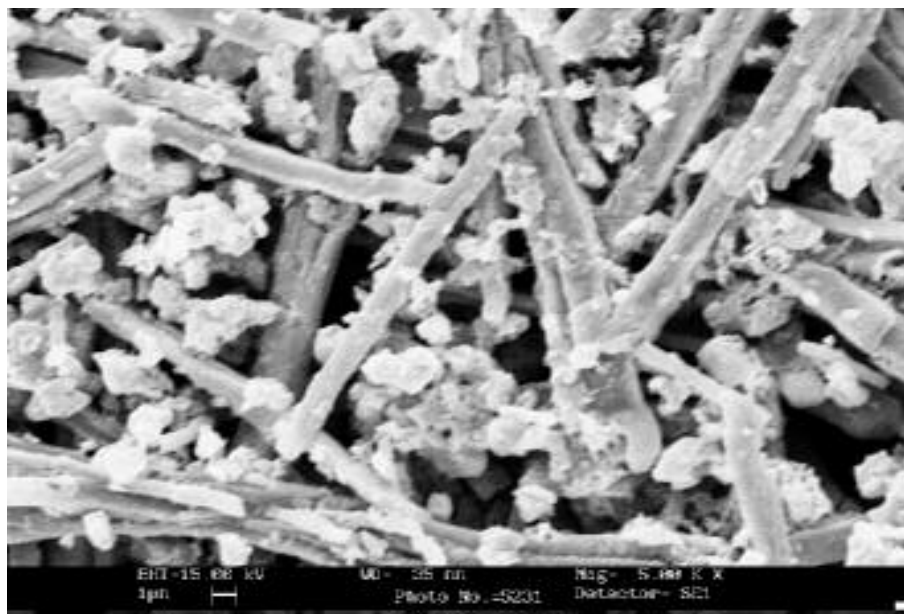
(a2) (Enlarge x 10000)

(a) Cu-Mn-O

Figure 7.2. SEM micrographs of the fresh metal oxide sorbents

(a) Cu-Mn-O, (b)Cu-Mn-V-O, (c) Cu-V-O
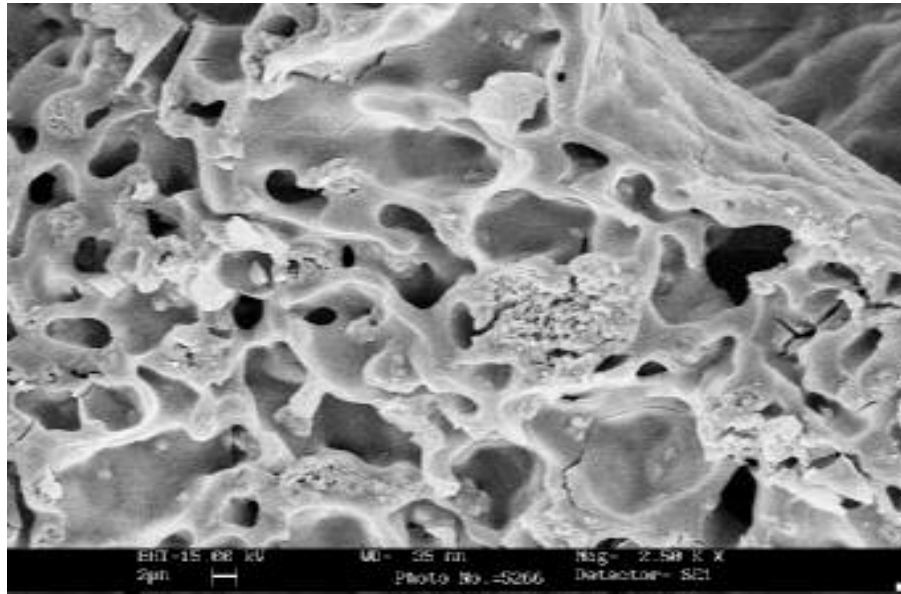
(b1) (Enlarge x 5000)
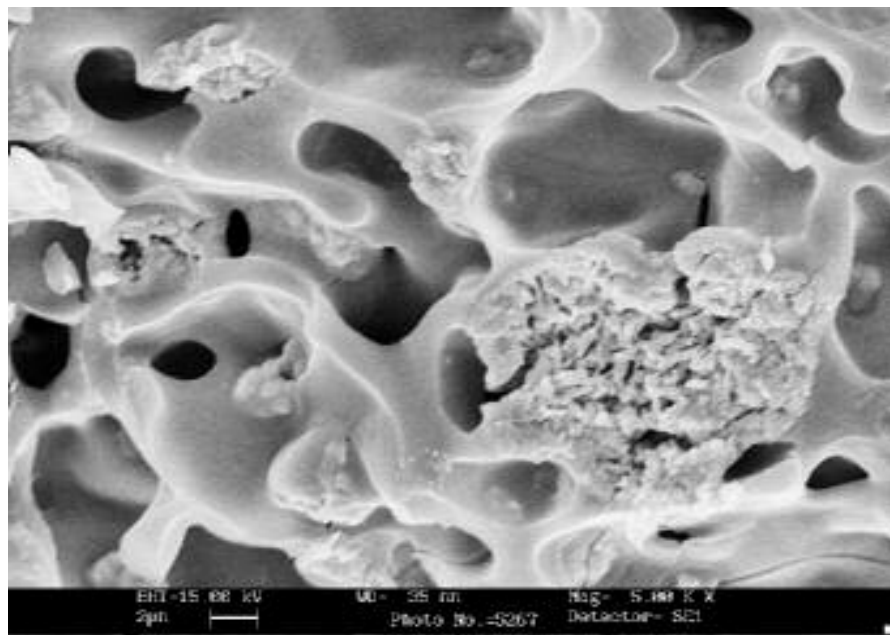
(**b2) (Enlarge x 10000)**

(b) Cu-Mn-V-O

Figure 7.2. (continued)
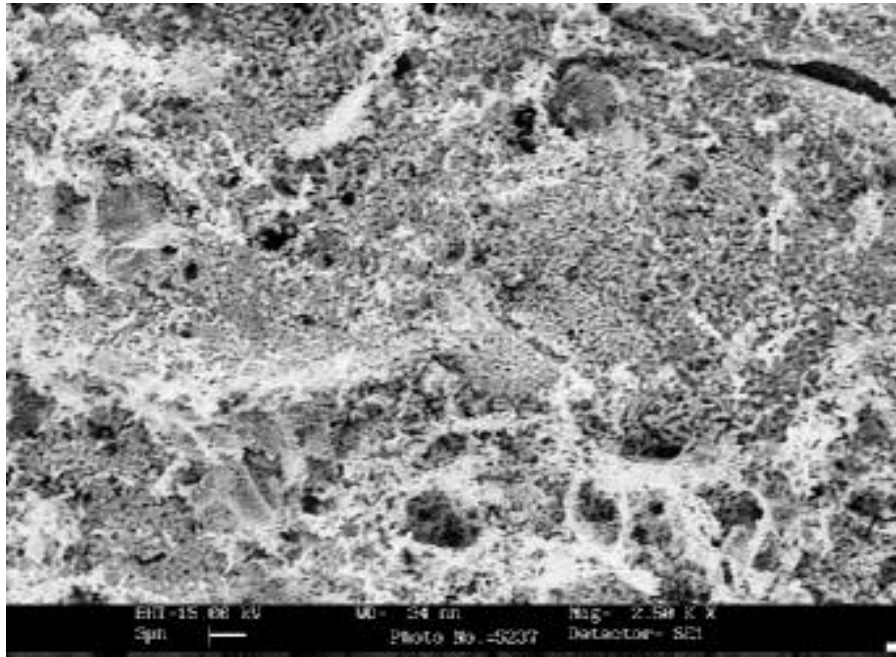
(c1) (Enlarge x 5000)
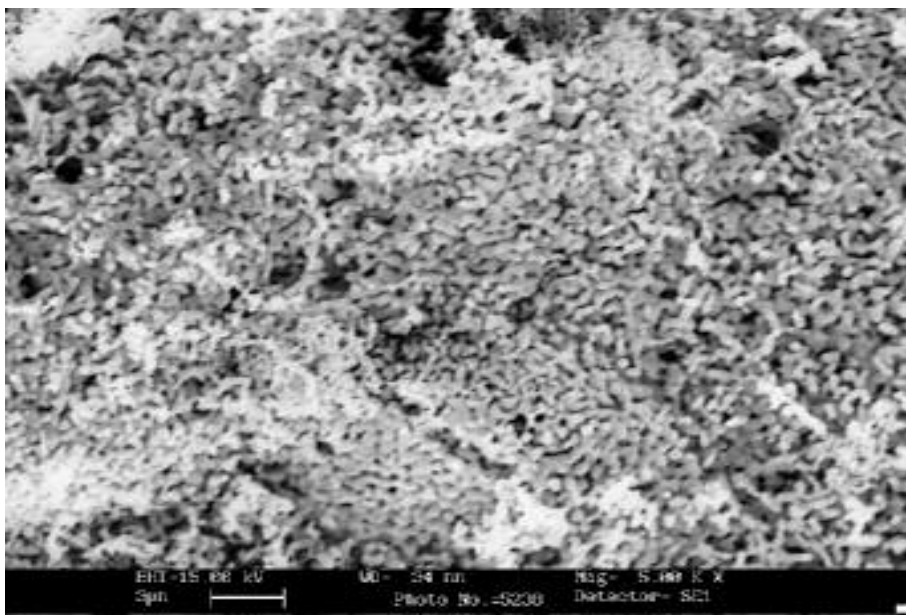
(c2) (Enlarge x 10000)

(c) Cu-V-O

Figure 7.2. (continued)

7.2   Multicycle Tests

In this work, to determine the sorbent regenerability, six cycles of consecutive sulfidation-regeneration tests were performed with Cu-Mn-O, Cu-Mn-V-O and Cu-V-O sorbents in a packed bed quartz microreactor .

The performance of sorbents were studied with 0.2 g of sorbent at atmospheric pressure. Sulfidation was carried out with a gas mixture containing (vol) %1 H_2S - %10 H_2 in balance He for about 80 min at 627 ^{o}C. Sulfided solids were purged in nitrogen for about 30 min and then regenerated with a %6 O_2 – N_2 mixture for about 40 min at 700 ^{o}C. Exit compositions of H_2S and SO_2 were evaluated with breakthrough curves. The total flow rate of the gas mixture (100 ml/min) and the gas mixture composition were kept constant in most of the experiments.

7.3   Sorption of H_2S on Cu-Mn-O in the Presence of Hydrogen

H_2S sorption experiment with fresh Cu-Mn-O sorbent (experiment name: CM1) was performed in a packed bed quartz microreactor with a gas mixture containing %1 H_2S and %10 H_2 in balance He for about 80 min at 627 ^{o}C. To confirm the experimental results of CM1 and to test the reliability of experimental setup before keeping on 6 cycles of consecutive sulfidation-regeneration tests, sorption experiment with the same fresh Cu-Mn-O sorbent (experiment name: CM2) was performed again.

Results of the sulfidation experiments are given in Table 7.3 and Figure 7.3. As it was shown in Table 7.3 and Figure 7.3, experimental results of CM2 consistent with experimental results of CM1. Also, standat error bars within ±

0.05 region for two experiments can be seen from Figure 7.3. By this way, the reliability of the experimental setup was also tested, and then six cycles of consecutive sulfidation-regeneration tests were continued with sulfided Cu-Mn-O sorbent (CM1).

Table 7.3 Results of sulfidation experiments carried out with the same fresh Cu-Mn-O sorbent (T=627 ^{o}C; %1 H_2S + %10 H_2 in balanced He)

Fresh Sorbent / Experiment Name	Q (ml/min)	$H_2S_{adsorbed}$ x10^3 (mol)	g S_{ads} / g Sorbent	$SO_{2formed}$ (mol)
Cu-Mn-O / CM1	91	0.95	0.152	0
Cu-Mn-O / CM2	91	0.97	0.155	0
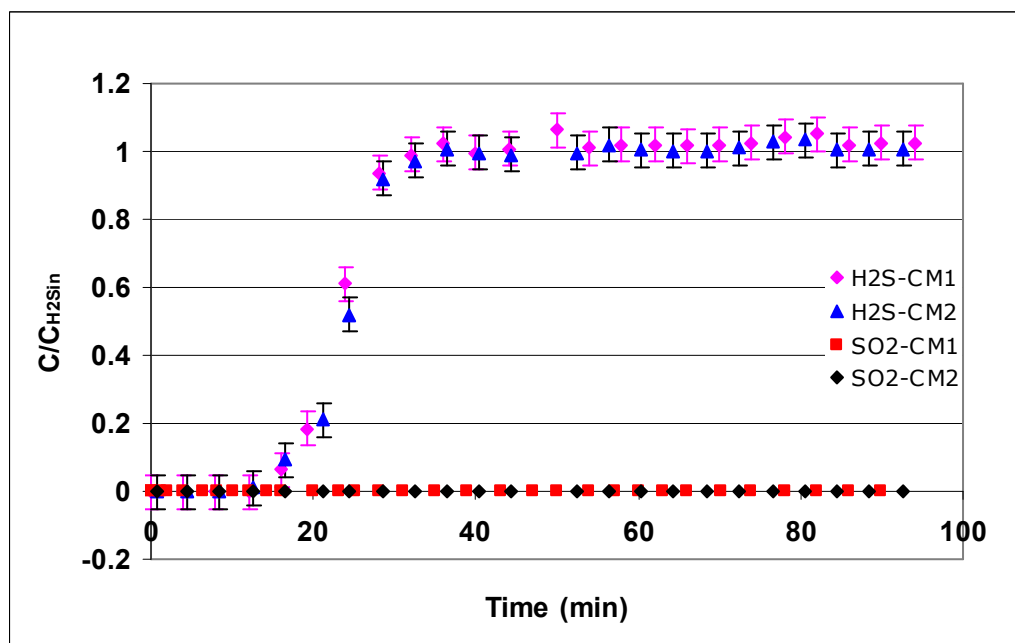
Figure 7.3 Exit compositions of H_2S and SO_2 in sulfidation experiments, CM1 and CM2, carried out with same fresh Cu-Mn-O sorbent (T=627 ^{o}C; %1 H_2S + %10 H_2 in balanced He)

Six cycles of consecutive sulfidation-regeneration tests were continued with sulfided Cu-Mn-O sorbent (CM1). As a result of material balance for sulfur around reactor, results for each sulfidation are given in Table 7.4. Because of experimental error in the fourth sulfidation of Cu-Mn-O sorbent, the graph of the fourth H_2S breakthrough curve and sulfidation results are given in Appendix I. Additionally, it must be noted that in sorption experiments carried out with Cu-Mn-O sorbent, SO_2 formation was not observed.

Table 7.4. Experimental results from the six sulfidation cycles carried out with Cu-Mn-O sorbent (T=627 ^{o}C; t≈80 min; %1 H_2S + %10 H_2 in balanced He)

Sulfidation No	Q (ml/min)	$H_2S_{adsorbed}$ x10^3 (mol)	g S_{ads} / g Sorbent
1	91	0.95	0.152
2	90	0.92	0.147
3	88	0.90	0.144
5	91	0.88	0.141
6	89	0.80	0.128

Table 7.4. (continued)

Sulfidation No	% H_2S	H_2S_{in} (mol)x10^3	H_2S_{out} (mol)x10^3	$H_2S_{adsorbed}$ (mol)x10^3
1	1.20	3.24	2.29	0.95
2	1.20	3.20	2.28	0.92
3	1.20	3.13	2.23	0.90
5	1.20	3.24	2.36	0.88
6	1.25	3.30	2.50	0.80

The most significant result in multicycle tests was that the Cu-Mn-O sorbent efficiency didn't change much as the number of cycles increases. As it was seen in Table 7.4, the sulfur retention capacity of the Cu-Mn-O sorbent decreased slightly from 0.152 to 0.128 (g of sulfur)/(g of sorbent) during 6 sulfidation/regeneration cycles.

The results from the six sulfidation cycles typically obtained with the developed Cu-Mn-O sorbent are also shown in Figure 7.4. The results indicated that the Cu-Mn-O sorbent prepared in this study removed sulfur without apparent performance decay during 6 sulfidation/regeneration cycles.
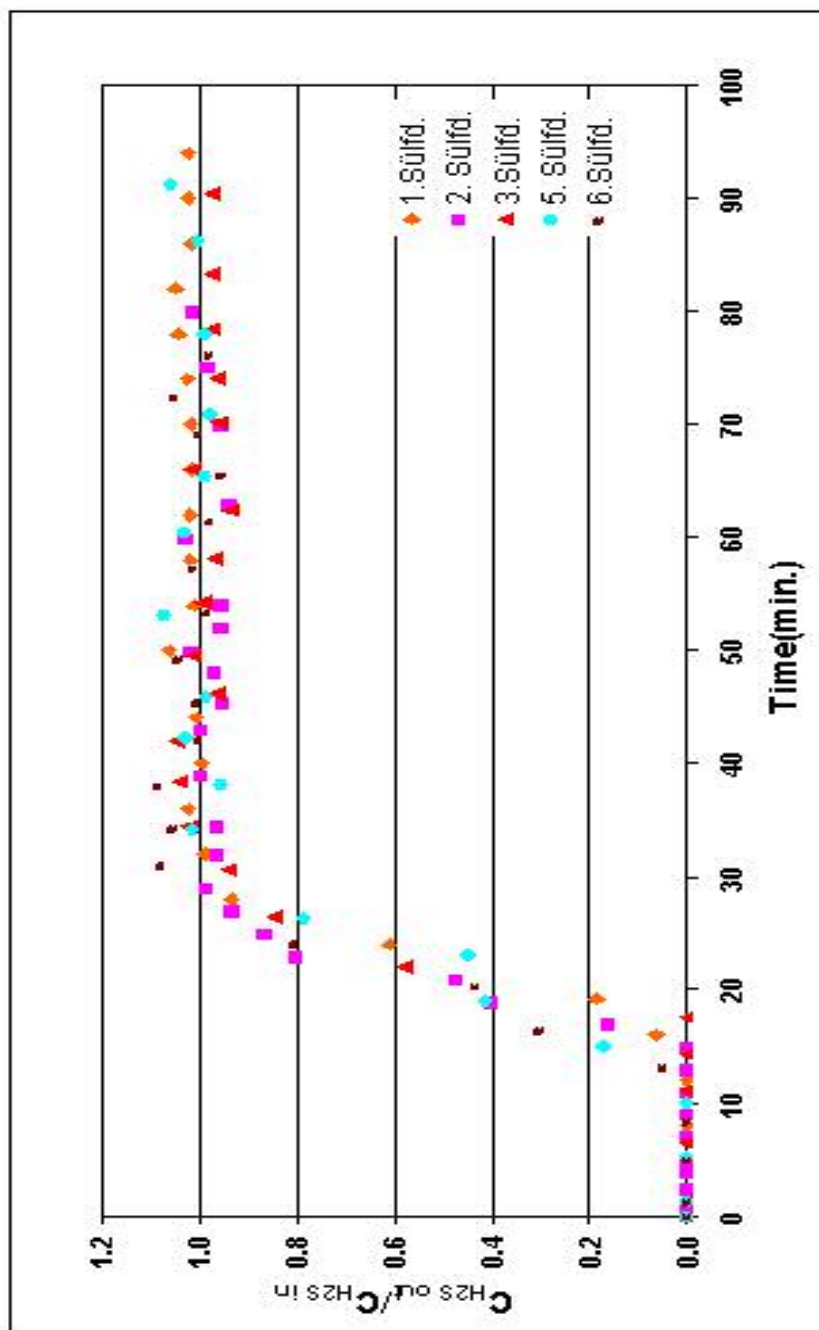
Figure 7.4. Exit compositions of H_2S in packed bed sorption experiments carried out with Cu-Mn-O sorbent in the presence of H_2 (T= 627 °C; 1% H_2S + 10% H_2 in He)

7.3.1 Application of Deactivation Model to Sulfidation Experiment Results of Cu-Mn-O

The results of the regression analysis of the data obtained with the Cu-Mn-O sorbent are given in Table 7.5. Mathematica 5.0 was used to calculate rate parameters and G^2 values that term goes to zero to minimize an error. Because of an experimental error in the fourth sulfidation of Cu-Mn-O sorbent, rate parameters obtained from the fourth sulfidation breakthrough data are given in Table I.3.

Table 7.5. Rate Parameters Obtained from the Breakthrough Data for Cu-Mn-O Using Eqn.6.18 (W=0.2 g; T=627 ^{o}C; 1 % H_2S + 10 % H_2 in He)

Sulfidation No	Q (ml/min)	k_oW/Q	$k_d(min^{-1})$ x10^2	$k_o(ml/g.min)$ x10^{-2}	G^2
1	91	6.35	91	88	0.0219
2	90	6.12	97	85	0.0332
3	88	7.71	112	103	0.0216
5	91	3.59	54	48	0.0479
6	89	4.51	72	60	0.0554

The results showed in Table 7.5 indicated that as the number of cycles increases, the Cu-Mn-O sorbent efficiency didn't change much. As said before, the Cu-Mn-O sorbent prepared in this study removed sulfur effectively during cycling. The predicted breakthrough curves for the six sulfidation experiments were also given in Figure 7.5 and Figure 7.6. As shown in figures, regression analysis of the experimental breakthrough data obtained for H_2S sorption on Cu-Mn-O gave very good agreement with the breakthrough equation derived.
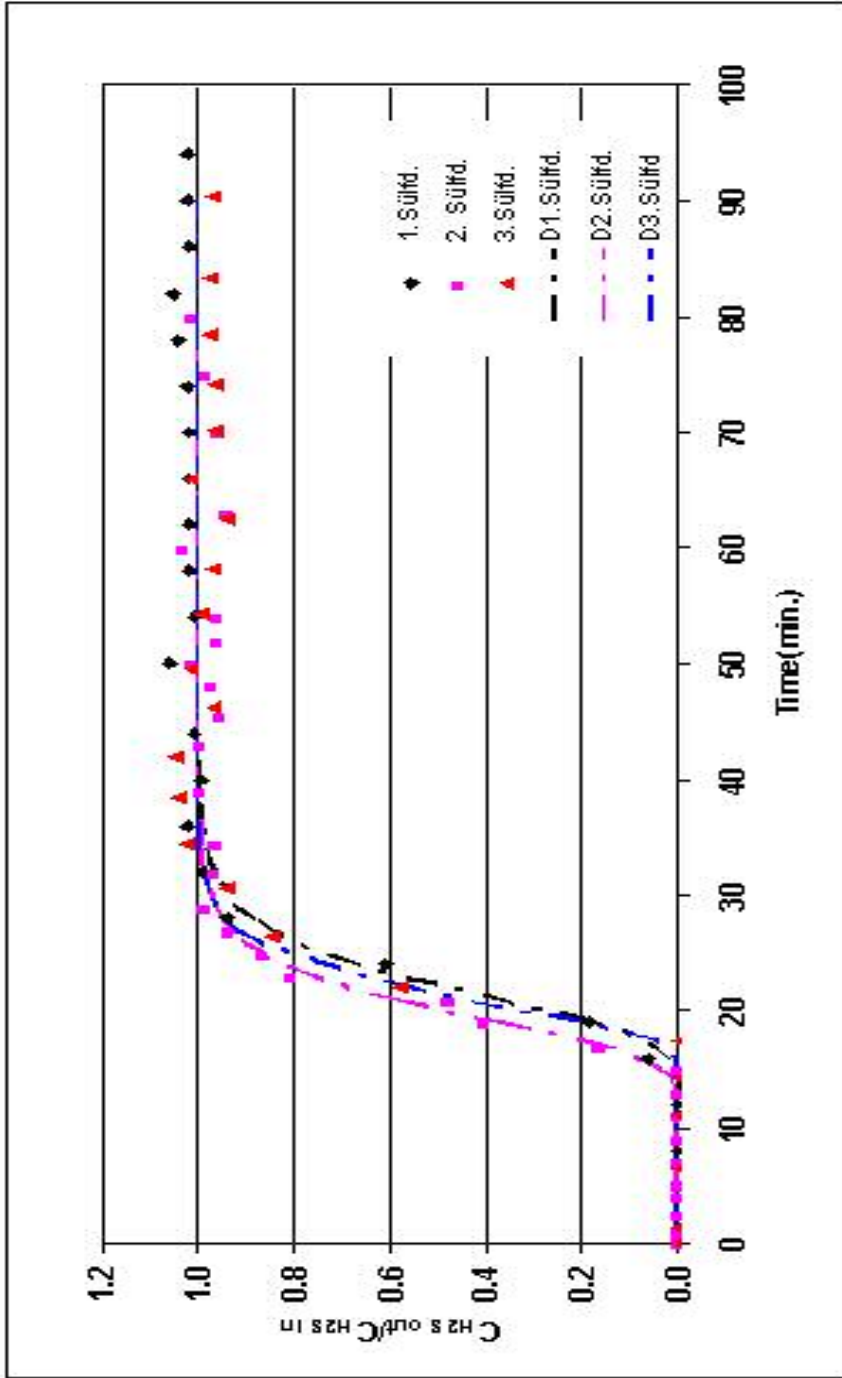
Figure 7.5. Breakthrough curves for H$_2$S using Cu-Mn-O sorbent at 627 °C.

The lines correspond to deactivation model predictions
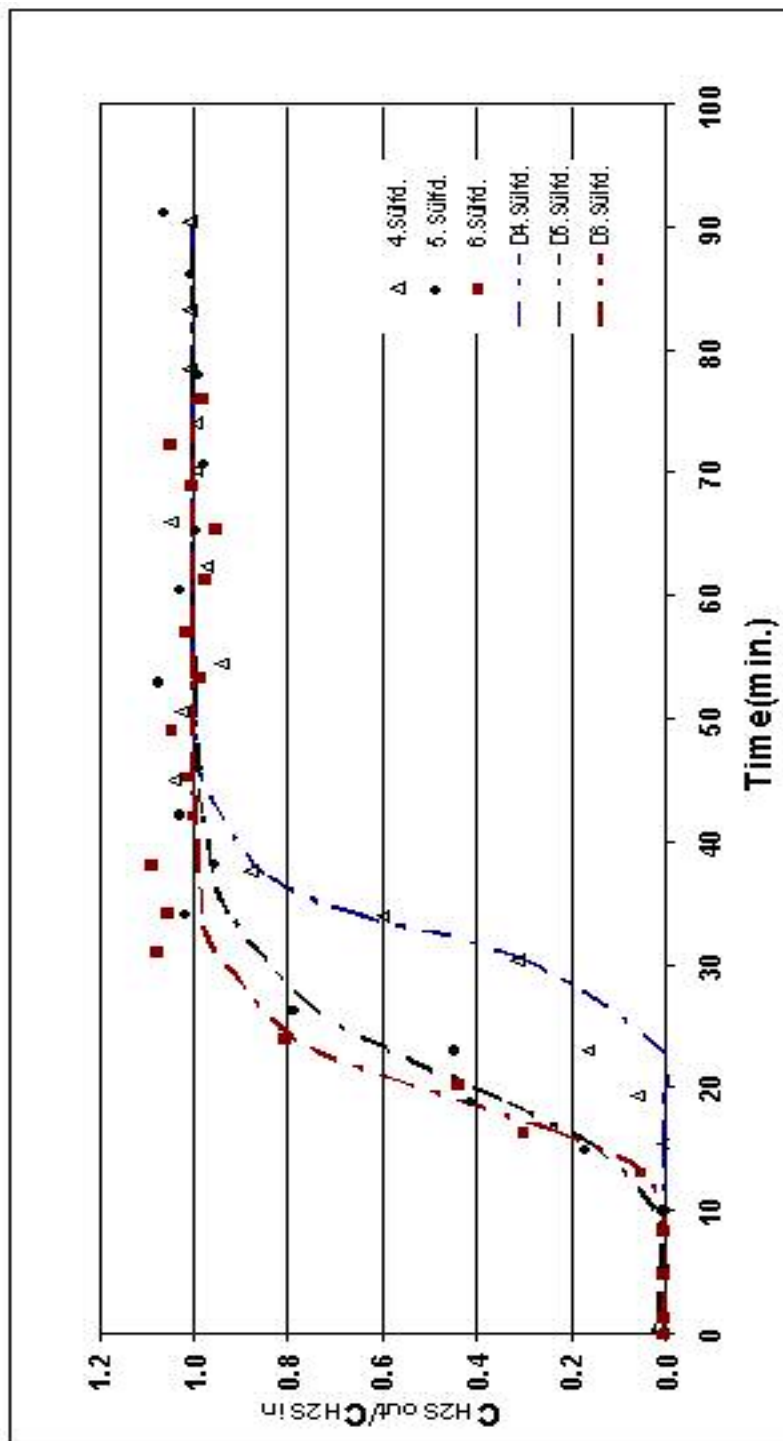
Figure 7.6. Breakthrough curves for H_2S using Cu-Mn-O sorbent at 627 °C. The lines correspond to deactivation model predictions

7.3.2 Reaction Mechanism of H$_2$S Sorption with Cu-Mn-O Sorbent in the Presence of Hydrogen

As has also been mentioned in the literature (Patrick et al., 1989), CuO was expected to be reduced in the presence of hydrogen. The reduction of CuO can go all the way to metallic copper or to Cu$_2$O before reaction with H$_2$S. The following reaction sequences are possible (Yasyerli et al., 2001)

Case 1

$$2CuO + 2H_2 \rightarrow 2Cu + 2H_2O \qquad\qquad (R.7.1)$$

$$\underline{2Cu + H_2S \rightarrow Cu_2S + H_2} \qquad\qquad (R.7.2)$$

$$2CuO + H_2S + H_2 \rightarrow Cu_2S + 2H_2O \qquad\qquad (R.7.3)$$

Case 2

$$2CuO + H_2 \rightarrow Cu_2O + H_2O \qquad\qquad (R.7.4)$$

$$\underline{Cu_2O + H_2S \rightarrow Cu_2S + H_2O} \qquad\qquad (R.7.5)$$

$$2CuO + H_2S + H_2 \rightarrow Cu_2S + 2H_2O \qquad\qquad (R.7.3)$$

with calculated reaction entalpies, gibbs free energy of reactions and reaction equilibrium constants, at 627 ^{o}C listed in Table 7.6 (based on thermodynamic values given in Barrin and Knacke, 1979). The overall reaction is the same for both cases.

Since CuMn$_2$O$_4$ has a crystalline structure distinct from CuO it must be inquired about the relevance of R.7.3 in the thermodynamics and kinetics of sulfidation of the CuMn$_2$O$_4$. The reactions that are thermodynamically feasible during contact with the sulfiding gas (1% H$_2$S, 10% H$_2$ in balance He) include following reactions with calculated reaction entalpies, gibbs free energy of

reactions and equilibrium constants, at 627 °C listed in Table 7.6 (Barrin and Knacke, 1979).

$$3CuMn_2O_4 + H_2 \rightarrow 3CuO + 2Mn_3O_4 + H_2O \qquad \text{(R.7.6)}$$

$$2\ CuMn_2O_4 + 5H_2S + 3H_2 \rightarrow Cu_2S + 4MnS + 8H_2O \qquad \text{(R.7.7)}$$

$$2CuO + H_2S + H_2 \rightarrow Cu_2S + 2H_2O \qquad \text{(R.7.3)}$$

$$2Mn_3O_4 + 3H_2S + H_2 \rightarrow 3MnS + 4H_2O \qquad \text{(R.7.8)}$$
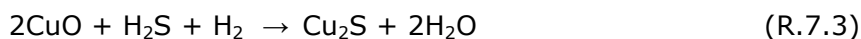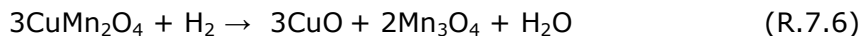
Reactions 7.6, 7.7 and 7.3 take place simultaneously, in view of the presence of unreacted $CuMn_2O_4$ along with the intermediate product Mn_3O_4 and the final products Cu_2S and MnS in sulfided Cu-Mn-O sorbent. The XRD patterns at the end of the sixth sulfidation/regeneration cycle (Figure 7.21) also indicated that the solid product in the presence of hydrogen was essentially $MnSO_4$, $Cu_{1.96}S$, Mn_3O_4.

Table 7.6. Sulfidation reaction enthalpies, Gibbs free energy of reactions and reaction equilibrium constants of Cu-Mn-O sorbent

Reaction	T=627 °C		
	ΔH_r (kj/mol)	ΔG_r (kj/mol)	log K
R.7.1	-190.650	-246.710	14.320
R.7.2	-40.058	-55.435	3.218
R.7.3	-230.708	-302.145	17.538
R.7.4	-111.783	-151.275	8.781
R.7.5	-118.925	-150.870	8.757
R.7.8	-168.332	-237.113	13.764

7.4   Sorption of H$_2$S on Cu-Mn-V-O in the Presence of Hydrogen

H$_2$S sorption experiment with fresh Cu-Mn-V-O sorbent (experiment name: CMV1) was performed in a packed bed quartz microreactor with a gas mixture containing %1 H$_2$S and %10 H$_2$ in balance He for about 80 min at 627°C. To confirm the experimental results of CMV1 and to test the reliability of experimental setup before keeping on 6 cycles of consecutive sulfidation-regeneration tests, sorption experiment with the same fresh Cu-Mn-O sorbent (experiment name: CM2) was performed again.

Results of the sulfidation experiments are given in Table 7.7 and Figure 7.7. As it was shown in Table 7.7 and Figure 7.7, experimental results of CMV2 consistent with the experimental results of CMV1. Error bars for experiments were also drawn in ±0.05 error region. By this way, the reliability of the experimental setup was also tested, and then six cycles of consecutive sulfidation-regeneration tests were continued with sulfided Cu-Mn-V-O sorbent (CMV1).

Table 7.7. Results of sulfidation experiments carried out with the same fresh Cu-Mn-V-O sorbent (T=627 $^{\circ}$C; %1 H$_2$S + %10 H$_2$ in balanced He)

Fresh Sorbent / Experiment Name	Q (ml/min)	H$_2$S$_{adsorbed}$ x10^3 (mol)	g S$_{ads}$ / g Sorbent	SO$_{2formed}$ (mol)
Cu-Mn-V-O / CMV1	92	0.68	0.110	0
Cu-Mn-V-O / CMV2	91	0.65	0.104	0
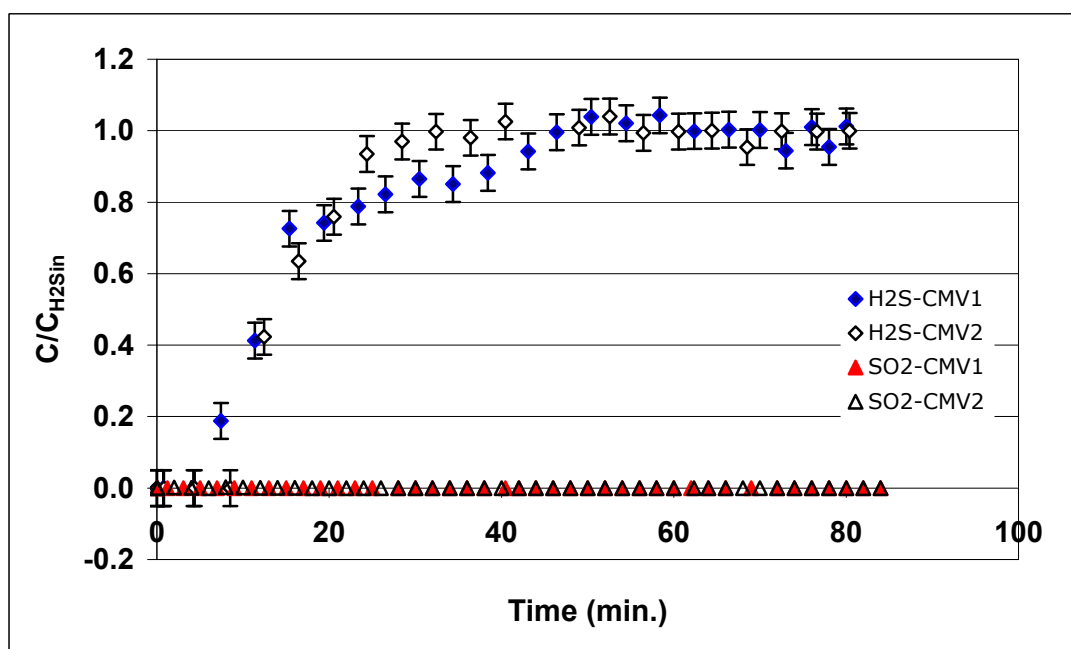
Figure 7.7. Exit compositions of H_2S and SO_2 in sulfidation experiments, CMV1 and CMV2, carried out with same fresh Cu-Mn-V-O sorbent (T=627 ^{o}C; %1 H_2S + %10 H_2 in balanced He)

Six cycles of consecutive sulfidation-regeneration tests were continued with sulfided Cu-Mn-V-O sorbent (CMV1). As a result of material balance for sulfur around reactor, results for each sulfidation are given in Table 7.8. Additionally, it must be noted that in sorption experiments carried out with Cu-Mn-V-O sorbent, SO_2 formation was not observed.

Table 7.8. Experimental results from the six sulfidation cycles carried out with Cu-Mn-V-O sorbent (T=627 $^{\circ}$C; ; t≈80 min; %1 H_2S + %10 H_2 in balanced He)

Sulfidation No	Q (ml/min)	$H_2S_{adsorbed}$ x10^3 (mol)	g S_{ads} / g Sorbent
1	92	0.68	0.110
2	93	0.54	0.086
3	90	0.45	0.072
4	87	0.42	0.067
5	88	0.36	0.058
6	91	0.34	0.054

Table 7.8. (continued)

Sulfidation No	% H_2S	H_2S_{in} (mol)x10^3	H_2S_{out} (mol)x10^3	$H_2S_{adsorbed}$ (mol)x10^3
1	1.20	3.28	2.60	0.68
2	1.20	3.31	2.77	0.54
3	1.24	3.31	2.86	0.45
4	1.22	3.15	2.73	0.42
5	1.13	2.95	2.59	0.36
6	1.15	3.11	2.77	0.34

As it was seen in Table 7.8, the sulfur retention capacity of the Cu-Mn-V-O sorbent decreased slightly from 0.110 to 0.054 (g of sulfur)/(g of sorbent) during 6 sulfidation/regeneration cycles. The results indicated that some loss of Cu-Mn-V-O sorbent efficiency was observed in cycles. Consequently, by increasing the number of cycles, the sorbent efficiency decreases because

porosity also decreases as a consequence of repetitive chemical and thermal stresses.

The results from the six sulfidation cycles typically obtained with the developed Cu-Mn-V-O sorbent are also shown in Figure 7.8. As the number of cycle increases breakthrough curves for Cu-Mn-V-O sorbent shifted left slightly.
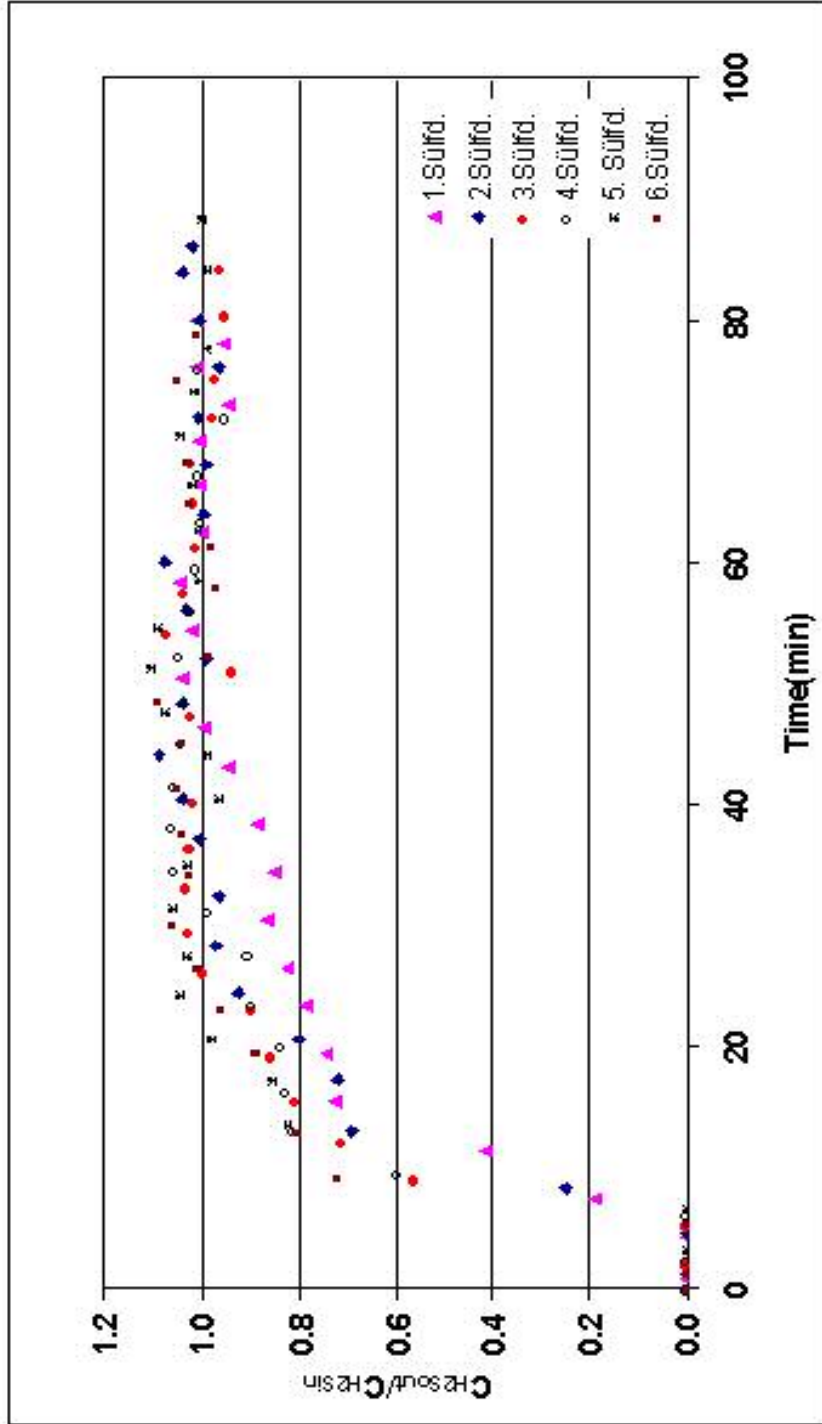
Figure 7.8. Exit compositions of H_2S in packed bed sorption experiments carried out with Cu-Mn-V-O sorbent in the presence of H_2 (T= 627 °C; 1% H_2S + 10% H_2 in He)

7.4.1 Application of Deactivation Model to Sulfidation Experiment Results of Cu-Mn-V-O

The results of the regression analysis of the data obtained with the Cu-Mn-V-O sorbent are given in Table 7.9.

Table 7.9. Rate Parameters Obtained from the Breakthrough Data for Cu-Mn-V-O Using Eqn. 6.18 (W=0.2 g; T=627 ^{o}C; 1 % H_2S + 10 % H_2 in He)

Sulfidation No	Q (ml/min)	k_oW/Q	$k_d(min^{-1})$ $x10^2$	$k_o(ml/g.min)$ $x10^{-2}$	G^2
1	92	2.43	57	33	0.1197
2	93	3.48	88	48	0.0950
3	90	2.98	100	39	0.1197
4	87	3.67	127	48	0.1197
5	88	4.34	132	57	0.1196
6	91	4.43	172	60	0.1197

The results indicated that deactivation rate constant increases as the sulfidation/regeneration cycle number increases. As mentioned before by increasing the number of cycles, the sorbent efficiency decreases because porosity also decreases as a consequence of repetitive chemical and thermal stresses.

The predicted breakthrough curves for the six sulfidation experiments were also given in Figure 7.9 and Figure 7.10. As shown in Figure 7.9 and Figure 7.10, regression analysis of the experimental breakthrough data obtained for H_2S sorption on Cu-Mn-V-O gave very good agreement with the breakthrough equation derived (Eqn. 6.18).
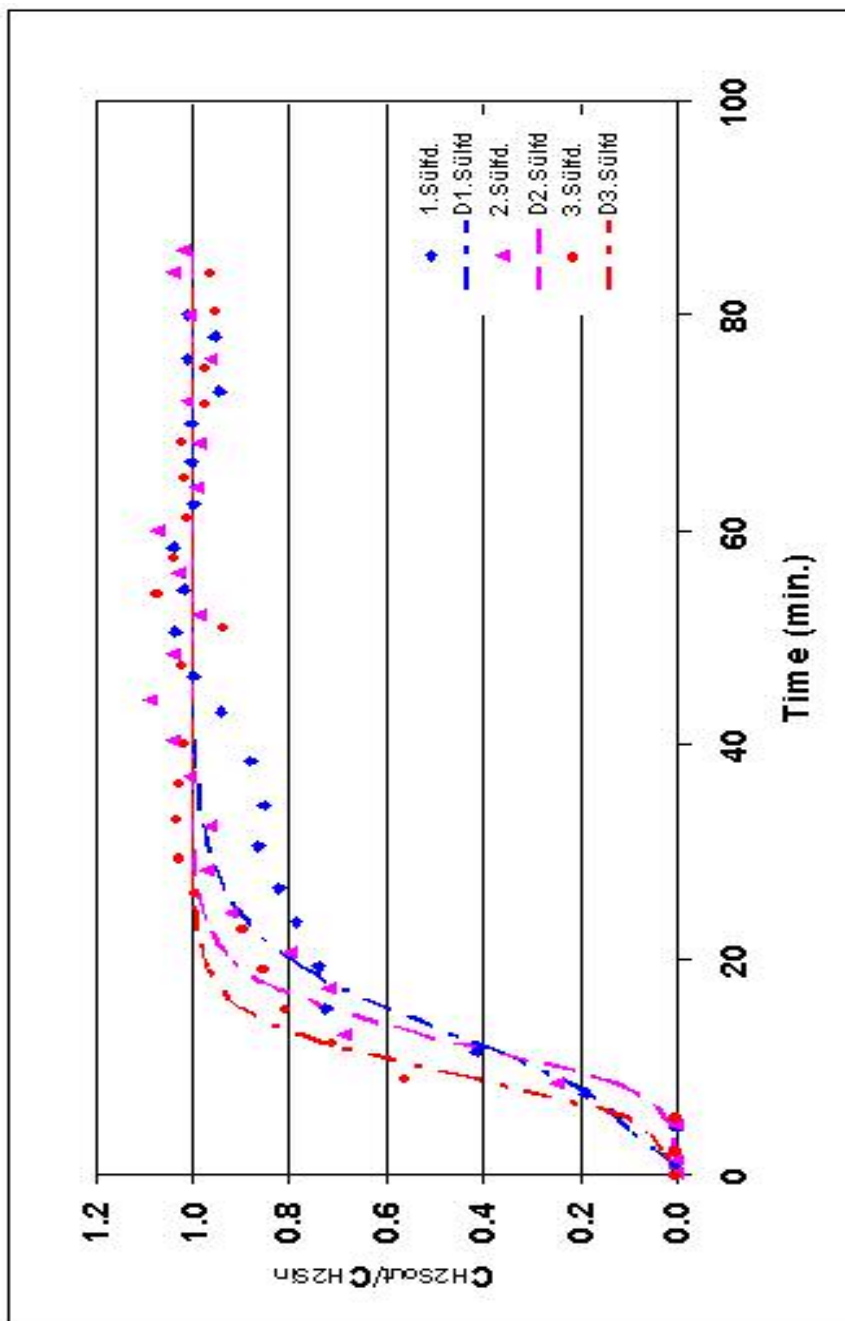
Figure 7.9. Breakthrough curves for H_2S using Cu-Mn-V-O sorbent at 627 °C. The lines correspond to deactivation model predictions

Figure 7.10. Breakthrough curves for H_2S using Cu-Mn-V-O sorbent at 627 °C.
The lines correspond to deactivation model predictions

7.5 Sorption of H_2S on Cu-V-O in the Presence of Hydrogen

H_2S sorption experiment with fresh Cu-V-O sorbent (experiment name: CV1) was performed in a packed bed quartz microreactor with a gas mixture containing %1 H_2S and %10 H_2 in balance He for about 80 min at 627 °C. To confirm the experimental results of CV1 and to test the reliability of experimental setup before keeping on 6 cycles of consecutive sulfidation-regeneration tests, sorption experiment with the same fresh Cu-V-O sorbent (experiment name: CV2) was performed again.

Results of the sulfidation experiments, CV1 and CV2, are given in Table 7.10 and Figure 7.11. As it was shown in Table 7.10 and Figure 7.11, experimental results of CV2 consistent with the experimental results of CV1. Error bars for experiments were drawn in ±0.05 error region. By this way, the reliability of the experimental setup was also tested.

Table 7.10. Results of sulfidation experiments carried out with the same fresh Cu-V-O sorbent (T=627 °C; %1 H_2S + %10 H_2 in balanced He)

| Fresh Sorbent / Experiment Name	Q (ml/min)	$H_2S_{adsorbed}$ x10^3 (mol)	g S_{ads} / g Sorbent	$SO_{2formed}$ (mol)
Cu-V-O / CV1	86	0.77	0.123	0.56
Cu-V-O / CV2	90	0.72	0.115	0.75
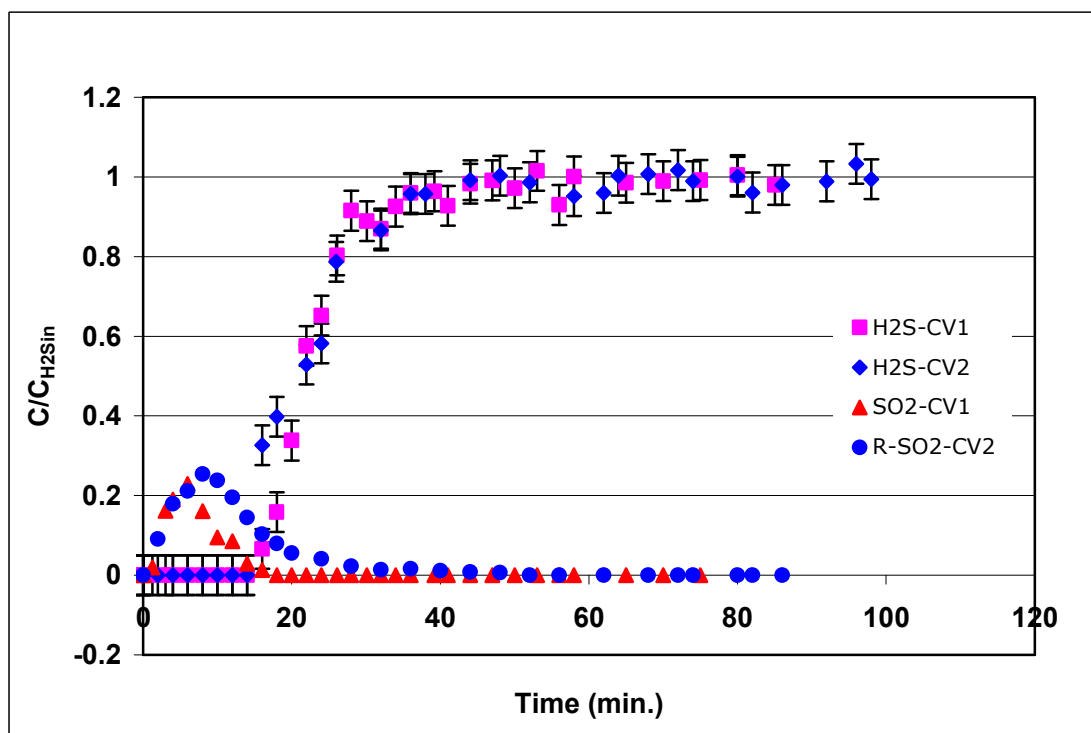
Figure 7.11. Exit compositions of H_2S and SO_2 in sulfidation experiments, CV1 and CV2, carried out with same fresh Cu-Mn-O sorbent (T=627 ^{o}C; %1 H_2S + %10 H_2 in balanced He)

As a result of material balance for sulfur around reactor, first sulfidation experimental results of Cu-V-O sorbent are given in Table 7.11. Because of an excessive thermal sintering in the first regeneration at 700 ^{o}C prevented further sulfidation/regeneration tests.

Table 7.11. Experimental results from the six sulfidation cycles carried out with Cu-V-O sorbent (T=627 ^{o}C; ; t≈80 min; %1 H_2S + %10 H_2 in balanced He)

Sulfidation Cycle No	Q (ml/min)	$H_2S_{adsorbed}$ x10^3 (mol)	gS_{ads} / gSorbent	$SO_{2\ formed}$ x10^4 (mol)
1	86	0.77	0.123	0.56

88

Table 7.11. (continued)

Sulfidation Cycle No	% H$_2$S	H$_2$S $_{in}$ (mol)x10^3	H$_2$S $_{out}$ (mol)x10^3	H$_2$S $_{adsorbed}$ (mol)x10^3
1	0.97	2.63	1.86	0.77

As can be seen from Table 7.11, Cu-V-O sorbent showed a very good performance in the first sulfidation at 627 ^{o}C. The sulfur retention capacity of the Cu-V-O sorbent is 0.123 (g of sulfur)/(g of sorbent) at the end of the first sulfidation.

The results from the sulfidation typically obtained with the developed Cu-V-O sorbent is shown in Figure 7.12. As can be seen from Figure 7.12, in experiments conducted with Cu-V-O sorbent SO$_2$ formation was observed.
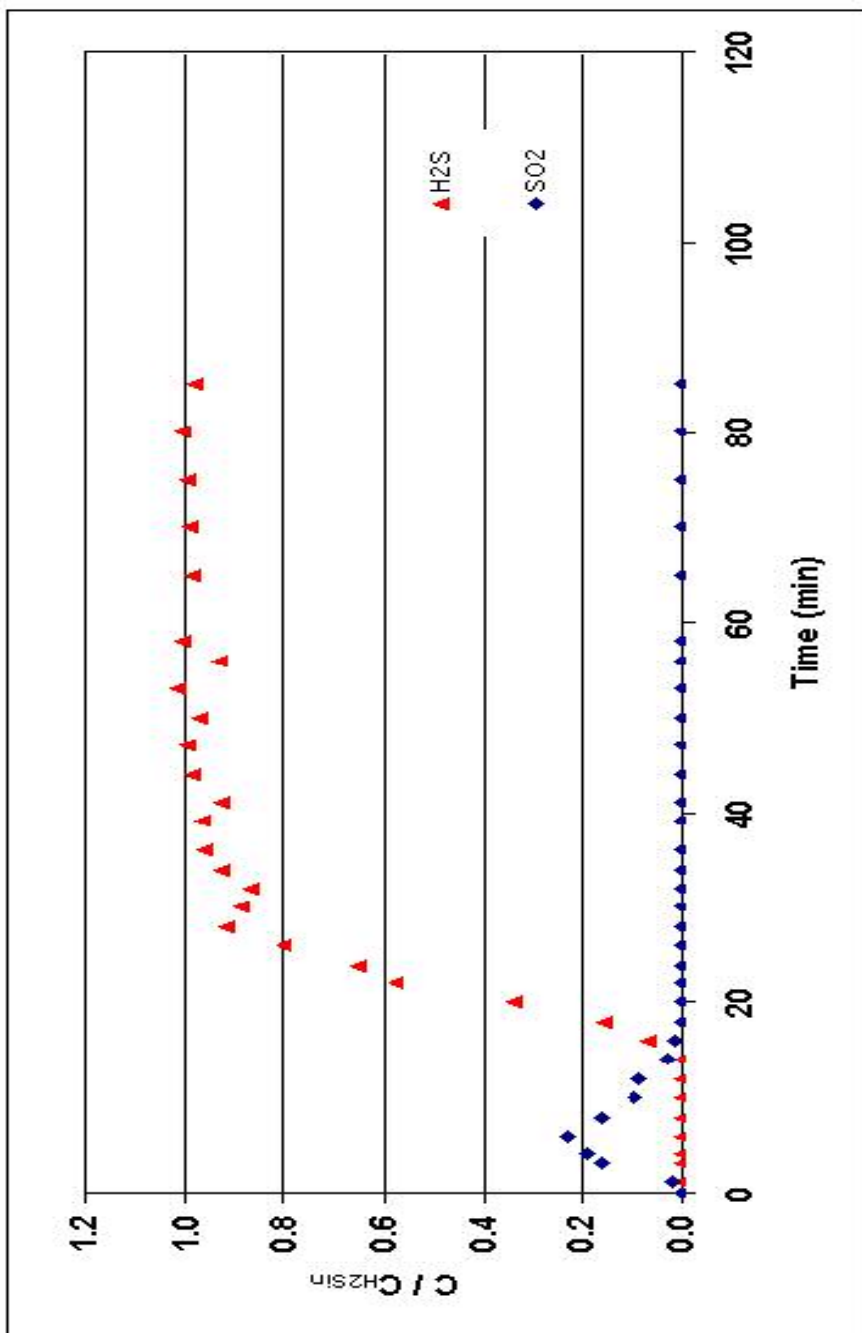
Figure 7.12. Breakthrough curves for H_2S and SO_2 using Cu-V-O sorbent at 627 °C

7.5.1 Application of Deactivation Model to Sulfidation Experiment Results of Cu-V-O

The results of the regression analysis of the data obtained with the Cu-V-O sorbent are given in Table 7.12.

Table 7.12. Rate Parameters Obtained from the Breakthrough Data for Cu-V-O Using Eqn. 6.18. (W=0.2 g; T=627 ^{o}C; 1 % H_2S + 10 % H_2 in He)

Sulfidation Cycle No	Q (ml/min)	k_oW/Q	$k_d(min^{-1})$ $x10^2$	$k_o(ml/g.min)$ $x\ 10^{-2}$	G^2
1	86	5.05	76	66	0.0279

The predicted breakthrough curves for the first sulfidation cycle are also given in Figure 7.13. As shown in Figure 7.13, regression analysis of the experimental breakthrough data obtained for H_2S sorption on Cu-V-O gave very good agreement with the breakthrough equation derived (Eqn. 6.18).
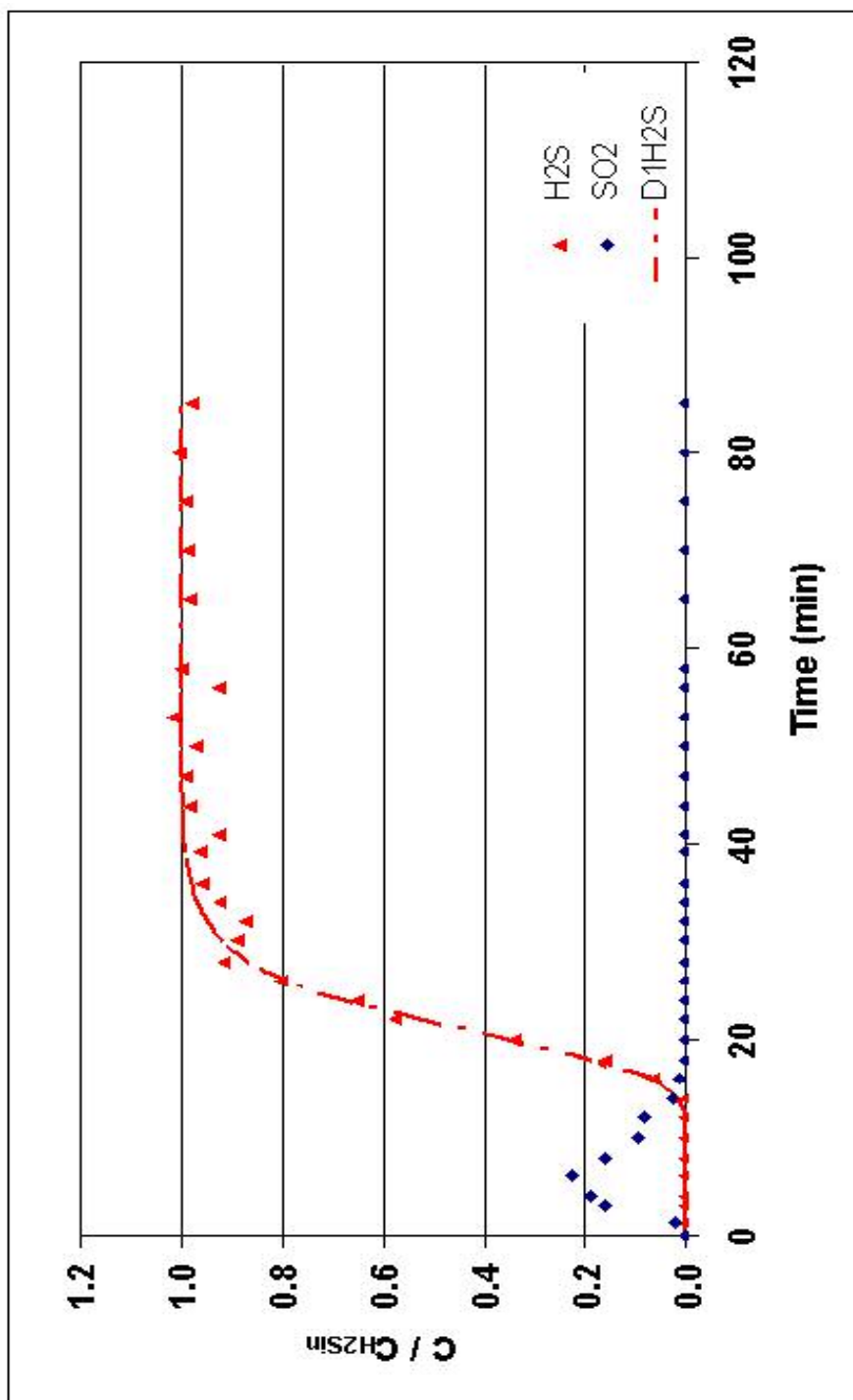
Figure 7.13. Breakthrough curves for H_2S and SO_2 using Cu-V-O sorbent at 627 °C.

The lines correspond to deactivation model predictions

7.5.2 Reaction Mechanism of H_2S Sorption with Cu-V-O Sorbent in the Presence of Hydrogen

The basic chemistry of the Cu-V-O sorbent may be summarized with a listing of the overall chemical reactions during sulfidation at 627^oC and regeneration at $700\,^oC$. Suggested reaction mechanism for desulfurization of Cu-V-O sorbent is given below (Yasyerli et al., 2001).

Sulfidation:

$$Cu_2V_2O_7 + H_2 \rightarrow Cu_2O + V_2O_5 + H_2O \qquad \text{(R.7.9)}$$

$$V_2O_5 + 2H_2 \rightarrow V_2O_3 + 2H_2O \qquad \text{(R.7.10)}$$

$$V_2O_3 + 3H_2S \rightarrow V_2S_3 + 3H_2O \qquad \text{(R.7.11)}$$

$$Cu_2O + H_2S \rightarrow Cu_2S + H_2O \qquad \text{(R.7.12)}$$

$$Cu_2V_2O_7 + 3H_2 + 4H_2S \rightarrow V_2S_3 + Cu_2S + 7H_2O \qquad \text{(R.7.13)}$$
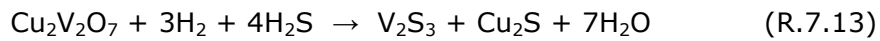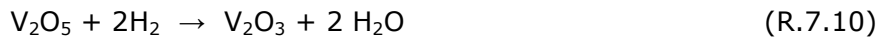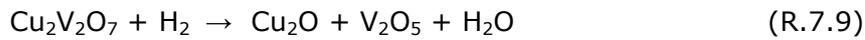
As stated by Westmoreland et al. (1976), V_2S_3 is the sulfided product up to the melting temperature of V_2S_3 near 650 ^oC. An additional reaction that is important in the absence of H_2 from the input gas is the direct reduction of V_2O_5 by H_2S:

$$V_2O_5 + (5-y)/2H_2S \rightarrow V_2O_y + (5-y)/2SO_2 + (5-y)/2H_2 \quad \text{(R.7.14)}$$
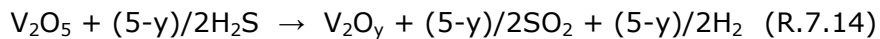
In the presence of H_2, reaction 7.14 is ineffective since V_2O_5 is reduced ahead of the sulfidation front. Neverthless at the beginning of sulfidation of fresh or regenerated sorbents, a small amount of SO_2 formation was observed. These

small peak of SO_2, fade away as sulfidation proceeds, evidently due to the conversion of V_2O_5 to a lower oxide by reduction with H_2 (Bagajewicz et al., 1988).

7.6 Comparison of The Sorbent Sulfidation Capacities

6-cycle series of sulfidation/regeneration experiments was completed to demonstrate the durability and regenerability of Cu-Mn-O and Cu-Mn-V-O sorbents. Under the following regeneration conditions, including 700 ^{o}C of regeneration temperature and %6 of oxygen concentration in balance N_2, the sulfur removal capacities of the sorbents underwent continuous desulfurization, and regeneration were represented in Figure 7.14 and Figure 7.15 as a function of the number of cycles respectively. This sulfur retention capacity is calculated using mass balances, based upon gas analyses for H_2S entering and leaving the reactor.

The sulfur retention capacities (defined as grams of sulfur per 100 g of sorbent) of the Cu-Mn-O sorbent decreased from %15.2 to %12.8 during 6 sulfidation/regeneration cycles. As can be seen from Figure 7.14 the Cu-Mn-O sorbent efficiency didn't change much as the number of cycles increases. The results indicated that the Cu-Mn-O sorbent prepared in this study removed sulfur without apparent performance decay during 6 sulfidation/regeneration cycles. Because of an experimental error in the fourth sulfidation of Cu-Mn-O, the fourth sulfur loading capacity is not drawn in Figure 7.14 but the fourth sulfidation experimental results are given in Appendix I.

The sulfur-loading capacity of the Cu-Mn-V-O sorbent shows some decrease with each cycle. This effect is noticable in the sixth cycle. Sulfur

retention capacity of Cu-Mn-V-O sorbent ranged from %11 to %5.4. The decrease in conversion with successive cycles observed in Figure 7.15 is predicted due to thermal sintering as well as loss of surface area which can be prevented by improving Cu-Mn-V-O sorbent regeneration conditions like choosing lower regeneration temperature or decreasing %O_2. Sample calculation of sulfur retention capacity for Cu-Mn-V-O sorbent is given in Appendix H.
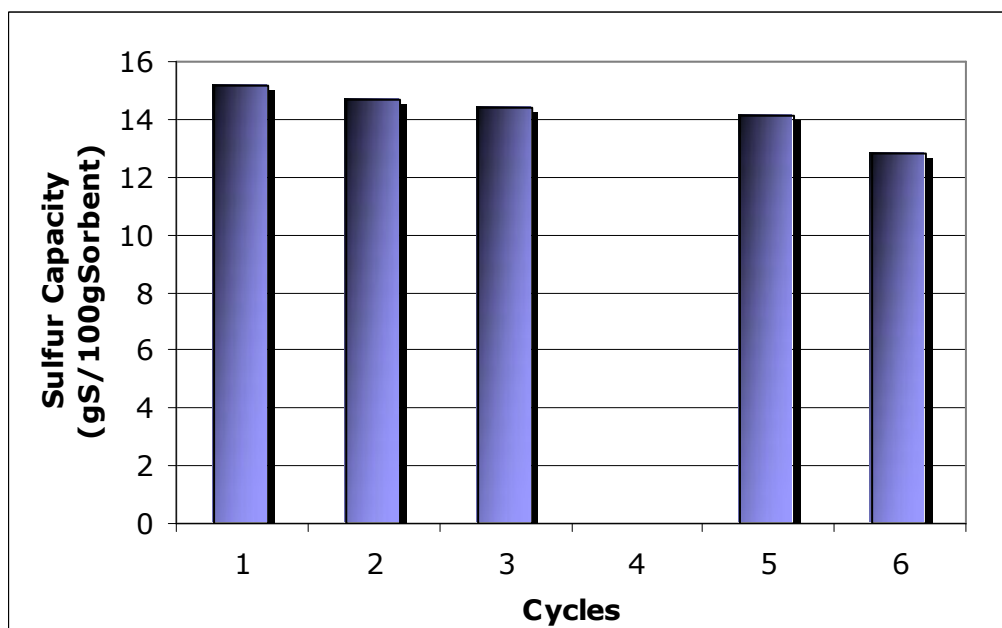
Figure 7.14. Effect of sulfidation/regeneration cycles on sulfur retention capacity of Cu-Mn-O. Sulfidation conditions: T: 627 $^{\circ}$C, inlet gas %1 H_2S-%10 H_2-balance He. Regeneration conditions: T: 700°C, inlet gas %6 O_2-balance N_2.
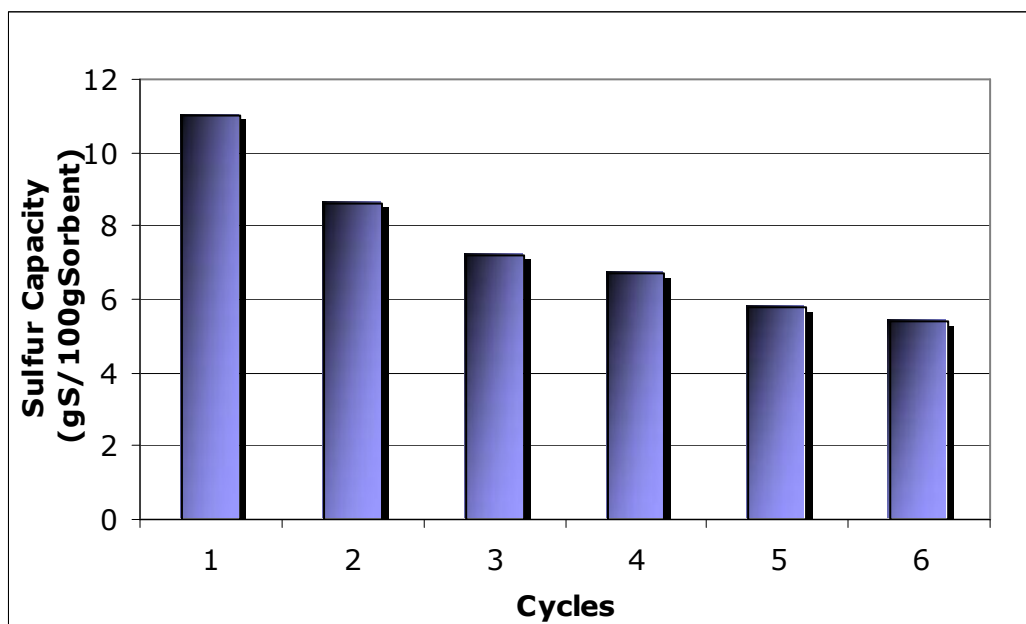
Figure 7.15. Effect of sulfidation/regeneration cycles on sulfur retention capacity of Cu-Mn-V-O. Sulfidation conditions: T: 627 $^{\circ}$C, inlet gas %1 H_2S-%10 H_2-balance He. Regeneration conditions: T: 700°C, inlet gas % 6O_2-balance N_2.

Concerning the selectivity to elemental sulfur, it is interesting to observe that the selectivity was maintained almost constant around %98-99   for Cu-Mn-O and Cu-Mn-V-O sorbents even though the conversion is varied through the cycle number. Because of the SO_2 formation, selectivity of Cu-V-O was %93.

7.7   Comparison of Deactivation Model Predictions for Sorbents

The results of regression analysis of the data obtained with prepared sorbents, Cu-Mn-O, Cu-Mn-V-O and Cu-V-O, for the first sulfidation cycle are given in Table 7.13. The predicted breakthrough curves for the first sulfidation cycle are also given in Figure 7.16.

Table 7.13. Rate Parameters Obtained from the Breakthrough Data for Prepared Sorbents Using Eqn.6.18. (W=0.2 g; T=627 $^\circ$C; 1 % H_2S + 10 % H_2 in He)

Sorbent	Q(ml/min)	k_oW/Q	$k_d(min^{-1})$ $x10^2$	$k_o(ml/g.min)$ $x\ 10^{-2}$
Cu-Mn-O	91	6.35	91	88
Cu-Mn-V-O	92	2.43	57	33
Cu-V-O	86	5.05	76	66

Deactivation model used in this work gave very good predictions of H_2S breakthrough curves obtained for sulfidation experiments. Another noticeable result of this analysis is that the rate parameters obtained with Cu-Mn-O are higher than the rate parameters obtained with Cu-Mn-V-O and Cu-V-O mixed oxides. From the study of sorbents Cu-Mn-O, Cu-Mn-V-O and Cu-V-O it may be concluded that the apparent decay of sorbent efficiency is exclusively associated with changes in the textural properties. It is well known that the pore volume of sulfided sorbents is always lower than that of the fresh sorbent, because of the higher molar volume of sulfided species with reference to that of the oxidized ones.
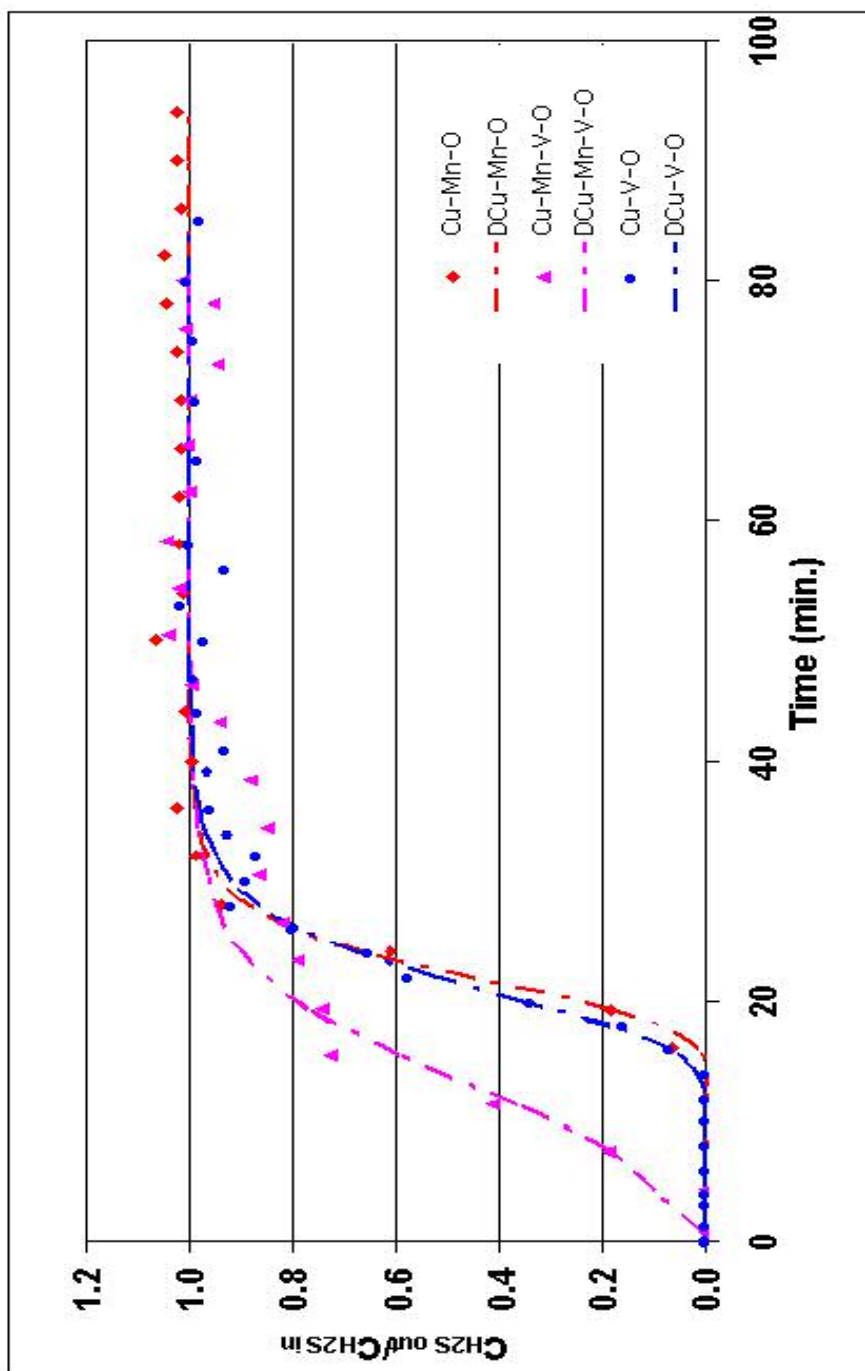
Figure 7.16. Comparison of first sulfidation H_2S breakthrough curves of sorbents. The lines correspond to deactivation model predictions($T=627^{\circ}C$, $1\%H_2S+10\%H_2$ in He)

7.8   Sorbent Regeneration Performance

Regeneration tests of sulfided Cu-Mn-O, Cu-Mn-V-O and Cu-V-O sorbents were conducted with 6 vol % O_2 in balance nitrogen at 700 ^{o}C. The results are shown in Table 7.14, Table 7.15 and Table 7.16 for Cu-Mn-O, Cu-Mn-V-O and Cu-V-O sorbents, respectively. All samples had been sulfided completely prior to regeneration under the same conditions.

Table 7.14. Regeneration test results of sulfided Cu-Mn-O sorbent

Regeneration No	Q (ml/min)	$n_{SO2\ out}$ x 10^4 (mol)
1	98	2.29
2	93	2.04
3	43	1.88
4	48	1.97
5	60	1.79
6	81	0.89

Table 7.15. Regeneration test results of sulfided Cu-Mn-V-O sorbent

Regeneration No	Q (ml/min)	$n_{SO2\ out}$ x 10^4 (mol)
1	92	2.17
2	86	1.46
3	75	1.52
4	83	0.73
5	98	1.44
6	94	1.16

Table 7.16. Regeneration test results of sulfided Cu-V-O sorbent

Regeneration No	Q (ml/min)	$n_{SO2\ out}$ x 10^4 (mol)
1	82	0.85

Results of 6 consecutive sulfidation/regeneration cycles carried out with Cu-Mn-O, Cu-Mn-V-O and Cu-V-O sorbents are also shown more detailly in Table 7.17, Table 7.18 and Table 7.19 respectively. As can be seen from Table 7.17 and Table 7.18, during Cu-Mn-O and Cu-Mn-V-O sorbent regeneration, the metal sulfide was reacted with oxygen to regenerate the metal oxide and liberate the sulfur as SO_2. At the end of each cycle about 1/3 of the adsorbed sulfur was emitted as SO_2 in the exhaust gas while the rest of it was collected as elementary sulfur at the end of the reactor outlet. Condensation of sulfur gases occurs at 444.60 ^{o}C. Hence, yellow color observed at the reactor outlet after each cycle except for first cycle of Cu-Mn-O and first sulfidation of Cu-Mn-V-O indicated the formation of elementary sulfur.

Table 7.17. Experimental results of 6 consecutive sulfidation/regeneration cycles carried out with Cu-Mn-O sorbent (Sulfidation conditions: T= 627 ^{o}C, t≈80 min, 1% H_2S + 10% H_2 in balance He ; Regeneration conditions: T= 700 ^{o}C, t≈40 min, 6% O_2 in balance N_2)

Cycle No	Experiment Type	Q (ml/min)	$H_2S_{adsorbed}$ X 10^3 (mol)	g $S_{adsorbed}$/ g Sorbent	$n_{SO2\ out}$ x 10^4 (mol)
1	Sulfidation	91	0.95	0.152	-
	Regeneration	98	-	-	2.29
2	Sulfidation	90	0.92	0.147	-
	Regeneration	93	-	-	2.04
3	Sulfidation	88	0.90	0.144	-
	Regeneration	43	-	-	1.88
4	Sulfidation	Exp. Error	Exp. Error	Exp. Error	Exp. Error
	Regeneration	48	-	-	1.97
5	Sulfidation	91	0.88	0.141	-
	Regeneration	60	-	-	1.79
6	Sulfidation	89	0.80	0.128	-
	Regeneration	81	-	-	0.89

Table 7.18. Experimental results of 6 consecutive sulfidation/regeneration cycles carried out with Cu-Mn-V-O sorbent (Sulfidation conditions: T= 627 ^{o}C, t≈80 min, 1% H_2S + 10% H_2 in balance He ; Regeneration conditions: T= 700°C, t≈40 min, 6% O_2 in balance N_2)

Cycle No	Experiment Type	Q (ml/min)	$H_2S_{adsorbed}$ X 10^3 (mol)	g $S_{adsorbed}$/ g Sorbent	$n_{SO2\ out}$ x 10^4 (mol)
1	Sulfidation	92	0.68	0.110	-
1	Regeneration	92	-	-	2.17
2	Sulfidation	93	0.54	0.086	-
2	Regeneration	86	-	-	1.46
3	Sulfidation	90	0.45	0.072	-
3	Regeneration	75	-	-	1.52
4	Sulfidation	87	0.42	0.067	-
4	Regeneration	83	-	-	0.73
5	Sulfidation	88	0.36	0.058	-
5	Regeneration	48	-	-	1.44
6	Sulfidation	91	0.34	0.054	-
6	Regeneration	94	-	-	1.16

Table 7.19. Experimental results of the first sulfidation/regeneration cycle carried out with Cu-V-O sorbent (Sulfidation conditions: T= 627 ^{o}C, t≈80 min, 1% H_2S + 10% H_2 in balance He ; Regeneration conditions: T= 700 ^{o}C, t≈40 min, 6% O_2 in balance N_2)

Cycle No	Experiment Type	Q (ml/min)	$H_2S_{adsorbed}$ X 10^3 (mol)	g $S_{adsorbed}$/ g Sorbent	$n_{SO2\ out}$ x 10^4 (mol)
1	Sulfidation	86	0.77	0.123	0.56
1	Regeneration	82	-	-	0.85

Additional chemical analysis of the solid products, Cu-Mn-O and Cu-Mn-V-O, obtained after the sixth regeneration experiment allowed the sulfur balance

around the reactor to be verified. For this purpose, a Leco SC 132 sulfur analyzer was used. Total sulfur amount in the Cu-Mn-O and Cu-Mn-V-O solid products obtained at the end of the sixth regeneration is 0.9×10^{-3} mol and 1.72×10^{-5} mol respectivelly. The results indicates that at the operating temperature of 700 ^{o}C the sorbents are regenerated almost completely.

7.9 Comparison of Sorbent Regeneration Capacity

In addition to the sulfur retention capacity and structural stability, regeneration characteristics are among the most important factors to be considered. The SO_2 breakthrough curves during the tests at 700 ^{o}C condition are plotted in Figure 7.17, Figure 7.18 and Figure 7.19 for Cu-Mn-O, Cu-Mn-V-O and Cu-V-O respectively.

From Figures, it was found out that the two sorbents were regenerated almost completely at 700 ^{o}C. However different regeneration characteristics were shown at 700 ^{o}C. It was observed for Cu-Mn-O sorbent that the concentration of SO_2 had a maximum value at approximately 10 min and then the outlet concentration of SO_2 slowly decreased gradually to the end.

In the case of Cu-Mn-V-O sorbent, however, it was found that most of the sulfur absorbed during sulfidation was desorbed over the process of regeneration at 700 ^{o}C for a short time. It was considered that a vanadium additive increased the regeneration capacity of Cu-Mn-O sorbent because it played an important role as the catalyst for oxidation. Sorbent Cu-V-O showed a very good performance in the first sulfidation, and excessive thermal sintering in the first regeneration prevented further testing.
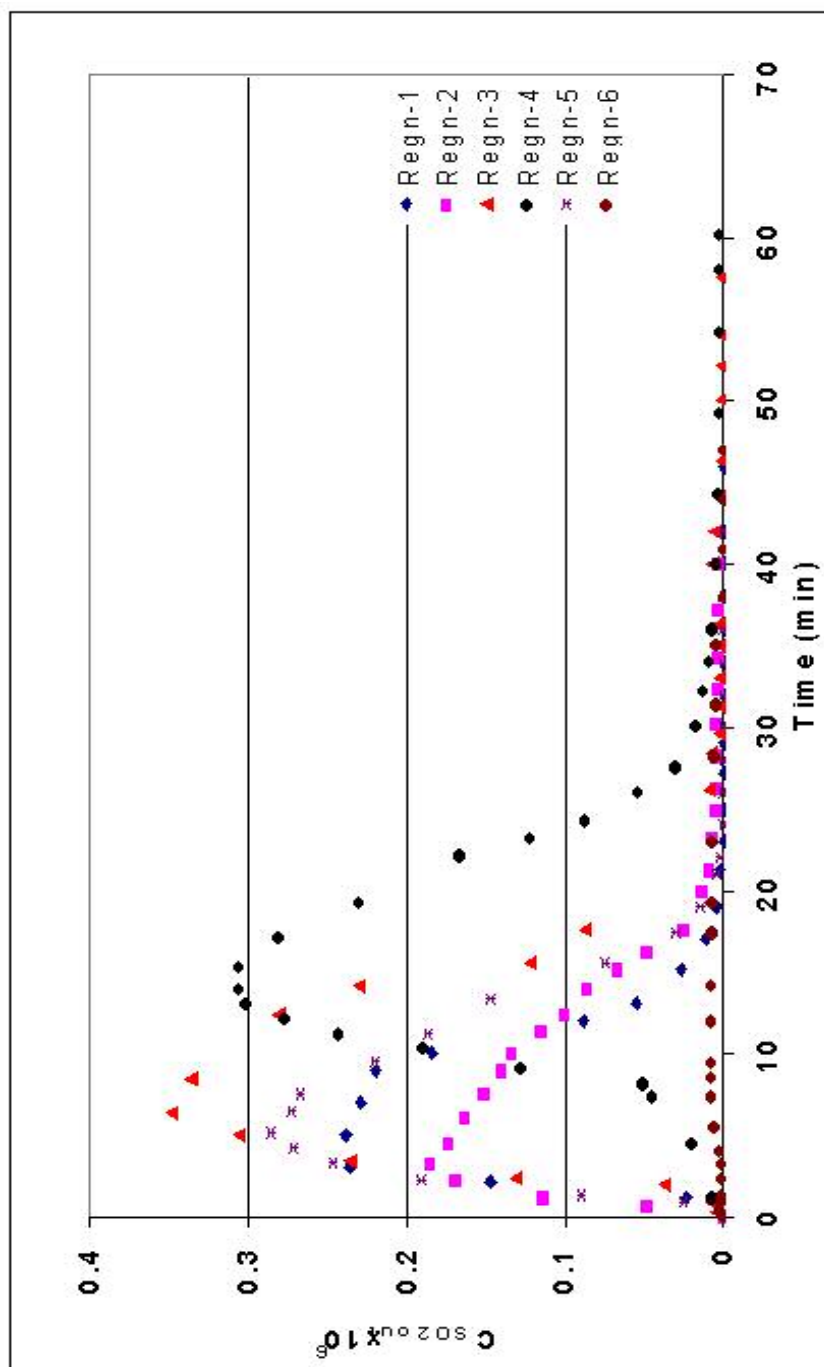
Figure 7.17. SO$_2$ breakthrough curves of Cu-Mn-O sorbent at 700 °C

103
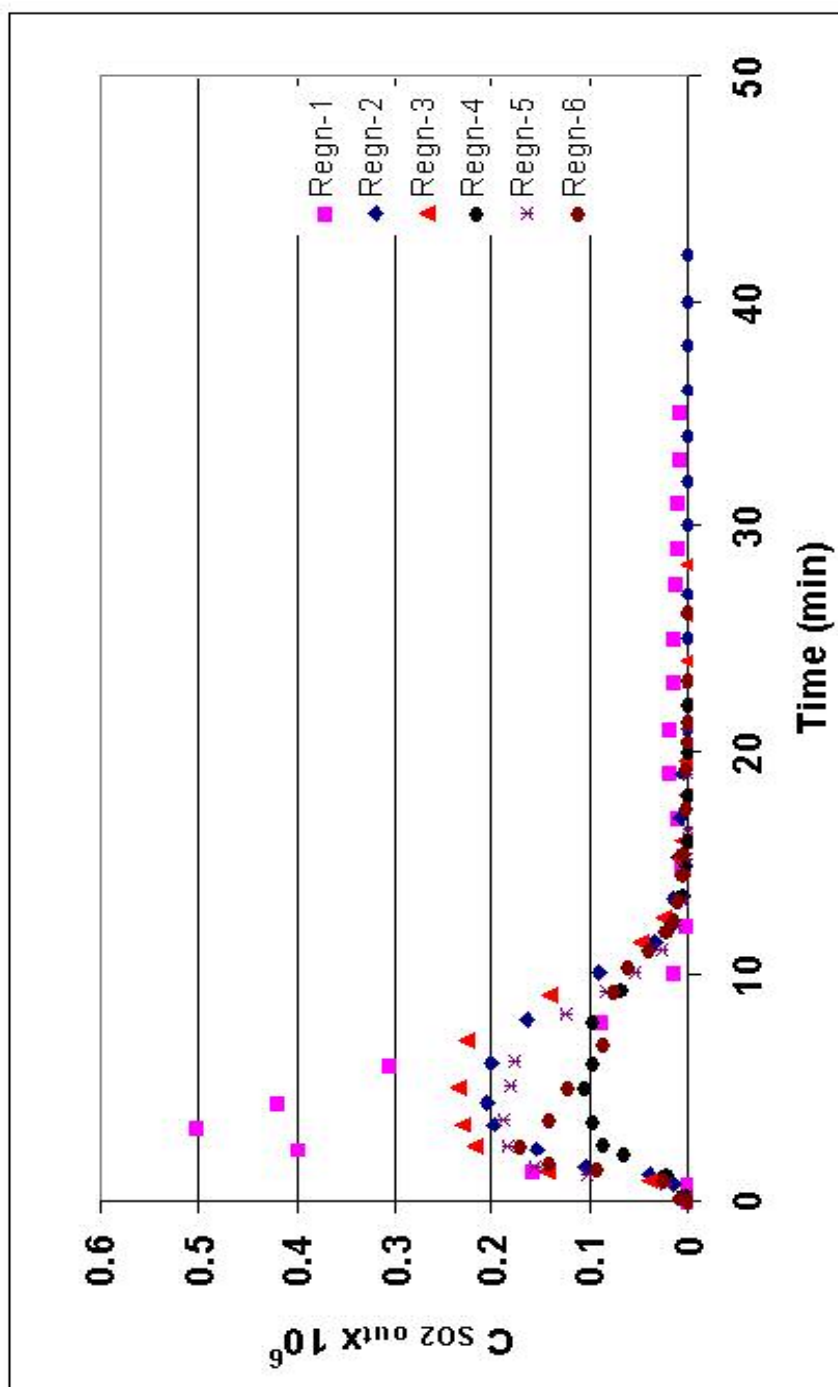
Figure 7.18. SO$_2$ breakthrough curves of Cu-Mn-V-O sorbent at 700 °C
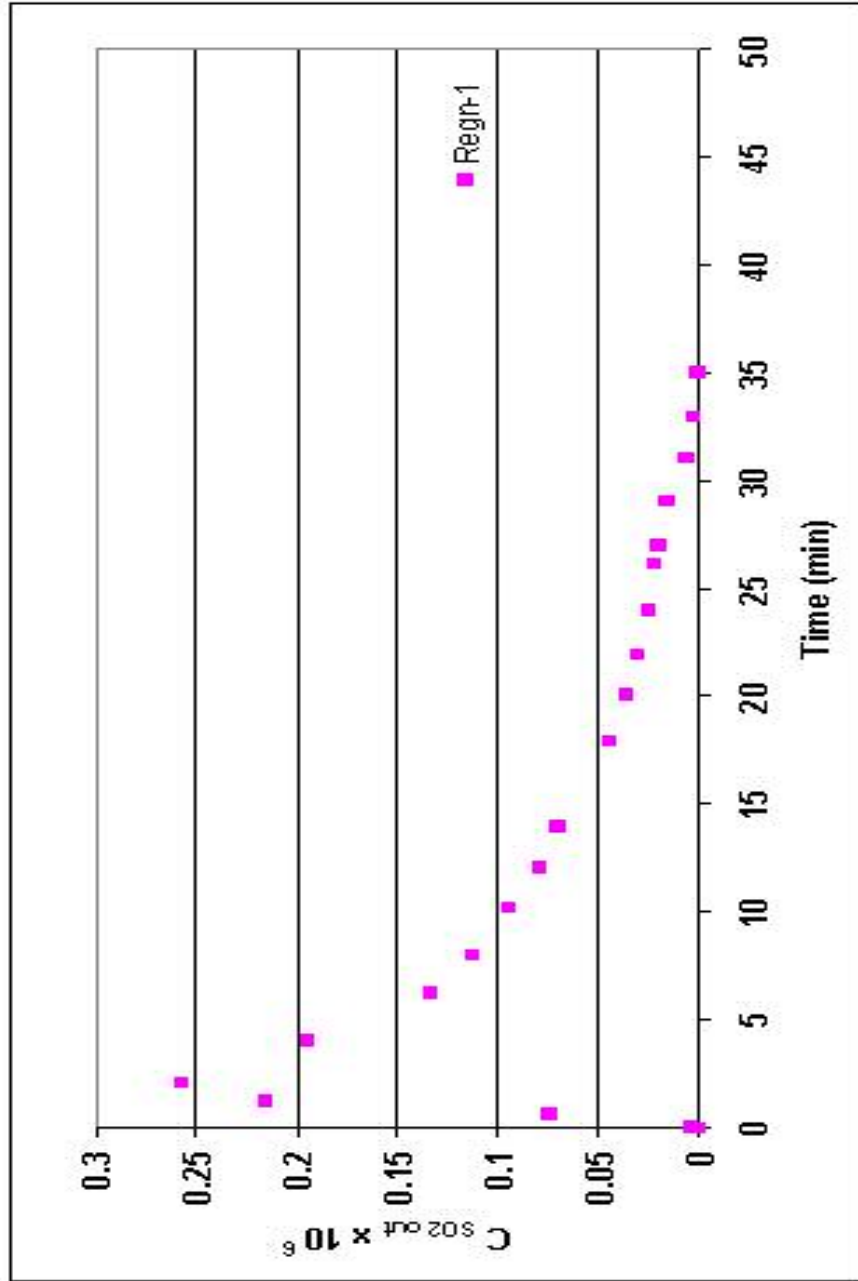
Figure 7.19. SO$_2$ breakthrough curves of Cu-V-O sorbent at 700 $^\circ$C

7.10 Oxidative Regeneration Reaction Mechanism of Cu-Mn-O Sorbent

Sulfidation of Cu-Mn-O sorbent produces manganese and copper sulfides. The phases, $CuMn_2O_4$, $Cu_{1.5}Mn_{1.5}O_4$, CuO, $MnSO_4$, $Cu_{1.96}S$, Mn_3O_4, observed in the XRD analyses (Figure 7.21) may be discussed qualitatively in terms of the following thermodynamically feasible phase transformations. The comparison of calculated XRD data with literature values is given in Table E.2 and Table E.3 for Cu-Mn-O sorbents.

The regeneration reaction proceeds initially according to the following reaction:

$$MnS + 3/2\ O_2 \rightarrow MnO + SO_2 \qquad\qquad (R.7.15)$$

Then MnO is readily converted to Mn_3O_4 because of the availability of O_2 in the gas:

$$MnO + 1/6\ O_2 \rightarrow 1/3\ Mn_3O_4 \qquad\qquad (R.7.16)$$

Consequently, under these conditions the overall regeneration reaction is given by

$$MnS + 5/3\ O_2 \rightarrow 1/3\ Mn_3O_4 + SO_2 \qquad\qquad (R.7.17)$$

It must be noted that in experiments conducted with Cu-Mn-O sorbent after each cycle except for the first one, yellow color was observed at the end of the reactor outlet which indicates the formation of elementary sulfur resulting from the reaction 7.18 given below. As said before, condensation of sulfur gases occurs at 444.60 $^{\circ}$C.

The oxygen in the reactant gas is virtually converted to SO_2. The regenerated manganese oxide would be in the form of Mn_3O_4 which would be

immediately reduced to MnO upon exposure to the hot reducing fuel gas during the sulfidation stage (Hepworth et al., 1994).

Regeneration is complicated by the tendency to form manganese and copper sulfates. This proposed reaction mechanism implies that manganese and copper sulfates are formed through reactions 7.19 and 7.20, from regenerated sorbent (oxide) located in the outer layers of the sample, SO_2 emitted by sorbent being regenerated located in inner layers of the sample and O_2 coming by diffusion from the feeding gas.
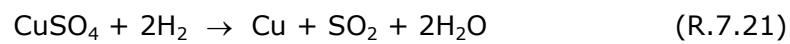
$$MnS + 1/2O_2 \rightarrow MnO + 1/2S_2 \hspace{3cm} (R.7.18)$$

$$MnO + SO_2 + 1/2 \ O_2 \rightarrow MnSO_4 \hspace{2.5cm} (R.7.19)$$

$$2Cu_2S + 4O_2 \rightarrow CuSO_4 + 2CuO + SO_2 \hspace{1.5cm} (R.7.20)$$

$$CuSO_4 + 2H_2 \rightarrow Cu + SO_2 + 2H_2O \hspace{2cm} (R.7.21)$$

Calculated reaction entalpies, gibbs free energy of reactions and reaction equilibrium constants, at 627 ^{o}C are listed in Table 7.20 (Barrin and Knacke, 1979). Taking into account thermodynamic data (Garcia et al.,2000) the stability curves for $MnSO_4$ and $CuSO_4$ are shown in Figure 7.20. Under the operating condition used (point A, 700 ^{o}C) $CuSO_4$ is unstable while $MnSO_4$ is stable, being the only sulfate phase presumably found in the regenerated sorbent. The formation of $MnSO_4$ during regeneration is a function of temperature and gas composition. Low temperature and high oxygen concentration promote sulfate formation.

From the above results it could be concluded that to prevent the presence of $MnSO_4$ the regeneration of Cu-Mn-O sorbent should be carried out above

900°C and then MnSO$_4$ is readily converted to Mn$_3$O$_4$ as given below. As stated before according to Garcia et al., (2000), MnSO$_4$ is also unstable at 850 °C. The amount of MnSO$_4$ decreases rapidly at 900 °C and at 1000 °C MnSO$_4$ is not evidenced.

$$MnSO_4 \rightarrow 1/3\ Mn_3O_4 + SO_2 + 1/3O_2 \qquad (R.7.22)$$
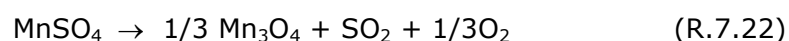
Table 7.20. Regeneration reaction enthalpies, gibbs free energy of reactions and reaction equilibrium constants of Cu-Mn-O Sorbent

Reaction	T=627 °C		
	ΔH$_r$ (kj/mol)	ΔG$_r$ (kj/mol)	log K
R.7.15	-469.081	-395.879	22.976
R.7.16	-76.727	-39.478	2.291
R.7.17	-545.808	-435.357	25.267
R.7.18	-107.067	-99.906	5.798
R.7.19	-371.495	-120.243	6.979
R.7.20	-1227.211	-681.341	39.542
R.7.21	-35.441	-396.386	14.75

It should be noted, however, that the oxidative regeneration of the oxide is highly exothermic. Accordingly, practical problems may be encountered in the control of the reactor temperature.
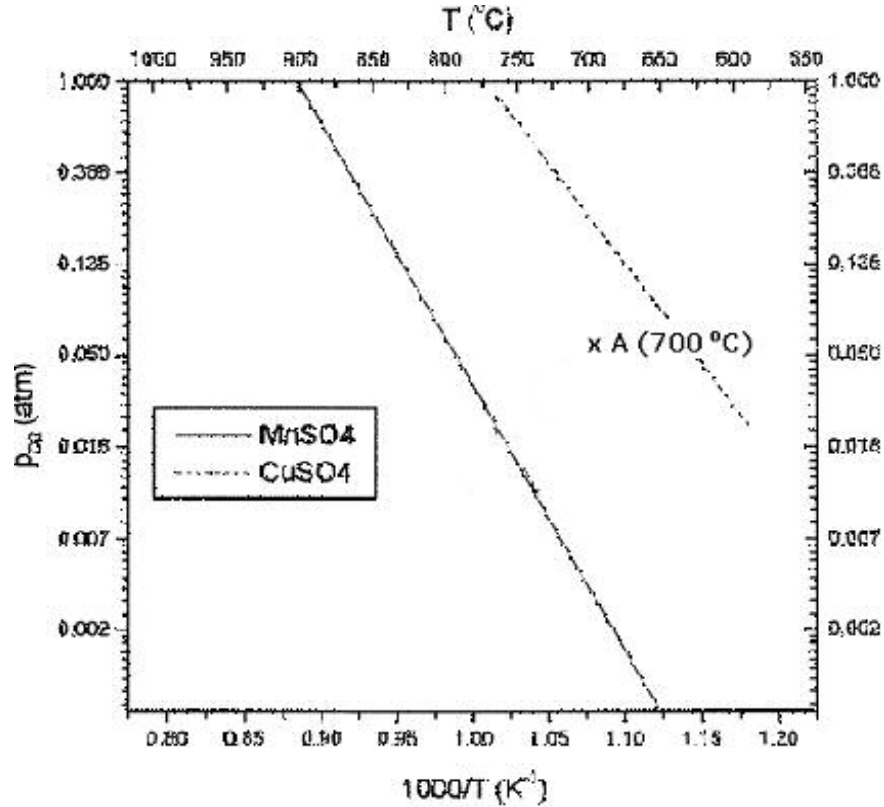
Figure 7.20.   Stability diagram of $MnSO_4$ and $CuSO_4$ as a function of partial pressure of O_2 (Garcia et al., 2000)

7.11   Oxidative Regeneration Reaction Mechanism of Cu-V-O Sorbent

During the nitrogen purge following sulfidation experiment , small amount of H_2S desorbed as elemental sulfur and was collected at the bed outlet. Since H_2 is not present in the purging gas, decomposition of H_2S takes place and, as reported by Fukuta et al., is catalyzed by the solid substrate. The amount of elemental sulfur collected was lower than the amount corresponding to the measured H_2S concentration at the reactor outlet. After nitrogen purge, the sorbent was regenerated by flow of a 6% O_2 in balance N_2 mixture and only trace of SO_2 was detected during this period.

The above results can be described by the following reaction sequence.

Chemisorption:

$$V_2O_y + H_2S \rightarrow V_2O_y \cdot H_2S \qquad\qquad (R.7.23)$$

N_2 Purge:

$$V_2O_y \cdot H_2S \rightarrow V_2O_y + (1-z)H_2S + zH_2 + (z/2)S_2 \qquad (R.7.24)$$

Regeneration:

$$V_2S_3 + (6+y)/2O_2 \rightarrow V_2O_y + 3SO_2 \qquad\qquad (R.7.25)$$

$$Cu_2S + V_2O_y + (w+(7-x)/2)O_2 \rightarrow Cu_2V_2O_7 + wSO_2 + (1-w)/2S_2 \qquad (R.7.26)$$
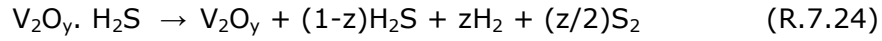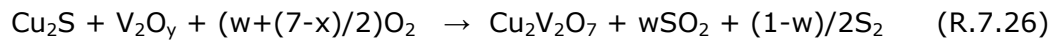
7.12 Change of Structure

The change of crystallographic form of regenerated Cu-Mn-O and Cu-Mn-V-O sorbents from cycle 6 were followed by the powder X-ray diffraction method. XRD patterns of the regenerated Cu-Mn-O and Cu-Mn-V-O sorbents after the sixth regeneration are given in Figure 7.21 and Figure 7.22 respectively.

Comparison of the X-ray diffraction patterns of the fresh Cu-Mn-O and Cu-Mn-V-O sorbents and after the sixth regeneration at 700 ^{o}C are shown in Figure 7.23 and 7.24 respectively.
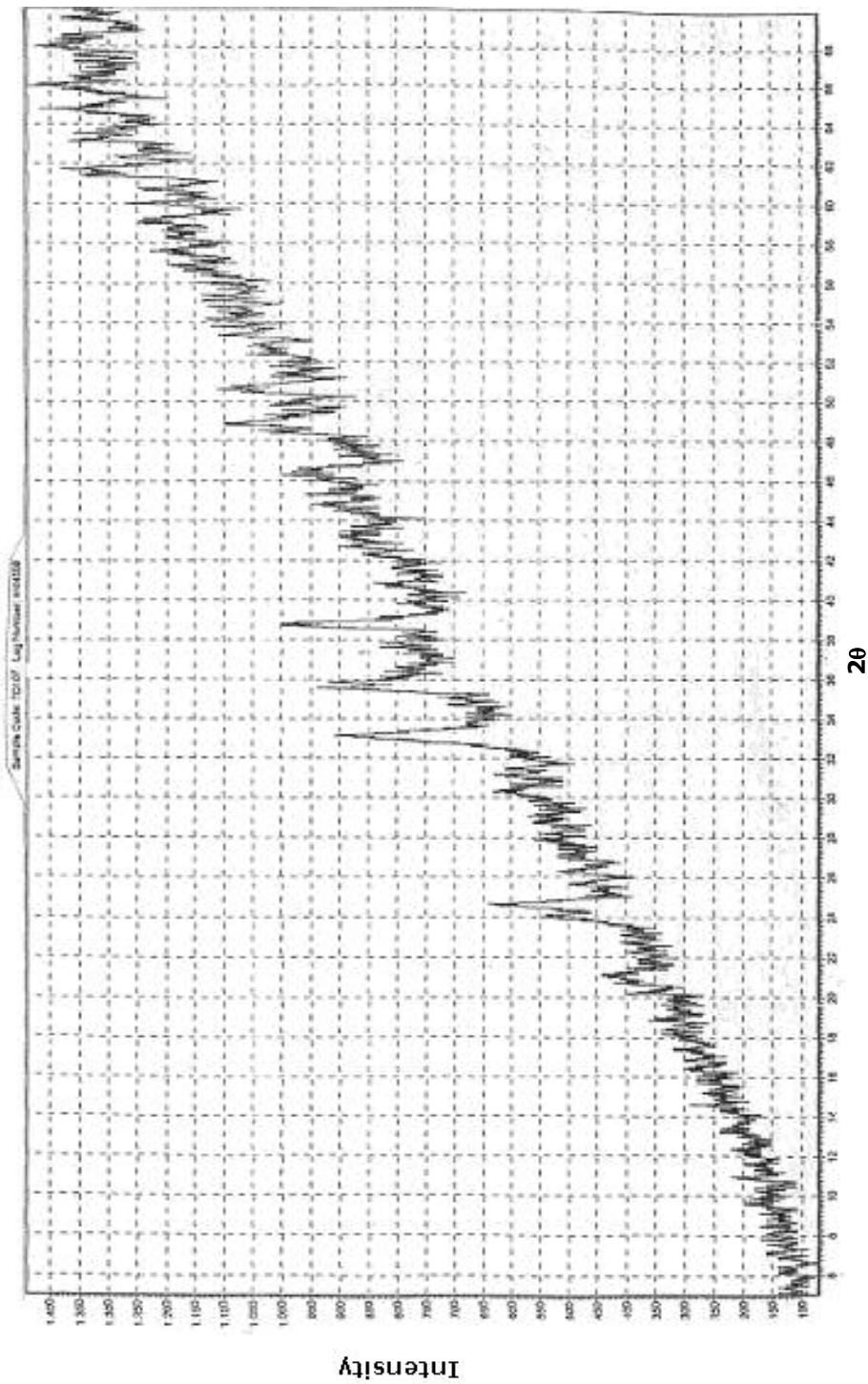
Figure 7.21. X-ray diffraction pattern of Cu-Mn-O sorbent after sixth regeneration

111
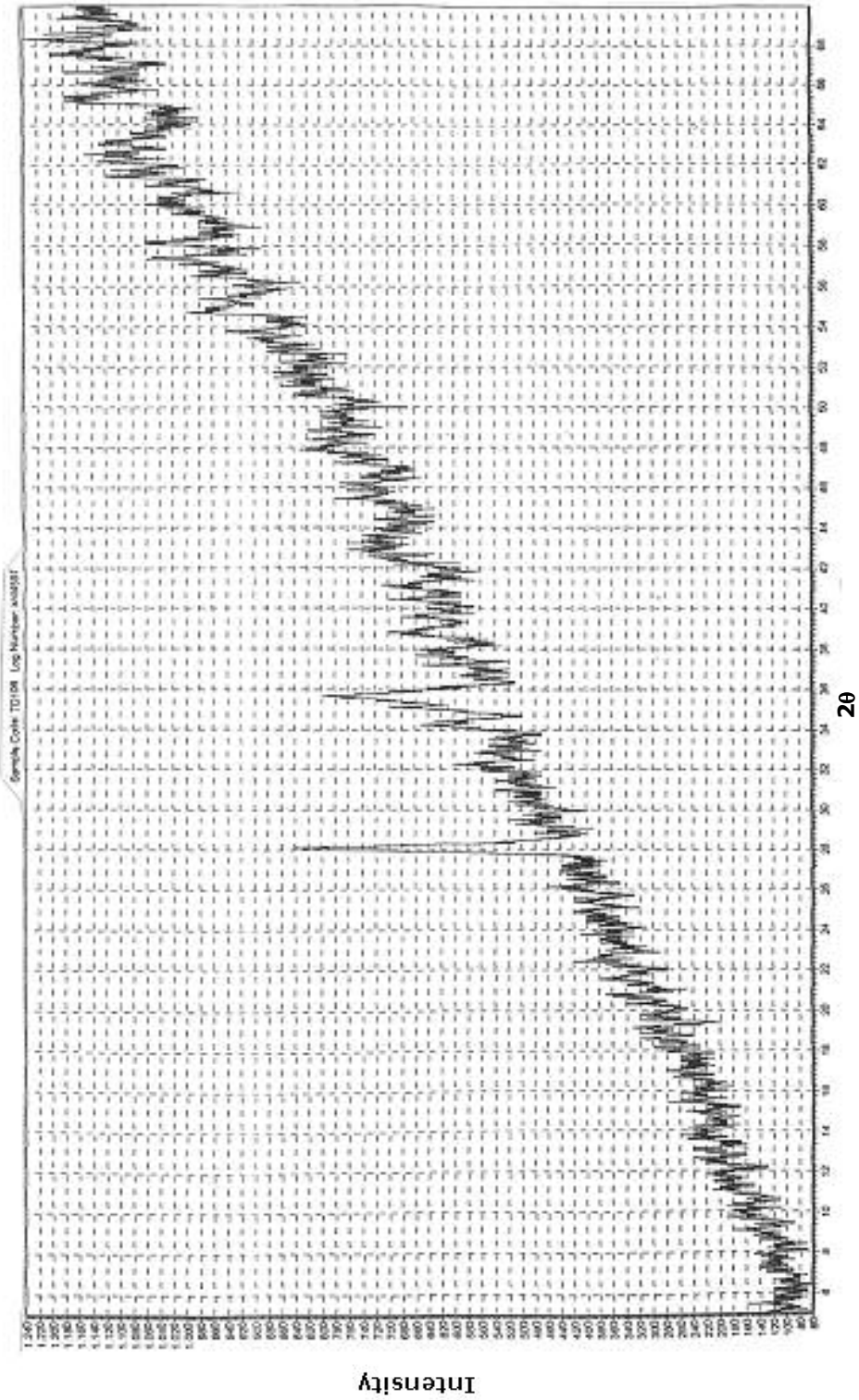
Figure 7.22. X-ray diffraction pattern of Cu-Mn-V-O sorbent after sixth regeneration

112

Figure 7.23. XRD patterns of the Cu-Mn-O sorbent before and after reaction
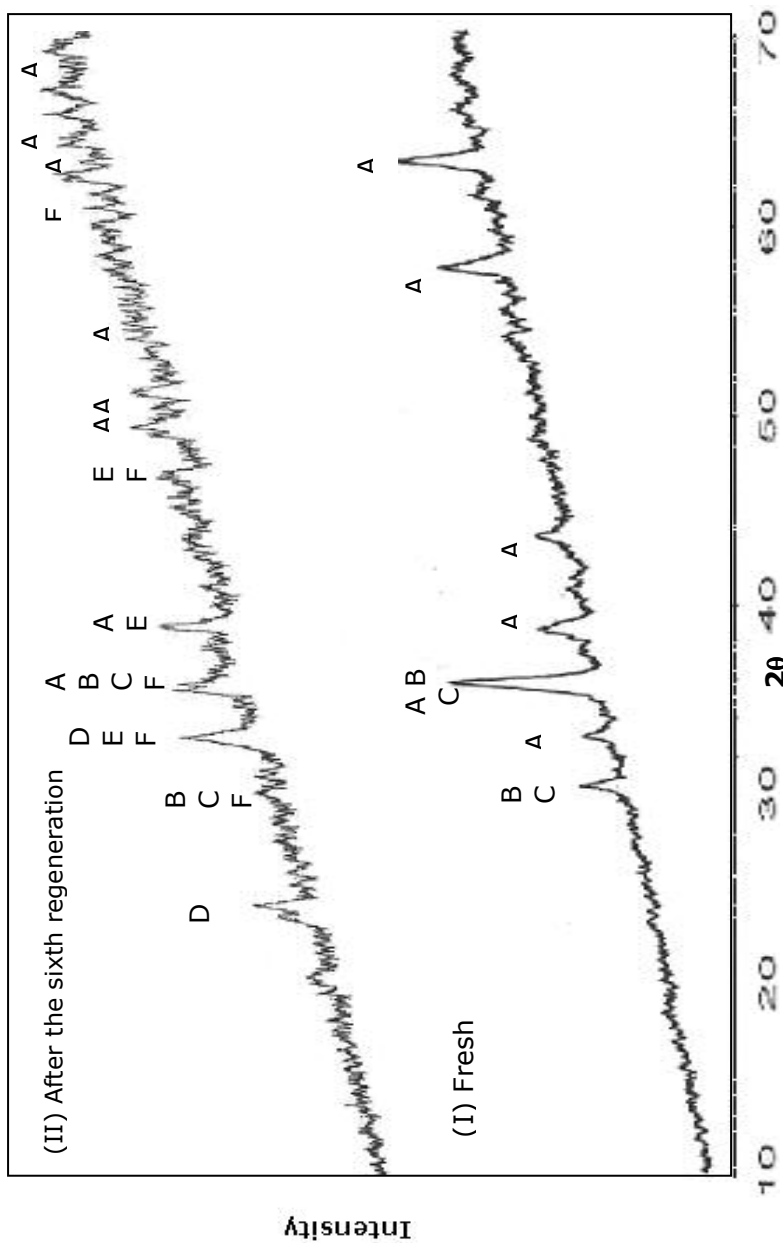
(A: CuO ; B: CuMn$_2$O$_4$; C: Cu$_{1.5}$Mn$_{1.5}$O$_4$; D: MnSO$_4$; E: Cu$_{1.96}$S ; F : Mn$_3$O$_4$)

113
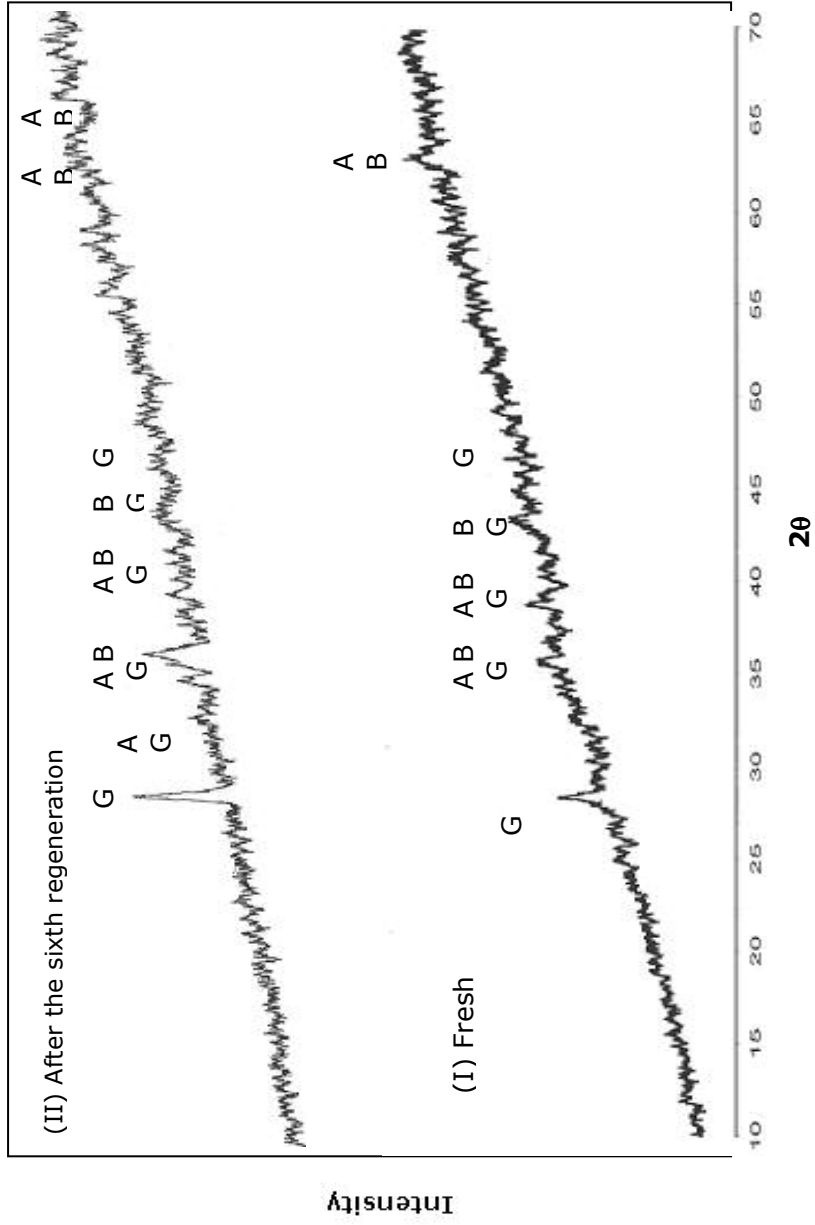
Figure 7.24. XRD patterns of the Cu-Mn-V-O sorbent before and after reaction

(A: CuO ; B: $CuMn_2O_4$; G: β-$Cu_2V_2O_7$)

As can be seen from Figure 7.23, the XRD pattern of the regenerated Cu-Mn-O sorbent, corresponding to samples extracted from the bed reactor in the sixth cycle is very similar to that of the fresh sorbent indicating that the most sulfides were converted into the initial phases of $Cu_{1.5}Mn_{1.5}O_4$, $CuMn_2O_4$, CuO with a little sulfate formation. The presence of $MnSO_4$ in the regenerated sorbent indicates that the sorbent reactivity decreases slightly as the number of cycles increases. Mn_3O_4, a nonexistent phase in the fresh sorbent, was also observed in the XRD of the regenerated Cu-Mn-O sorbent. The XRD results are also summurized in Table 7.21.

In the case of Cu-Mn-V-O sorbent, after the sixth regeneration process at 700 ^{o}C, the XRD pattern was almost the same as that of fresh Cu-Mn-V-O sorbent (Figure 7.24). The XRD results for Cu-Mn-V-O sorbent are also given in Table 7.21. As can be seen from the figure and table, it was found to be largely amorphous phase with some crystalline phase of CuO, $CuMn_2O_4$, and β-$Cu_2V_2O_7$.

From results obtained in XRD, therefore, it was concluded that vanadium promoted sorbent, Cu-Mn-V-O, prevented the sulfate formation and increased the regeneration capacity of Cu-Mn-O sorbent because it played an important role as the catalyst for oxidation.

The comparison of calculated XRD data with fresh sample XRD data and literature values are also given in Table E.2, Table E.3 and Table E.4 for regenerated Cu-Mn-O and Cu-Mn-V-O sorbents after sixth regeneration respectively.

Table 7.21. XRD Results of Cu-Mn-O and Cu-Mn-V-O Sorbents after the sixth regeneration process

Sorbent	XRD Identification
Cu-Mn-O	$CuMn_2O_4$, $Cu_{1.5}Mn_{1.5}O_4$, CuO, $MnSO_4$, $Cu_{1.96}S$, Mn_3O_4 and an amorphous phase
Cu-Mn-V-O	An amorphous phase, $CuMn_2O_4$, CuO, β-$Cu_2V_2O_7$

CHAPTER 8

CONCLUSIONS AND RECOMMENDATIONS

In this study, several copper-based sorbents, Cu-Mn-O, Cu-V-Mn-O and Cu-V-O, were prepared by using a complexation method. The reactivities of sorbents for hot coal gas desulfirization applications were studied in a packed-bed quartz micro reactor over 6 sulfidation/regeneration cycles. A sequence of sulfidation and regeneration reactions by using these sorbents was investigated under reducing atmosphere. Also, detailed study of characterization of the fresh sorbents was performed with the aid of Hg porosimetry, N_2 sorptometry, X-ray diffraction and Scanning electron microscopy. The change of crystallographic form of regenerated Cu-Mn-O and Cu-Mn-V-O sorbents from cycle 6 were followed by the powder X-ray diffraction method. Taking into account these characterization results, the reactivity and performance of copper-based sorbents in multicycle sulfidation/regeneration tests were investigated. Additionally, deactivation model was used for the prediction of breakthrough curves of H_2S in a fixed–bed reactor to confirm the experimental data and to calculate the rate parameters for each cycle. Major conclusions reached as a result of this work are,

1) XRD patterns of fresh sorbents indicated that the crystal structures of the Cu-Mn-O sorbent are consistent with $Cu_{1.5}Mn_{1.5}O_4$, $CuMn_2O_4$, CuO and an amorphous phase. The Cu-Mn-V-O sorbent consists of an amorphous phase while β-$Cu_2V_2O_7$ is the only detected phase in the Cu-V-O sorbent.

2) The sulfur retention capacity of the Cu-Mn-O sorbent decreased from 0.152 to 0.128 (g of sulfur)/(g of sorbent) during 6 sulfidation/regeneration cycles. The results indicated that the Cu-Mn-O sorbent efficiency didn't change much as the number of cycle increases.

Consequently, Cu-Mn-O sorbent prepared in this study removed sulfur without apparent performance decay during 6 sulfidation/regeneration cycles.

3) The sulfur retention capacity of the Cu-Mn-V-O sorbent decreased slightly from 0.110 to 0.054 (g of sulfur)/(g of sorbent) during 6 sulfidation/regeneration cycles. The results indicated that some loss of Cu-Mn-V-O sorbent efficiency was observed in cycles.

As the number of cycle increases breakthrough curves for Cu-Mn-V-O sorbent shifted left sligthly.

The decrease in conversion with successive cycles is predicted due to thermal sintering as well as loss of surface area which can be prevented by improving Cu-Mn-V-O sorbent regeneration conditions like choosing lower regeneration temperature (< 700 ^{o}C) or oxygen concentration (< %6 O_2).

4) During Cu-Mn-O and Cu-Mn-V-O sorbent regeneration the metal sulfide was reacted with oxygen to regenerate the metal oxide and liberate the sulfur as SO_2. At the end of each cycle about 1/3 of the adsorbed sulfur was emitted as

SO_2 in the exhaust gas while the rest of it was collected as elementary sulfur at the end of the reactor outlet.

5) Cu-V-O sorbent showed a very good performance in the first sulfidation at 627 ℃. The sulfur retention capacity of the Cu-V-O sorbent was 0.123 (g of sulfur)/(g of sorbent) at the end of the first sulfidation.

The results showed that excessive thermal sintering in the first regeneration at 700℃ prevented further sulfidation/regenration tests that can be explained with highly exothermic reaction between sulfided Cu-V-O sorbent and O_2 which complicates the reactor temperature control and may hasten sorbent deterioration.

To prevent the excessive thermal sintering in the first regeneration at 700℃ of Cu-V-O sorbent, experiment must be done below 650℃. Essentially high desulfurization, with V_2S_3 as the sulfided product, is predicted up to the melting temperature of V_2S_3 near 650℃. Moreover, SO_2 or steam can be used prevent the excessive thermal sintering during regeneration.

6) To confirm the results of the sulfidation experiments of prepared sorbents, sorption experiments repeated at the same operating conditions (%1 H_2S + %10 H_2 in balance He at 627 ℃). It was found that the repeated experimental results consistent with the results of the experiment carried out before.

7) Concerning the selectivity to elemental sulfur, it is interesting to observe that the selectivity was maintained almost constant around %98 and %99 for Cu-Mn-O and Cu-Mn-V-O sorbents even though the conversion is varied through the cycle number. Additionally, selectivity of Cu-V-O was %93 because of the SO_2 formation.

8) Additional chemical analysis of the solid products, Cu-Mn-O and Cu-Mn-V-O, obtained after the sixth regeneration experiment allowed the sulfur balance around the reactor to be verified. For this purpose, a Leco SC 132 sulfur analyzer was used.

Total sulfur amount in the Cu-Mn-O and Cu-Mn-V-O solid products obtained at the end of the sixth regeneration is 0.9×10^{-3} mol and 1.72×10^{-5} mol respectivelly. The results indicates that at the operating temperature of 700 ºC the sorbents are regenerated almost completely.

9) XPS analysis of the sorbents especially for Cu-V-O sorbent should be made before and after the reactions.

10) Although Cu-Mn-O and Cu-Mn-V-O sorbents were regenerated almost completely at 700 ºC, they showed different regeneration characteristics. It was observed for Cu-Mn-O sorbent that the concentration of SO_2 had a maximum value at approximately 10 min and then the outlet concentration of SO_2 slowly decreased gradually to the end.

In the case of Cu-Mn-V-O sorbent, however, it was found that most of the sulfur observed during sulfidation was desorbed over the process of regeneration at 700 ºC for a short time.

It was considered that a vanadium additive increased the regeneration capacity of Cu-Mn-O sorbent because it played an important role as the catalyst for oxidation.

11) At the end of the sixth regeneration experiment of Cu-Mn-O sorbent, under the operating condition used (700 ºC and %6 O_2 in balance N_2) $CuSO_4$ is unstable while $MnSO_4$ is stable, being the only sulfate phase presumably found in

the regenerated sorbent. Because the formed sulphate is inert with respect to the desulfurization and thus there is a loss of active material.

Low temperature and high oxygen concentration result in sulfate formation and a lower sulfur removal efficiency. Hence to prevent the presence of $MnSO_4$ the regeneration of Cu-Mn-O sorbent should be carried out above 900ºC or at lower oxygen concentration(<%6 O_2).

12) In sulfidation experiments conducted with Cu-Mn-O and Cu-Mn-V-O sorbents SO_2 formation was not observed while with Cu-V-O sorbent SO_2 formation was observed, indicating less sulfur loading capacity of Cu-V-O compared to Cu-Mn-O.

13) Regression analysis of the experimental breakthrough data obtained for H_2S sorption on prepared sorbents, Cu-Mn-O, Cu-Mn-V-O and Cu-V-O gave very good agreement with the breakthrough equation derived.

14) Variation in k_o values is predicted due to changes in chemical structure of sorbent after each sulfidation/regeneration cycles such as sintering of sorbent and sulfate formation during reaction can cause variation in k_o values.

15) XRD pattern of the regenerated Cu-Mn-O sorbent, corresponding to samples extracted from the bed reactor after the sixth cycle is very similar to that of the fresh sorbent indicating that the most sulfides were converted into the initial phases of $Cu_{1.5}Mn_{1.5}O_4$, $CuMn_2O_4$ and CuO with a little sulfate formation.

In the case of Cu-Mn-V-O sorbent, after the sixth regeneration process at 700 ºC, the XRD pattern was almost the same as that of fresh one. It was found

to be largely amorphous phase with some crystalline phase of CuO, $CuMn_2O_4$ and β-$Cu_2V_2O_7$.

16) From results obtained in XRD therefore, it was concluded that vanadium promoted sorbent, Cu-Mn-V-O, prevented the sulfate formation and increased the regeneration capacity of Cu-Mn-O sorbent because vanadium played an important role as the catalyst for oxidation.

17) Cu-Mn-V-O and Cu-Mn-O sorbents developed in this study exhibited promising properties as high temperature desulfurization sorbents. However, some further studies are recommended to improve and understand the reaction mechanisms beter:

• Sorbents with different vanadium loadings should be prepared and phsical and chemical analysis of these sorbents should be compleated for a better understanding of sorbent structure.

• XRD analysis of the sorbents at various steps of the sulfidation reaction should be carried out.

• The regeneration step is a highly exothermic oxidation process requiring careful temperature control. Regeneration studies should be carried out at different conditions to prevent thermal sintering of Cu-V-O sorbent.

18) Calcination should be made at the same temperature with reaction to observe the changes in chemical structure of prepared sorbents .

REFERENCES

Akyurtlu, A., and Akyurtlu, J., 1995, "Hot gas desulfurization with vanadium-promoted zinc ferrite sorbents", Gas Separation and Purification, Vol.9(1), pp.17-25.

Akyurtlu, A., 1996, "Mixed metal oxide sorbents", Presented in NATO Advanced Study Institude on Desulfurization of Hot Coal Gas with Regenerable Metal Oxide Sorbents: New Developments, Kuşadası, İzmir.

Al-Shamma, L.M., Naman, S.A., 1989, "Kinetic study for thermal production of hydrogen from H_2S by heterogeneous catalysis of vanadium sulfide in a flow system", Vol.14(3), pp.173-179.

Anderson, G.L., and Berry, F.O., 1987, "Development of a hot gas cleanup system", Proceedings of the 7 th Annual Gasification and Gas Stream Cleanup Systems Review Meeting, DOE/METC-87/6079 (DE87006496), Vol. II.

Atakül, H., Öner, G., Yardım, M.F., 1993, "Fluidized bed combustion in Turkey", Energy Sources, Vol.15, pp.1-15.

Atakül, H., Wakker, J.P., Gerritsen A.W., Van Den P., 1996, "Regeneration of MnO/γ-Al_2O_3 used for high temperature desulfurization of fuel gases", Fuel, Vol.75 (3), pp.373-378.

Ayala, R.E. and Venkataramani, V.S., "Development of sorbents for moving-bed and fluidized-bed applications, Volume:1 Development of sorbents for moving-bed", U.S. Department of Energy Federal Energy Technology Center, Morgantown, WV, September 1998, Final Report No. DE-AC21-94MC31089-02.

Atımtay, A.T., Gasper-Galvin L.D. and Poston J.A., 1993, "Novel supported sorbent for hot gas desulfurization", Environmental Science and Technology, Vol.27(7), pp.1295-1303.

Ayala, R.E., 1996a, "Application of IGCC technology in power generation", NATO/ASI, 7-19 Temmuz, Kuşadası, İzmir, Türkiye.

Ayala, R.E., 1996b, "Assesment of coal gasification processes-relevance to sorbent development", Presented in NATO Advanced Study Institude on Desulfurization of Hot Coal Gas with Regenerable Metal Oxide Sorbents: New Developments, Kuşadası, İzmir.

Bagajewicz, M.J., Tamhankar, S.S., Flytzani-Stephanopoulos M. And Gavalas G.R., 1988, "Hydrogen sulfide removal by supported vanadium oxide", Environ. Sci. And Tech., Vol.22 (4), pp.467-470.

Balcı, S., 1992, "Kinetics of Activated carbon production from Almond Shell, Hazelnut Shell and Beech Wood and characterization of products", Ph. D. Thesis, Middle Technical University, Depertmant of Chemical Engineering.

Barrin, I. And Knacke, O., 1973, "Thermochemical Properties of Inorganic Substances", Springer Verlag, Berlin.

Barrin, I., 1989, "Thermochemical data of pure substances", VCH Verlagsgesellschaft, Weinheim, Germany.

Ben-Slimane, R., Hepworth, M.T., 1994a, "Desulfurization of hot gases with manganese based regenerable sorbents. 1.Loading (sulfidation) tests", Energy and Fuels, Vol.8 (6), pp.1175-1183.

Ben-Slimane, R., Hepworth, M.T., 1994b, "Desulfurization of hot gases with manganese based regenerable sorbents. 2. Regeneration and multicycle tests", Energy and Fuels, Vol.8 (6), pp.1184-1191.

Ben-Slimane, R., Hepworth, M.T., 1995, "Desulfurization of Hot Gases with Manganese Based Regenerable Sorbents. 3. Fixed-Bed Testing, Energy and Fuels", Vol.9 (2), pp.372-378.

Copeland, R.J., et al., 1994, "High temperature hydrogen sulfide removal with stannic oxide", Proceedings of the Coal-Fired Power Systems Advances in IGCC and PFBC Review Meeting, DOE/METC-94/1008 (DE94012252), Vol. I, pp.444.

De Moss, T.B., 1997, "Deregulation can play savior or spoiler for clean coal progress", Power Engineering, January.

Derinöz, C., 1998, "Development of a novel sorbent for hot gas desulfurization", Master Thesis, ODTÜ, Ankara.

Derinöz, C. And Atımtay A., 1997, "Hava kirliliğini azaltacak yeni enerji dönüşüm teknolojileri ve kükürtlü hidrojen gazının absorplanması için geliştirilen sorbentler", Yanma ve Hava Kirliliği Kontrolü IV. Ulusal Sempozyumu, Antalya, Türkiye, pp.219-229.

Efthimiadis, E.A., Sotirchos, S.V., 1993, "Effects of pore structure on the performance of coal gas desulfurization sorbents", Chemical Engineering Science, Vol.48, No.1, pp. 1971-1984.

Elseviers, W.F., Verelst, H., 1999, "Transition metal oxides for hot gas desulfurization", Fuel, Vol.78, pp.601-612.

Flytzani-Stephanopoulos, M., Tamhankar, S. S., Sharma, P. K. and Gavalas, G. R., "Novel sorbents for high-temperature regenerative H_2S removal," Jet Propulsion Laboratory Final Report No. DOE/MC/20417-1898, October 1985.

Flytzani-Stephanopoulos, M. et al., Final Report to DOE, DOE/MC22193-2582, October 1987.

Garcia, E., Cilleruelo C., Ibarra J.V., Pineda M. and Palacios J.M., 1997, "Kinetic study of high-temperature removal of H_2S by novel metal oxide sorbents", Ind.Eng.Chem.Res., Vol.36, pp.846-853.

Gasper-Galvin, L.D., Atımtay A.T. and Gupta R.P., 1998, "Zeolite-supported metal oxide sorbents for hot gas desulfurization", Ind.Eng.Chem.Res., Vol.37, pp.4157-4166.

Grindley, T., and Steinfeld, G., 1981, "Development and testing of regenerable gas desulfurization sorbents", DOE/MC/16545-1125.

Harrison, D.P., 1995, "Control of gaseous contaminants in IGCC processes, an overview", Pittsburgh Coal Conference, Pittsburgh, Pennsylvania.

Harrison, D.P., 1996, "Performance Analysis of ZnO-based sorbents in removal of H_2S from fuel gas", Presented in NATO Advanced Study Institude on Desulfurization of Hot Coal Gas with Regenerable Metal Oxide Sorbents: New Developments, Kuşadası, İzmir.

Huang, J. H.; Rosen, E.,1992, "Solid state emf studies of equilibria in the Mn-S-O system at 900 K-1300 K", Scand. J. Metall., Vol.21 (3), pp.116-120.

Ingraham, T. R. ,1966, Thermodynamics of the Mn-S-O system between 1000 °K and 1250 °K, Can.Metall. Q., Vol.5, pp.109-122.

Joshi, D.K., et al.,1979, "Hot low-Btu producer gas desulfurization in fixed-bed of Iron oxide fly ash", DOE/FE-2257-3.

Jun, H.K., Lee, T.J., Ryu, S.O., and Kim, J.C., 2001, A study of Zn-Ti based H_2S removal sorbents promoted with cobalt oxides, Ind. Eng. Chem. Res., Vol.40, pp.3547-3556.

Kay, D.A.R., and Wilson, W.G., 1989, "Method for the regeneration of sulfided cerium oxide back to a form that is again capable of removing sulfur from fluid materials", U.S. Patent 4,857,280.

Kay, D.A.R., et al., 1993, "High temperature thermodynamics and application of rare earth compounds containing oxygen and sulfur in fuel gas desulfurization and SO_x and NO_x removal", J. Of Alloys and Compounds, Vol.192, pp.11.

Lee H.S., Kang M.P., Rhee Y.M., 2001 "Effect of Fe_2O_3 additive on reactivities of CuO-based sorbents", In: The 7th International Joint Symposium of Beijing University of Chemical Technology and Chungnam National University, Beijing, China, pp.43.

Lew, S., Jothimurugesan, K. and Flytzani-Stephanopoulos, M., 1989, "High temperature H_2S removal from fuel gases by regenerable zinc oxide-titanium dioxide sorbents", Ind. Eng. Chem. Res., Vol.28, pp.535.

Li, Z. Ve Flytzani-Stephanopoulos M., 1997, "Cu-Cr-O and Cu-Ce-O regenerable oxide sorbents for hot gas desulfurization", Ind.Eng.Chem.Res., Vol.36, pp.187-196.

Liang, B., Korbee, R., Gerritsen, A.W., Van den Bleek, C.M., 1999, "Effect of manganese content on the properties of high temperature regenerative H_2S acceptor", Fuel, Vol.78, pp.319-325.

Marcilly, C., Courty, P., Delmon, B., 1970, "Preparation of highly dispersed Mixed oxides and oxide solid solutions by pyrolysis of amorphous organic precursors", J. Am. Ceram. Soc., Vol.53, pp.56.

Nielsen, P.E.H., et al.,1991, "Steam regenerable sulfur absorption masses and their application in IGCC plants", paper presented at EPRI Coal Gasification Conference, San Francisco.

Patrick, V., Gavalas, G. R., Flytzani-Stephanopoulos, M. and Jothimurugesan, K.,1989, "High temperature sulfidation-regeneration of $CuO-Al_2O_3$ sorbents", Ind. Eng. Chem. Res., Vol.28, pp.931-940.

Patrick, V. And Gavalas, G.R., 1993, "Reduction, sulfidation and regeneration of mixed ıron-aluminum Oxide sorbent", Industrial and Engineering Chemistry Research, Vol.32, pp.519.

Perry, H.R., and C.H. Chilton, 1973, "Chemical Engineer's Handbook", 5th. Edition. McGraw-Hill, New York.

Sage, P.W., 1996a, "World energy resources, their use and environment", NATO/ASI, 7-19 Temmuz, Kuşadası, İzmir, Türkiye.

Sage, P.W. and Mills S.J., 1996b, "Overview of clean technologies and current status of the air blown gasification cycle", NATO/ASI, 7-19 Temmuz, Kuşadası, İzmir, Türkiye.

Schrodt, J.T., and Best, J.E., 1978, "Sulfur recovery from fuel gas desulfurization sorbent", AIChE Symposium Series, Vol.74 (175), pp.189.

Skeaff, J. M.; Espelund, A. W., 1973, "An E.M.F. method for the determination of sulphate-oxide equilibria results for the Mg, Mn, Fe, Ni, Cu and Zn systems", Can. Metall. Q. ,Vol.12, pp. 445-454.

Slimane, R.B., Abbasian, J., 2000, "Regenerable mixed metal oxide sorbents for coal gas desulfurization at moderate temperatures", Vol.4, pp.147-162.

Sohn, H.Y., and Kim, D., 1987, "Intrinsic kinetics of the reaction between zinc sulfide and water vapor", Metal. Trans. B., Vol.18B, pp.451.

Suyadal, Y., Erol, M., Oğuz, H., 2000, "Deactivation model for the adsorption of Trichloroethylene vapor on an activated carbon bed", Ind. Eng. Chem. Res., Vol.39, pp.724.

Tamhankar SS, Hasatani M, Wen CY., 1981, "Kinetic studies on the reactions involved in the hot gas desulfurization using a regenerable iron oxide sorbent", Chem. Eng. Sci., Vol.36, pp.1181-91.

Tamhankar, S.S., et al., 1985, "Kinetic study of the reactions ınvolved in hot gas desulfurization using a regenerable Iron oxide sorbent III. Reaction of the sulfided sorbent with steam and steam-air mixtures", Chemical Engineering Science, Vol.40, pp.1019.

Tamhankar S.S., Bagajewicz M., Sharma P.K. and Flytzani-Stephanopoulos M., 1986, "Mixed oxide sorbents for high temperature removal of hydrogen sulfide", Ind.Eng.Chem.Process Des.Dev., Vol.25, pp.429-437.

Tseng, S.C., et al., 1981, "Kinetic studies on the reactions involved in hot gas desulfurization using a regenerable iron oxide sorbent II. Reactions of iron sulfide with oxygen and sulfur dioxide", Chemical Engineering Science, Vol.36, pp.1287.

Turkdoğan, E. T.; Olsson, R. G.; Vinters, J. V., 1977, "Sulfate and sulfide reactions in the Mn-S-O system", Metall. Trans., Vol.8B, pp.59-65.

Turkdogan, E.T. and Olsson, R.G., April 16-20, 1978, " Desulfurization of hot reducing gases with mangasese oxide pellets", Proceedings of the Third Inı'ı Iron and Steel Congress, Chicago, Vol.II, pp.277-288.

Van Der Ham, A.G.J., Vanderbosch, R.H., Prins, W., Van Swaaji, W.P.M., 1996b, "Desulfurization process of fuel gas and stagewise desulfurization", Presented in NATO Advance Study Institute on Desulfurization of Hot Coal Gas with Regenerable Metal Oxide Sorbents: New Developments, Kuşadası, İzmir.

Van Der Ham, A.G.J., Heesink, A.B.M., Prins, W., Van Swaaij, W.P.M., 1996a, "Proposal for a regenerative high temperature process for coal gas cleanup with calcined limestone", Ind. And Eng. Chem. Res., Vol.35 (5), pp.1487-1495.

Van der Wal, W.J.J., 1987, "Desulfurization of process gas by means of iron oxide on silica sorbents", Ph.D. Dissertation, University of Utrecht.

Yasyerli, S., 2001, "Kimyasal proseslerde oluşan H_2S'in yenilenebilir adsorbentler ile tutulması", Ph.D. Thesis, Gazi University, Ankara.

Yasyerli, S., Doğu, T., Doğu, G., Ar, I., 2001, Activities of copper oxide and Cu-V and Cu-Mo mixed oxides for H_2S removal in the presence and absence of hydrogen and prediction of a deactivation, Ind. Eng. Chem. Res., Vol.40, pp.5206.

Zhang J., Wang Y., Wu D., 2003, "Effect investigation of ZnO additive on Mn-Fe/γ-Al_2O_3 sorbents for hot gas desulfurization", Energy Conversion and Management, Vol.44, pp.357-367.

Wakker, J.P., et al., 1993, "High temperature H_2S and COS removal with MnO and FeO on γ-Al_2O_3 acceptors", Industrial and Engineering Chemistry Research, Vol.32, pp.139.

Watkinson, A.P., Lucas J.P., Lim, C.Y., 1991, "A Prediction of Performance of Commercial Coal Gasifier", Fuel, Vol.70, April, pp.519-609.

Westmoreland, P.W., and D. P. Harrison. 1976, "Evaluation of candidate solids for high-temperature desulfurization of low-Btu gases". Env. Sci. Tech., Vol.10, pp.659.

Wheast, R.C., and M.J. Astle, 1978, "CRD Handbook of Chemistry and Physics", CRD Press, Inc. West Palm Beach, Florida, 33409.

APPENDIX A

CALIBRATION OF FTIR DEVICE WITH H$_2$S AND SO$_2$

Exit gas compositions from the outlet of the packed reactor were analyzed by FTIR Spectrometer. Calibration graph of FTIR with SO$_2$ and H$_2$S are given in Figure A.1 and Figure A.2 respectively.
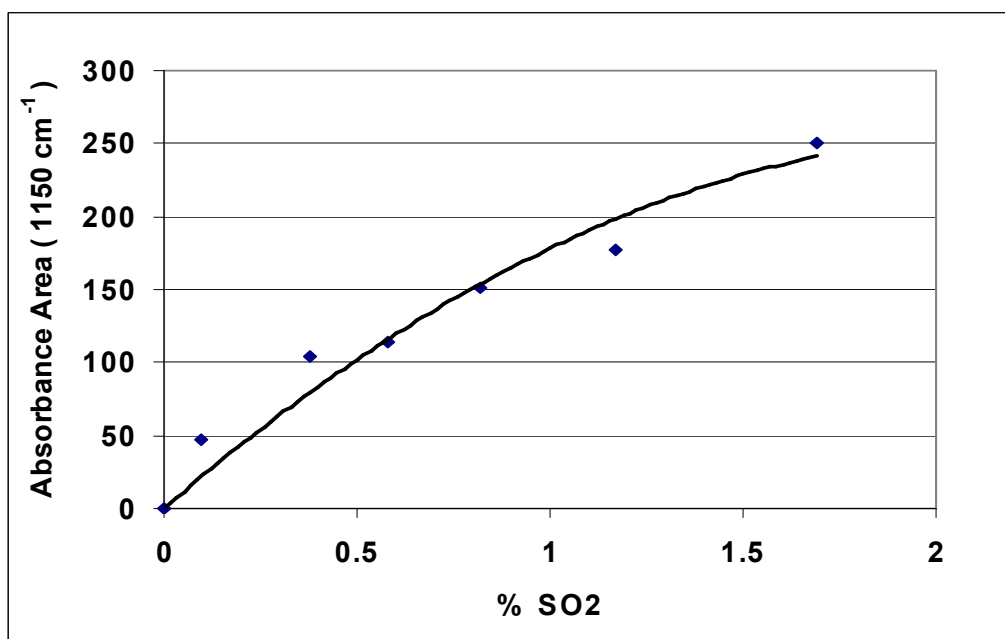
Figure A.1. Calibration graph of FTIR with SO$_2$
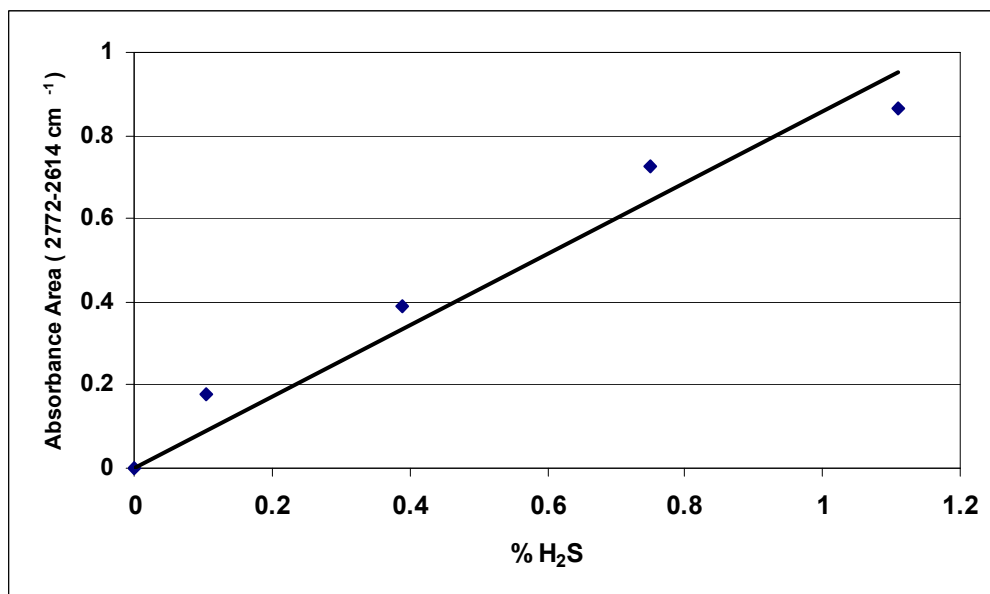
Figure A.2. Calibration graph of FTIR with H_2S

APPENDIX B

CALIBRATION OF FTIR DEVICE WITH H_2O

B.1 Followed Procedure of FTIR Calibration with H_2O

H_2O gas taken from the outlet of reactor was analysed by FTIR. How to make calibration is summarized step by step in the following.

1.   While carrier gas (He) passing through the gas cell, the humidity in the gas cell is removed by heating it up to 110 ^{o}C.

2.   Reference spectrum is taken after the device reach to steady state. All of the flow lines between the FTIR spectrometer and the wet gas are heated to eliminate any condensation.

3.   Before taking the absorbance spectrum, wet gas prepared in known amount is send to the FTIR.

4.   This procedure is repeated for each different amount of wet gas prepared. Then, the calibration graph of % H_2O versus absorbance area is drawn.

B.2 Sample calculation for finding the amount of wet gas prepared

The amount of wet gas prepared was calculated by using the following method.

1.   Flow rate of wet gas = 30.94 ml/min

2.   Total (dry+wet) flow rate of He = 191 ml/min

$$= (191 \text{ ml/min}) \times (1 \text{ mol/22400 ml}) = 0.0085 \text{ mol/min}$$

3.   Amount of adsorbed H_2O by $MgClO_4$ in 15 min = 0.043 gr.

4. H_2O = 0.00029 gr/min = 0.000016 mol/min

5.   % H_2O = [(0.000016 mol/min)/(0.0085 mol/min)]x100

$$= \% \ 0.19$$

Calibration graph of FTIR with H_2O is given in Figure B.1.
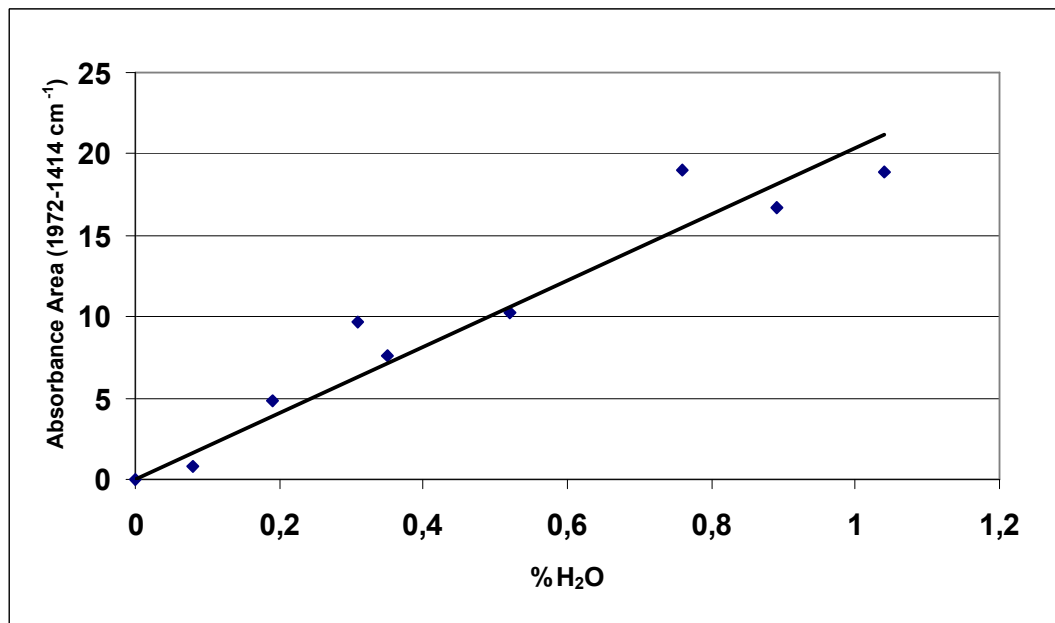
Figure B.1. Calibration graph of FTIR with H_2O

APPENDIX C

CALIBRATION OF GAS CHROMATOGRAPH WITH H$_2$S

Exit H$_2$S gas composition from the outlet of the packed reactor were analyzed by using gas chromatograph. Calibration graph of GC with H$_2$S is given in Figure C.1.
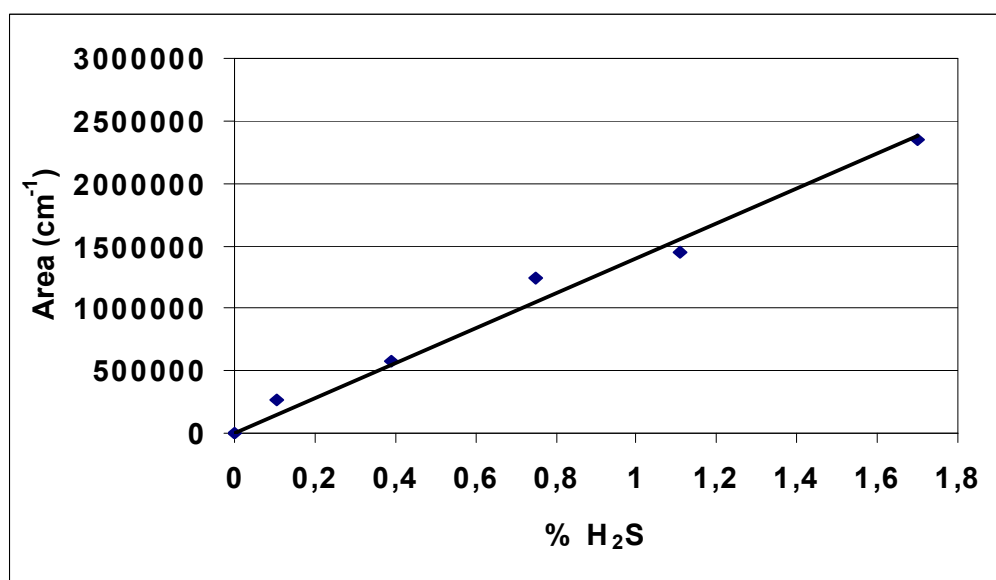
Figure C.1. Calibration graph of GC with H$_2$S

APPENDIX D

PREPARATION AND TESTING OF PORAPAK-T GAS CHROMATOGRAPH ADSORPTION COLUMN

Porapak-T adsorption column was prepared and tested to analyze the H_2S and SO_2 exit gases from outlet of the quartz-micro reactor. In order to determine the separation conditions of the reactor outlet gas analysis were done at different column and detector temperatures and at different carrier gas (He) flow rates. As column and detector temperature 80, 100, 150^oC and 150, 200^oC were tried respectively.The best chromatograms were obtained at 80^oC for column and 200^oC for detector. In addition, at different carrier gas flow rates, 30, 40, 60 cm^3/min He, the best carrier gas flow rate was found as 60 cm^3/min Separate peaks for H_2S and SO_2 were obtained from chromotograms at 2.2 min and at 5.6 min respectively. The chromatograms taken from GC for H_2S and SO_2 were given in Figure D.1 and Figure D.2 respectively.

Properties of the Porapak T adsorption column and sample calculation to prepare column are given in the following**.**

Porapak T

Composition : Ethyleneglycoldimethacrylate (EGDM)

Maximum Operating Temperature : 165 ^oC

Surface Area : 250 m^2/g

Tapped Bulk Density : 0.381 g/cc

Polaraty : 10

Stainless Steel

Inner Diameter : 2.2 mm

Outer Diameter : 1/8 in : 3.18 mm

Length : 184 cm

Sample Calculation to Prepare Porapak-T Adsorption Column

V (porapak T) = 0.55 x V (stainless steel)

V (stainless steel) = (ID^{2}π/4) x 184cm = 6.994 cm^3

V (porapak T) = 0.55 x 6.994 cm^3 = 3.85 cm^3

m (porapak T) = ρ (porapak T) x V(porapak T)

$\quad\quad\quad\quad$ = 0.381 g/cc x 3.85 cc

$\quad\quad\quad\quad$ = 1.47 g
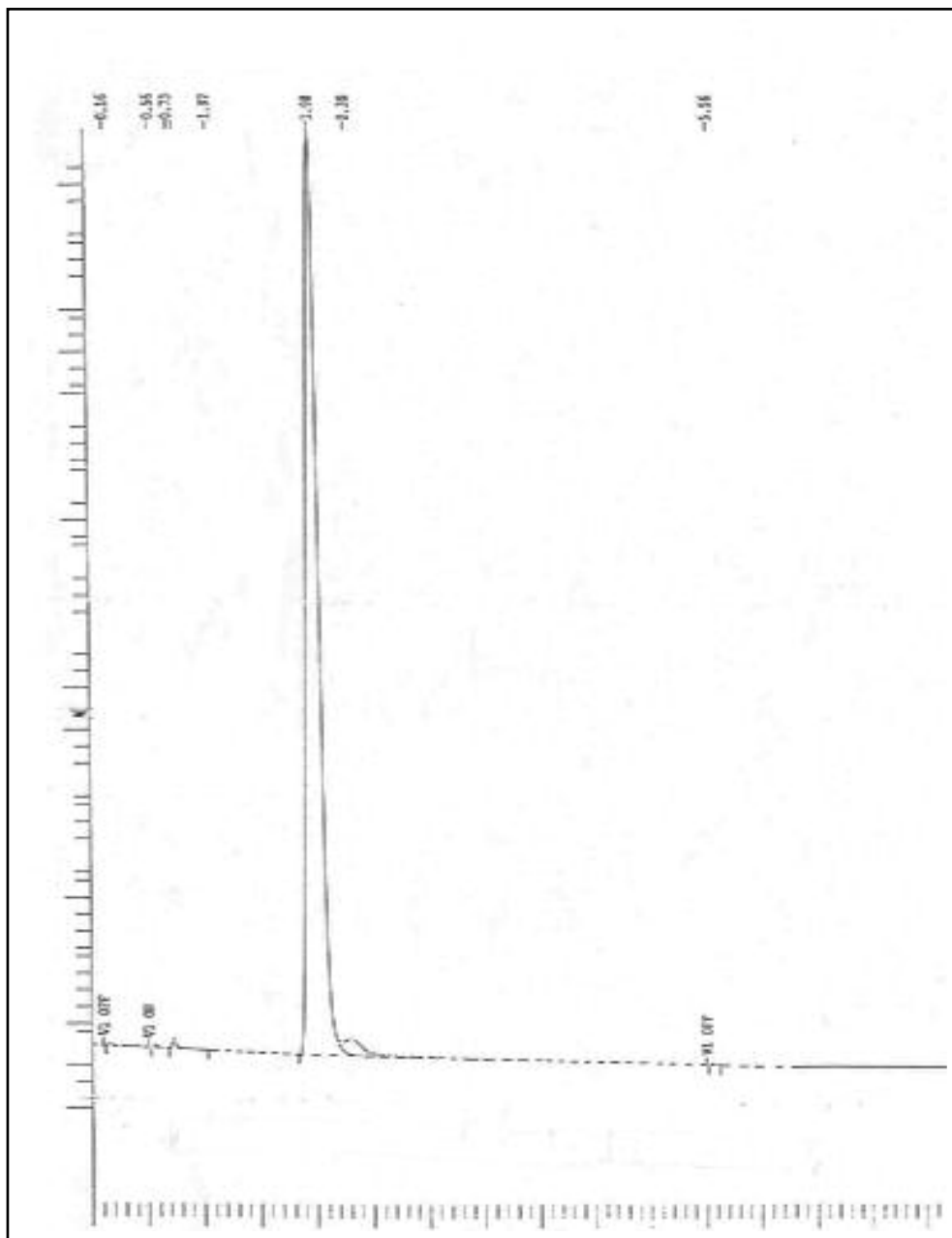
Figure D.1. H$_2$S chromatogram taken from GC
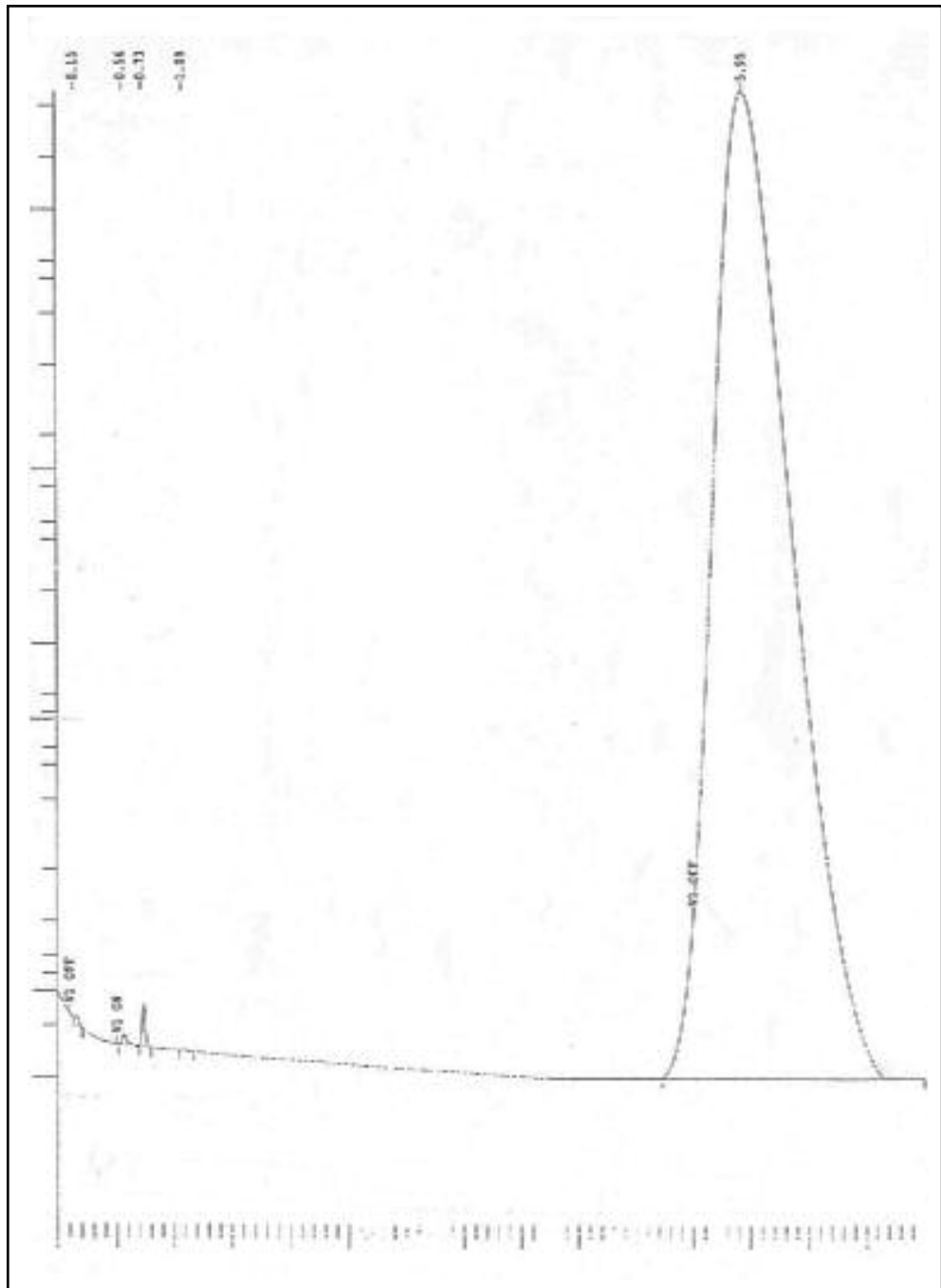
Figure D.2. SO$_2$ chromatogram taken from GC

137

APPENDIX E

COMPARISON OF CALCULATED XRD DATA WITH

LITERATURE ONE FOR PREPARED FRESH SORBENTS

Table E.1. Comparison of calculated XRD data with literature one for fresh Cu-V-O Sorbent

β-$Cu_2V_2O_7$ (26-569)			Cu-V-O (Sample)		
d	I/I_o	2θ	d	I/I_o	2θ
5.34	80	16.59	5.317	19.3	16.66
4.21	40	21.09	-	-	-
4.11	40	21.60	4.103	9.6	21.64
3.98	10	22.32	4.021	7.2	22.09
3.68	40	24.17	3.633	10.8	24.48
3.60	100	24.71	3.596	100	24.74
3.160	20	28.22	3.114	16.8	28.64
3.09	100	28.87	-	-	-
3.06	100	29.16	3.057	100	29.19
2.771	10	32.28	2.775	14.5	32.23
2.641	60	33.92	2.634	27.7	34.01
2.494	40	35.98	2.514	7.2	35.69
2.459	20	36.51	2.487	18.0	36.09
2.405	10	37.36	2.418	14.5	37.16
2.365	60	38.02	2.364	25.3	38.04
2.349	10	38.29	-	-	-
2.302	80	39.10	2.296	26.5	39.21
2.111	80	42.80	2.100	18.1	40.16
2.088	80	43.30	2.084	22.9	43.39
2.057	40	43.98	-	-	-

1.955	10	46.41	-	-	-
1.946	10	46.64	-	-	-
1.852	20	49.16	1.842	37.3	49.44
1.835	60	49.64	-	-	-
1.824	10	49.96	-	-	-
1.778	40	51.35	1.776	19.3	51.42
1.740	10	52.55	-	-	-
1.693	60	54.13	-	-	-
1.674	40	54.79	-	-	-
1.642	10	55.95	-	-	-
1.606	80	57.32	1.603	38.6	57.42
1.564	20	59.01	1.563	27.7	59.07
1.560	20	59.18	-	-	-

Table E.2. Comparison of calculated XRD data with literature one for fresh Cu-Mn-O Sorbent

$Cu_{1.5}Mn_{1.5}O_4$ (P35-1172)			$CuMn_2O_4$ (P34-1400)		
d	I/I_o	2θ	d	I/I_o	2θ
4.82	6	18.39	4.82	10	18.39
2.934	30	30.44	2.957	40	30.20
2.492	100	36.01	2.522	100	35.57
2.396	9	37.51	2.412	4	37.25
2.071	20	43.67	2.09	18	43.25
1.693	14	54.13	1.705	8	53.72
1.594	50	57.80	1.609	25	57.21
1.457	60	63.83	1.477	30	62.87
1.312	6	71.91	1.322	2	71.30
1.264	14	75.09	1.275	5	74.34
1.247	9	76.30	1.207	1	79.31
1.197	4	80.11	1.117	4	87.20
1.17	2	82.35	1.089	9	90.04
1.106	7	88.29	-	-	-
1.079	20	91.11	-	-	-
1.037	8	95.94	-	-	-

Table E.2. (continued)

CuO/Tenorite-syn (P41-0254)			Cu-Mn-O (Sample)		
d	I/I$_o$	2θ	d	I/I$_o$	2θ
2.752	8	32.53	2.935	26	30.43
2.531	60	35.45	2.699	20	33.16
2.524	100	35.59	2.500	100	35.89
2.311	100	38.96	2.318	34	38.82
1.960	3	46.28	2.176	12	41.37
1.866	25	48.65	2.070	16	43.72
1.712	7	53.55	1.689	18	54.28
1.581	12	58.36	1.631	14	56.36
1.506	16	61.35	1.594	46	57.81
1.417	12	65.70	1.491	16	62.26
1.409	14	66.23	1.466	58	63.39
1.378	9	67.86	1.407	16	66.41
1.375	14	68.42	1.367	16	68.6
1.304	6	72.67	1.293	16	73.12
1.265	6	74.68	1.260	16	75.35
1.262	7	75.37	-	-	-
1.196	2	79.87	-	-	-
1.169	4	82.35	-	-	-
1.161	4	83.22	-	-	-
1.155	4	84.11	-	-	-
1.124	2	86.91	-	-	-
1.091	5	89.93	-	-	-

Table E.3. Comparison of calculated XRD data with fresh sample XRD data and literature one for Cu-Mn-O sorbent after sixth regeneration

Cu-Mn-O (after sixth regeneration)			Cu-Mn-O (Sample)		
d	I/I$_o$	2θ	d	I/I$_o$	2θ
3.693	56	24.08	-	-	-
2.938	29	30.40	2.935	26	30.43
2.712	80	33.00	2.699	20	33.16
2.534	100	35.40	2.500	100	35.89
2.387	31	37.65	2.318	34	38.82

d	I/I$_o$	2θ	d	I/I$_o$	2θ
2.320	92	38.80	-	-	-
2.199	39	41.00	2.176	12	41.37
2.090	39	43.20	2.070	16	43.72
1.865	86	48.80	1.689	18	54.28
1.802	81	50.60	-	-	-
1.629	42	56.65	1.631	14	56.36
1.595	47	57.75	1.594	46	57.81
1.562	42	59.10	-	-	-
1.504	92	61.60	-	-	-
1.476	61	62.90	1.491	16	62.26
1.441	67	64.65	1.466	58	63.39
1.414	64	66.00	1.407	16	66.41
1.410	19	66.20	-	-	-
1.378	56	68.00	1.367	16	68.60
1.350	50	69.60	1.293	16	73.12

Table E.3. (continued)

MnSO$_4$ (main three peaks)*			Mn$_2$O$_3$ (P06-0540)		
d	I/I$_o$	2θ	d	I/I$_o$	2θ
-	-	-	4.93	40	17.98
-	-	-	3.08	60	28.97
3.70	70	24.03	2.74	70	32.66
2.70	100	33.15	2.48	100	36.19
2.39	40	37.60	2.39	40	37.60
-	-	-	2.03	20	44.60
-	-	-	1.83	30	49.79
-	-	-	1.79	20	50.98
-	-	-	1.59	30	57.95
-	-	-	1.55	60	59.60

Table E.3. (continued)

Cu$_{1.96}$S (main three peaks)*		
d	I/I$_o$	2θ
2.74	100	32.7
2.30	80	39.1
1.99	40	45.5

* From Powder Diffraction File Alphabetical Index, Inorganic Phases, 1989.

Table E.4. Comparison of calculated XRD data with fresh sample XRD data for
Cu-Mn-V-O sorbent after sixth regeneration

Cu-Mn-V-O (after sixth regeneration)			Cu-Mn-V-O (Sample)		
d	I/I_o	2θ	d	I/I_o	2θ
3.160	100	28.22	3.147	100	28.34
2.769	29	32.30	-	-	-
2.620	40	34.20	2.512	77	35.72
2.520	67	35.60	2.508	83	35.77
2.372	29	37.90	2.319	88	38
2.092	19	43.20	2.081	77	43.44
1.996	25	45.40	1.986	38	45.65
1.940	23	46.80	1.947	54	46.61
1.587	38	58.05	1.587	80	58.08
1.472	21	63.10	1.475	92.3	62.97
1.422	35	65.60	-	-	-
1.384	37	67.65	-	-	-

APPENDIX F

MERCURY-POROSIMETRY DATA AND CALCULATION OF POROSITY

The porosities of sorbents and the distribution of the pore volumes were determined by Quantachrome Hg-porosimeter. The original porosimeter data and porosity calculation of each sorbents are given in the following.

F.1 Sorbent: Cu-Mn-O

F.1.1 Porosity Calculation

ρ_{Hg}= 13.5681 g/cc   (T = 11°C)

1. Sample Weight = 0.2013 g

2. Penetrometer + Sample Weight = 36.5803 g

3. Penetrometer + Sample + Hg Weight = 87.4237 g

4. Hg Weight = 87.4237-36.5803 = 50.8434 g

5. Hg Volume (Hg Weight / ρ_{Hg}) = 3.7473 cc

6. Penetrometer Volume = 3.8863 cc

7. Sample Volume (Pen. Vol.–Hg Vol.) = 0.139 cc

8. Bulk Density (1/7) = 1.4482 g/cc

9. Apparent (Skeletal) Density = 6.2130 g/cc (taken from Hg porosimetry)

10. Total Intruded Vol. = 0.5296 cc/g

11. Porosity Calculation

$$\varepsilon = 1 - \frac{\rho_{bulk}}{\rho_{apparent}}$$

ε = 0.77

F.1.2 Check: Calculation of Apparent Density

1. Pore Vol. = Total Intruded Vol. x Sample Weight

$\qquad$ = 0.5296 cc/g x 0.2013 g

$\qquad$ = 0.1066 cc

2. Solid Vol. = Sample Vol. – Pore Vol.

$\qquad$ = 0.139cc – 0.1066 cc

$\qquad$ = 0.0324 cc

3. Apparent Density **=** Sample Weight / Solid Vol.

$\qquad$ = 0.2013/0.0324

$\qquad$ = 6.2130 g/cc

F.1.3 Average Pore Radius Calculation

The values of the average pore radius can be evaluated from pore volume vs. radius data. The expression used for calculation is given below.

$$r(nm) = \frac{\sum r \times \Delta V}{V}$$

r : Pore radius

V : Intruded vol. Hg.

The original mercury porosimetry data for Cu-Mn-O are given in Table F.1.

The Surface Area vs. Radius graph taken from mercury porosimetry is also given in Figure F.1.

Table F.1. The Original Mercury Porosimetry Data for Cu-Mn-O

INTRUSION DATA

PRESSURE PSIA	PORE RADIUS nm	INTRUDED VOL Hg cc/g	% VOLUME INTRUDED %	dV/dP cc/(PSIA-g)	dV/dlogP cc/g	Ds(r) m²/(nm-g)	CUMULATIVE SURF AREA m²/g
33	3232.15	0.0124	2.35	2.73E-04	2.75E-02	1.73E-06	0.000
75	1422.15	0.1436	27.11	5.76E-03	9.65E-01	3.86E-06	0.155
120	888.84	0.3467	65.48	2.44E-03	6.42E-01	7.04E-06	0.506
187	570.38	0.4148	78.33	5.54E-04	2.21E-01	5.96E-06	0.683
252	423.26	0.4332	81.80	1.66E-04	9.50E-02	4.59E-06	0.767
323	330.22	0.4411	83.30	9.77E-05	7.11E-02	5.58E-06	0.810
401	265.99	0.4471	84.43	7.06E-05	6.52E-02	7.82E-06	0.850
519	205.51	0.4536	85.65	5.02E-05	5.96E-02	1.21E-05	0.906
735	145.12	0.4600	86.87	2.76E-05	4.67E-02	1.88E-05	0.981
1048	101.76	0.4665	88.09	1.82E-05	4.29E-02	3.52E-05	1.087
1527	69.85	0.4729	89.31	1.06E-05	3.66E-02	6.35E-05	1.240
2412	44.22	0.4794	90.53	7.20E-06	3.94E-02	1.69E-04	1.476
3317	32.16	0.4858	91.74	9.45E-06	7.19E-02	6.01E-04	1.826
4158	25.65	0.4928	93.06	8.77E-06	6.38E-02	1.09E-03	2.315
4976	21.44	0.5002	94.47	8.28E-06	9.40E-02	1.74E-03	2.954
5895	18.09	0.5067	95.68	6.50E-06	8.69E-02	2.25E-03	3.612
7039	15.15	0.5127	96.81	5.10E-06	8.21E-02	3.02E-03	4.329
9769	10.92	0.5191	98.03	1.49E-06	3.36E-02	2.36E-03	5.315
21237	5.02	0.5266	99.44	4.25E-07	1.78E-02	5.68E-03	7.283

Average Pore Radius **r (nm) = 814 nm**
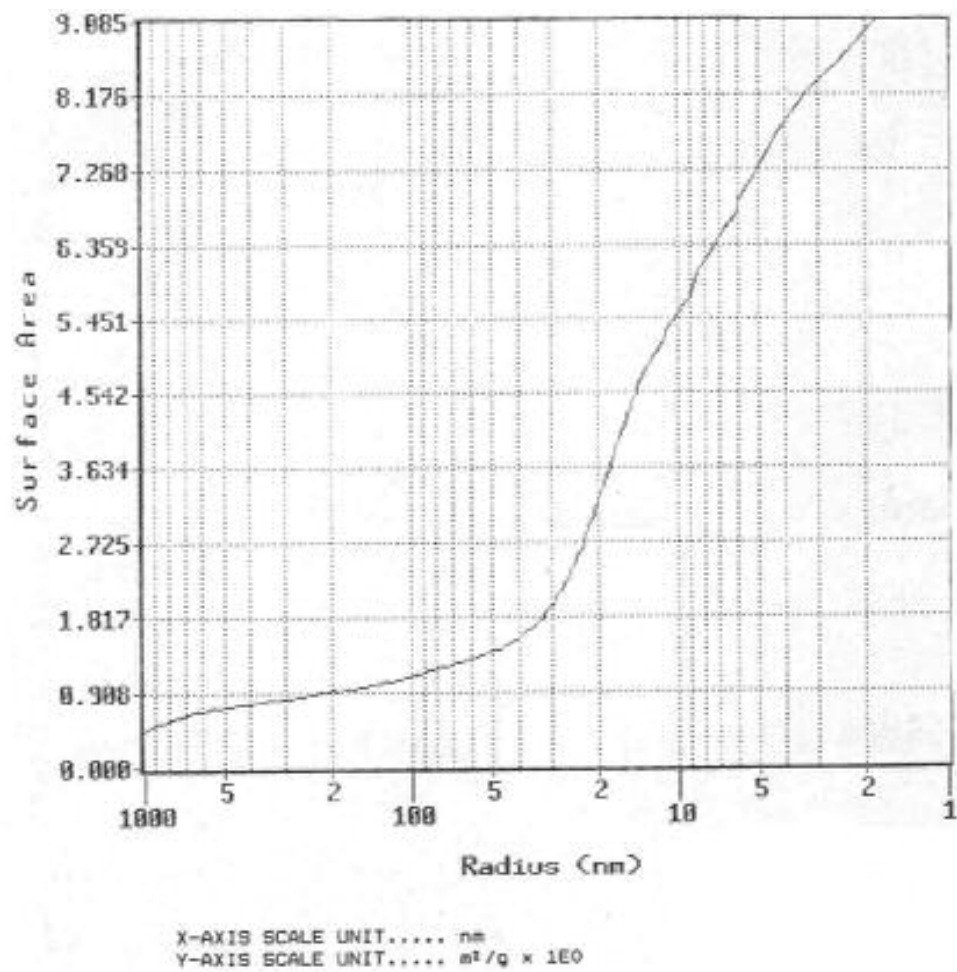
Figure F.1. The Surface Area vs. Radius graph for Cu-Mn-O

F.2 Sorbent: Cu-V-O

F.2.1 Porosity Calculation

ρ_{Hg}= 13.5705 g/cc (T = 10°C)

1. Sample Weight = 0.1044 g

2. Penetrometer + Sample Weight = 36.4851 g

3. Penetrometer + Sample + Hg Weight = 87.6339 g

4. Hg Weight = 51.1488 g

5. Hg Volume (Hg Weight / ρ_{Hg}) = 3.7691 cc

6. Penetrometer Volume = 3.8615 cc

7. Sample Volume (Pen. Vol.–Hg Vol.) = 0.0924 cc

8. Bulk Density (1/7) = 1.1299 g/cc

9. Apparent (Skeletal) Density = 2.2795 g/cc

10. Total Intruded Vol. = 0.4464 cc/g

11. Porosity Calculation

$$\varepsilon = 1 - \frac{\rho_{bulk}}{\rho_{apparent}}$$

ε = 0.51

F.2.2 Average Pore Radius Calculation

The original mercury porosimetry data for Cu-V-O are given in Table F.2.

The Surface Area vs. Radius graph taken from mercury porosimetry is also given in Figure F.2.

Table F.2. The Original Mercury Porosimetry Data for Cu-V-O

INTRUSION DATA

PRESSURE PSIA	PORE RADIUS nm	INTRUDED VOL Hg cc/g	% VOLUME INTRUDED %	dV/dP cc/(PSIA-g)	dV/dlogP cc/g	Ds(r) m²/(nm-g)	CUMULATIVE SURF AREA m²/g
52	2051.18	0.0000	0.00	3.75E-03	5.22E-01	9.26E-07	0.000
94	1134.69	0.1561	34.98	2.71E-03	5.59E-01	3.71E-06	0.208
144	740.70	0.2423	54.29	1.24E-03	3.99E-01	6.05E-06	0.394
208	512.79	0.2989	66.95	6.29E-04	2.94E-01	9.39E-06	0.576
289	369.07	0.3400	76.18	4.23E-04	2.74E-01	1.70E-05	0.765
353	302.16	0.3611	80.90	2.62E-04	2.12E-01	1.98E-05	0.892
436	244.64	0.3793	84.98	1.88E-04	1.85E-01	2.65E-05	1.026
570	187.12	0.3966	88.84	8.45E-05	1.08E-01	2.66E-05	1.186
1234	86.44	0.4138	92.70	1.54E-05	3.74E-02	4.07E-05	1.446
23432	4.55	0.4310	96.57	5.37E-07	2.65E-02	1.11E-02	3.780

Average Pore Radius **r (nm) = 698 nm**
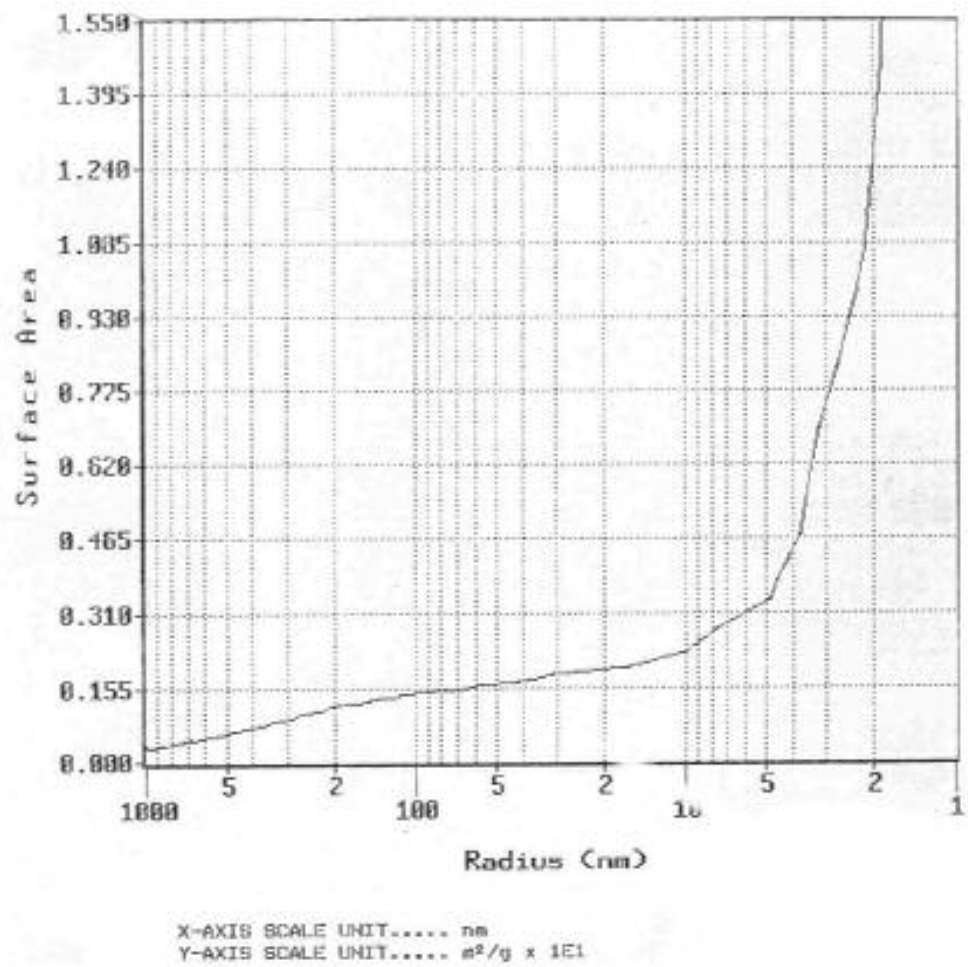
Figure F.2. The Surface Area vs. Radius graph for Cu-V-O

149

F.3. Sorbent: Cu-Mn-V-O

F.3.1 Porosity Calculation

ρ_{Hg}= 13.5705 g/cc   (T = 10°C)

1. Sample Weight = 0.1023 g

2. Penetrometer + Sample Weight = 36.4803 g

3. Penetrometer + Sample + Hg Weight = 88.4993 g

4. Hg Weight = 52.019 g

5. Hg Volume (Hg Weight / ρ_{Hg}) = 3.8332 cc

6. Penetrometer Volume = 3.8863 cc

7. Sample Volume (Pen. Vol.–Hg Vol.) = 0.0531 cc

8. Bulk Density (1/7) = 1.9266 g/cc

9. Apparent (Skeletal) Density = 6.2761 g/cc

10. Total Intruded Vol. = 0.3597 cc/g

11. Porosity Calculation

$$\varepsilon = 1 - \frac{\rho_{bulk}}{\rho_{apparent}}$$

ε = 0.70

F.3.2 Average Pore Radius Calculation

The original mercury porosimetry data for copper-manganese-vanadium oksit are given in Table F.3.

The Surface Area vs. Radius graph taken from mercury porosimetry is also given in Figure F.3.

Table F.3. The Original Mercury Porosimetry Data for Cu-Mn-V-O

INTRUSION DATA

PRESSURE PSIA	PORE RADIUS nm	INTRUDED VOL. Hg cc/g	% VOLUME INTRUDED %	dV/dP cc/(PSIA-g)	dV/dlogP cc/g	Ds(r) m²/(nm-g)	CUMULATIVE SURF AREA m²/g
25	4266.44	0.0186	5.16	8.87E-04	1.28E-01	2.44E-08	0.000
102	1045.70	0.0880	24.46	1.35E-03	2.98E-01	2.27E-06	0.100
150	711.07	0.1378	38.32	7.68E-04	2.61E-01	4.38E-06	0.217
228	467.81	0.1740	48.37	3.07E-04	1.53E-01	6.06E-06	0.340
355	300.45	0.1935	53.80	1.04E-04	8.06E-02	7.42E-06	0.443
809	131.84	0.2111	58.70	3.59E-05	6.66E-02	2.98E-05	0.623
1276	83.59	0.2297	63.86	4.14E-05	1.18E-01	1.41E-04	0.986
1840	57.97	0.2473	68.75	2.84E-05	1.18E-01	2.99E-04	1.494
2794	38.18	0.2649	73.64	1.46E-05	9.14E-02	5.12E-04	2.240
4662	22.88	0.2835	78.80	8.05E-06	8.31E-02	1.33E-03	3.517
7605	14.03	0.3011	83.70	6.08E-06	1.04E-01	4.42E-03	5.555
11341	9.40	0.3187	88.59	3.82E-06	9.55E-02	9.16E-03	8.619
21299	5.01	0.3363	93.48	1.27E-06	5.98E-02	2.00E-02	13.782
43741	2.44	0.3539	98.37	6.22E-07	5.76E-02	8.73E-02	24.107

Average Pore Radius **r (nm) = 399 nm**
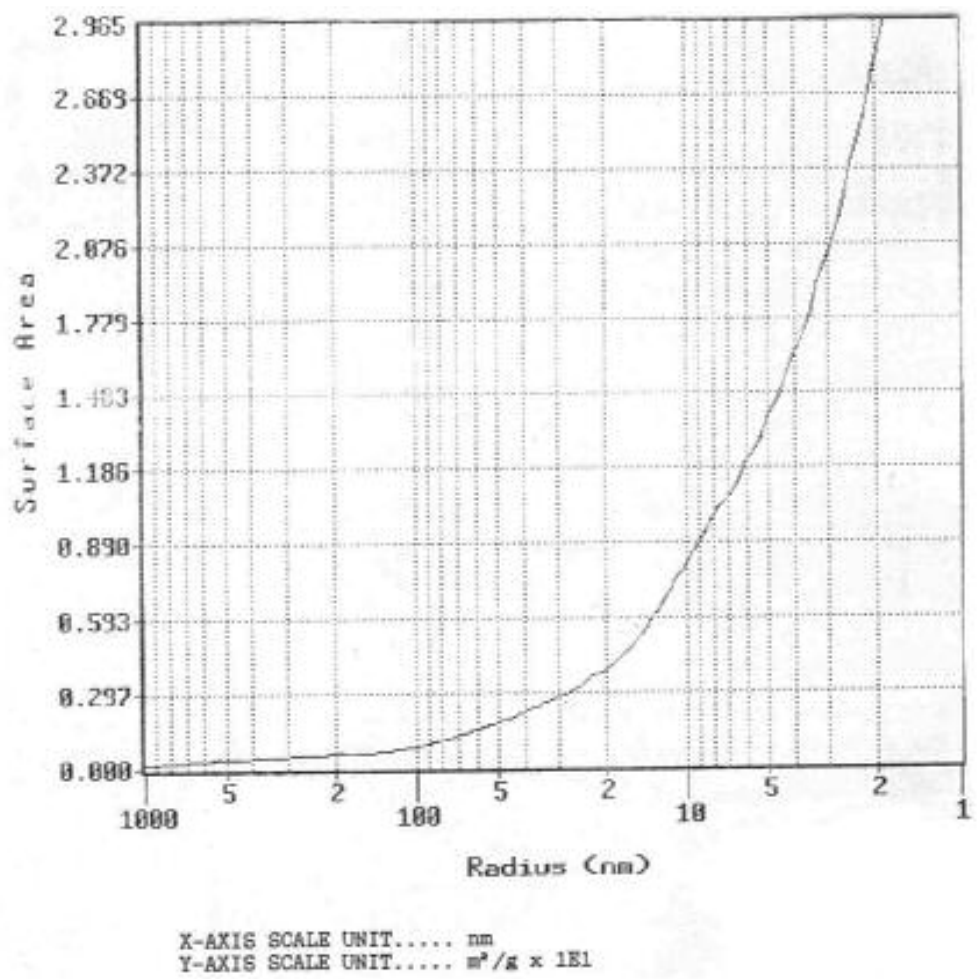
Figure F.3. The Surface Area vs. Radius graph for Cu-Mn-V-O

APPENDIX G

N$_2$ SORPTOMETRY EXPERIMENTAL DATA

The surface areas were measured in a Quantachrome Monosorb model BET apparatus. N$_2$-sorptometry experimental data and BET surface area calculation of sorbents were given in the following.

G.1 Sorbent: Cu-Mn-O

Sample Weight: 0.086 g

BET Surface Area = 3.87 m^2 (1. measure)

3.85 m^2 (2. measure) $\quad$ 3.86 m^2

BET Surface Area = 3.86 m^2 / 0.086 g = **45 m^2/g**

G.2 Sorbent: Cu-V-O

Sample Weight: 0.082 g

BET Surface Area = 3.82 m^2 (1. measure)

3.40 m^2 (2. measure) $\quad$ 3.61 m^2

BET Surface Area = 3.61 m^2 / 0.082 g = **44 m^2/g**

G.3 Sorbent: Cu-Mn-V-O

Sample Weight: 0.0797 g

BET Surface Area = 4.61 m^2 (1. measure)

4.43 m^2 (2. measure) } 4.52 m^2

BET Surface Area = 4.52 m^2 / 0.0797 g = **57 m^2/g**

APPENDIX H

SAMPLE CALCULATION FOR BREAKTHROUGH ANALYSIS

Experimental results were evaluated with breakthrough curves obtained for exit composition of H_2S and SO_2 data taken with time.

Figure H.1 shows the first sulfidation breakthrough curves of H_2S and SO_2 obtained in the packed bed sorption experiment using Cu-Mn-V-O sorbent in the presence of hydrogen.
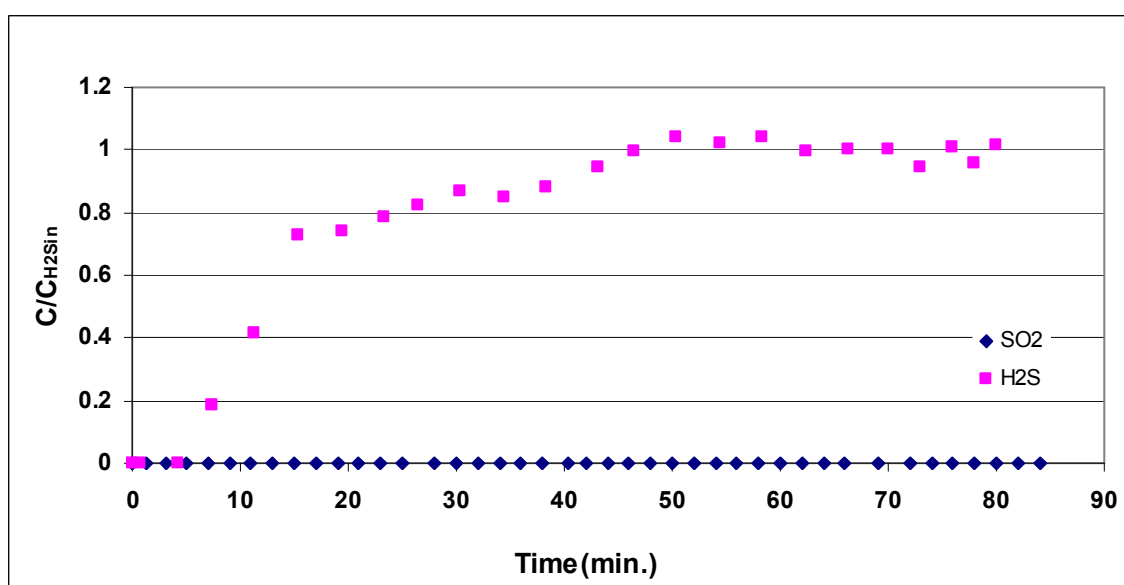

Figure H.1. Exit compositions of H_2S and SO_2 in packed-bed sorption experiment carried out with Cu-Mn-V-O in the presence of H_2
(T=627 ^{o}C; 1 % H_2S + 10 % H_2 in He)

Sample calculation for the first sulfidation of Cu-Mn-V-O sorbent at 627 $^{\circ}$C in reducing atmosphere (% 1 H_2S + % 10 H_2 in balance He) to calculate adsorbed H_2S amount and formed SO_2 were given in the following.

P=690 mmHg = 0.9079 atm

R=0.082 (ltxatm)/(molxK)

T=298 K

$$C_T = \frac{P}{RxT}$$

$$= \frac{0.9079\,atm}{0.082\,\dfrac{ltxatm}{molxK}\,x298K} = 3.71x10^{-5}\,mol/ml$$

$C_0 = C_T \; x \; (\%H_2S_{\;in})$

$\%H_2S_{\;in} = \% \; 1.2$

$C_0 = 4.45x10^{-7}$ mol/ml

$Q_0 = 92$ ml/min

t= 80 min

$H_2S_{in} = Q_0 \; x \; C_0 \; x \; t$

$$= (92\,\frac{ml}{min})x(4.45x10^{-7}\,\frac{molH2Sin}{ml})x(80min) = 3.28x10^{-3}\,mol$$

Area under the breakthrough curve calculated by using "Curve Expert 1.3" program.

Area under the H_2S breakthrough curve = Area 1

$$\text{Area 1} = 63.6176 \ \frac{\text{mol } H_2S_{out}}{\text{mol } H_2S_{in}} \times \text{min.}$$

$H_2S_{out} = Q_0 \times C_0 \times (\text{Area1})$

$$= (92 \ \frac{ml}{min}) \times (4.45 \times 10^{-7} \ \frac{\text{mol } H_2S_{in}}{ml}) \times (63.6176 \ \frac{\text{mol } H_2S_{out}}{\text{mol } H_2S_{in}} \times \text{min.})$$

$$= 2.60 \times 10^{-3} \ \text{mol}$$

$H_2S_{adsorbed} = H_2S_{in} - H_2S_{out}$

$$= (3.28 \times 10^{-3} \ \text{mol}) - (2.60 \times 10^{-3} \ \text{mol})$$

$$= 0.68 \times 10^{-3} \ \text{mol}$$

$m_{sorbent} = 0.2 \ g$

g S / g Sorbent $= (0.68 \times 10^{-3} \ \text{mol}) (32 \ \frac{g \, S}{mol}) / 0.2 \ g \ \text{Sorbent}$

$$= 0.110$$

$SO_{2formed} = 0$

SO_2 concentration profile of Cu-Mn-V-O sorbent at column outlet in the first regeneration experiment is given in Figure H.2.
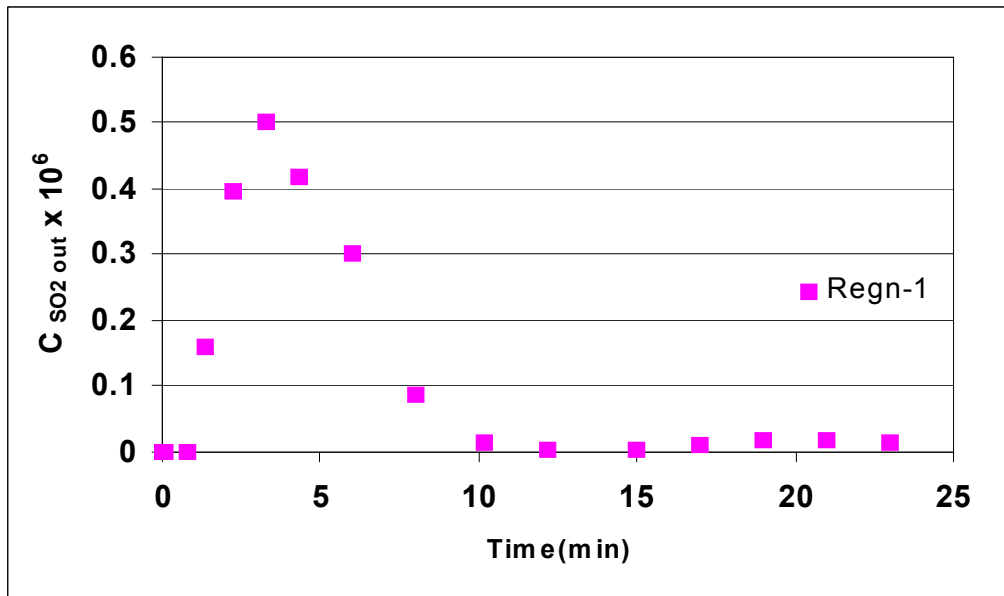
Figure H.2. SO_2 concentration at column outlet in the first regeneration experiment using Cu-Mn-V-O sorbent (T=700 °C; 6 % O_2 in balance N_2)

Sample calculation for formed SO_2 amount in regeneration experiment of Cu-Mn-V-O sorbent at 700 °C (6 % O_2 in balance N_2) was given in the following.

Q_{in} = 92 ml/min

Area under the curve was calculated with "Curve Expert 1.3" program.

Area = 2.36 x 10^{-6} (mol $SO_{2\ out}$ x min /ml)

$SO_{2\ formed}$ = Q_{in} x (Area)

$$= (92 \frac{ml}{min.}) \times (2.36 \times 10^{-6} \frac{mol\ SO_2 out}{ml} \times min.)$$

$$= 2.17 \times 10^{-4}\ mol$$

g S/g Sorbent = (2.17 x 10^{-4} mol) x (32 g S/mol) / (0.2 g Sorbent)

$$= 0.035$$

APPENDIX I

EXPERIMENTAL DATA

Because of an experimental error (time delay) in the fourth sulfidation experiment of Cu-Mn-O sorbent, sulfidation results and the fourth H_2S breakthrough curve are given in the following Table I.1, Table I.2 and Figure I.1. For comparison purpose, other experimental data obtained for Cu-Mn-O sorbent are also given in the same Tables and Figure.

Table I.1. The fourth sulfidation experimental results of Cu-Mn-O sorbent
at 627^oC

Sulfidation No	Q (ml/min)	$H_2S_{adsorbed}$ x10^3 (mol)	g S_{ads} / g Sorbent
4	84	1.24	0.198

Table I.1. (continued)

Sulfidation No	% H_2S	H_2S_{in} (mol)x10^3	H_2S_{out} (mol)x10^3	$H_2S_{adsorbed}$ (mol)x10^3
4	1.20	2.99	1.75	1.24
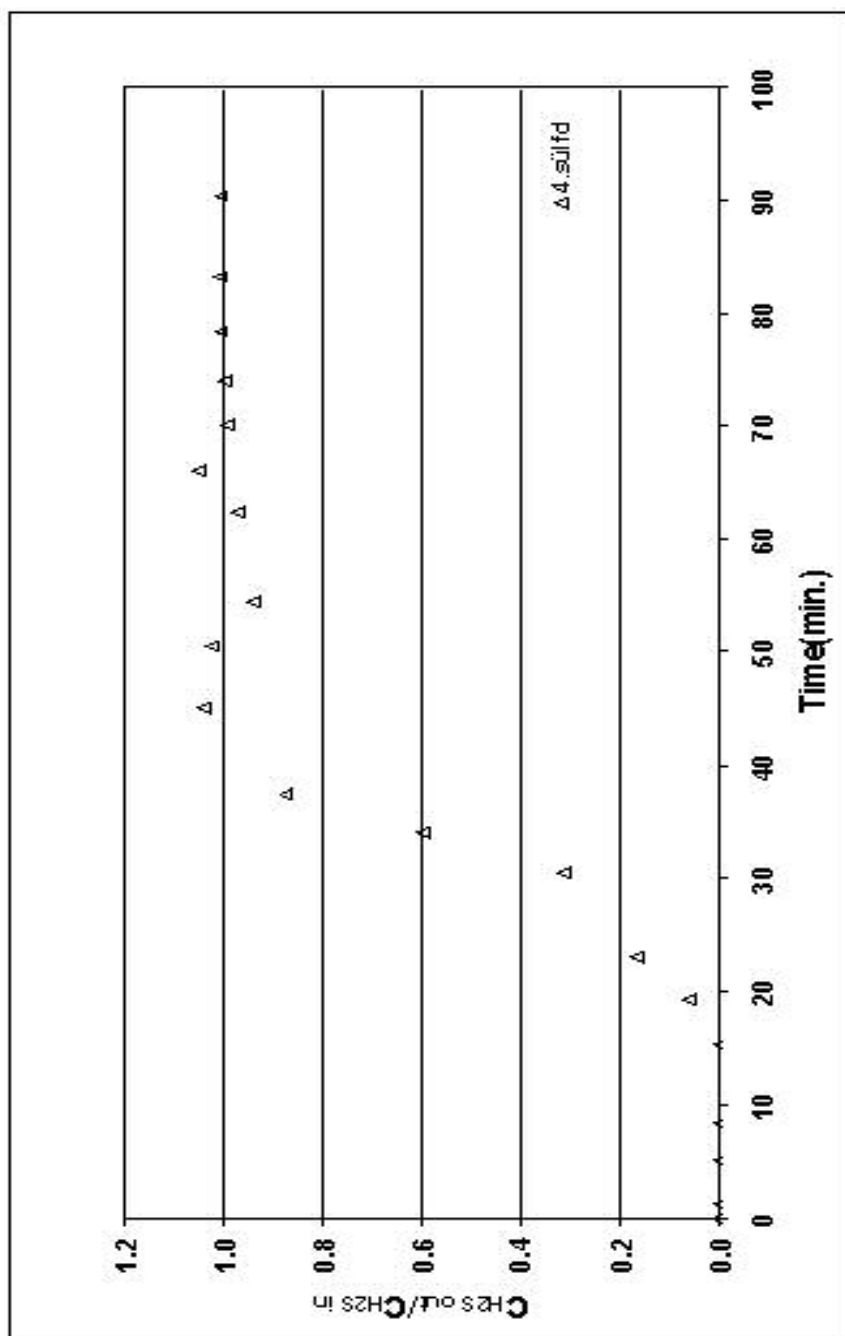
Figure I.1. H$_2$S breakthrough curve of the fourth sulfidation experiment for Cu-Mn-O sorbent at 627 °C

160

The results of the regression analysis of the data obtained with the Cu-Mn-O sorbent were given in Table I.2.

Table I.2. Rate parameters obtained from the breakthrough data of the fourth sulfidation experiment for Cu-Mn-O using Eqn.6.18 (W=0.2 g; T=627 $^{\circ}$C; 1 % H_2S + 10 % H_2 in He)

Sulfidation No	Q (ml/min)	k_oW/Q	$k_d(min^{-1})$ $x10^2$	$k_o(ml/g.min)$ $x10^{-2}$	G^2
4	84	8.82	28	37	0.0443

APPENDIX J

OUTPUT FILE OF PROGRAM

Mathematica 5.0 was used to apply nonlinear regression to experımantal data of sorbents.

J.1 Regression report of 1. sulfidation experiment carried out with Cu-Mn-V-O in the presence of H_2 (T= 627 $^{\circ}$C; 1% H_2S + 10% H_2 in He)

$a = k_ow/Q$

$b = k_d$

a1: dimensionless adsorption rate constant of the zeroth solution of the deactivation model,

b1: zeroth order deactivation rate constant,

a2: dimensionless adsorption rate constant of the first corrected solution for the breakthrough curve,

b2: first order deactivation rate constant,

Nonlinear Regression

**veri=**{{0.000001,0} , {0.73,0} , {4.25,0} , {7.44,0.1881} , {11.38,0.4125} , {15.38,0.7257} , {19.38,0.7419} , {23.38,0.7880} , {26.54,0.8223} , {30.46,0.8652} , {34.36,0.8504} , {38.40,0.8817} , {43.10,0.9422} , {46.41,0.9960} , {50.42,1.0387} , {54.44,1.0209} , {58.36,1.0429} ,

{62.36,0.9988} , {66.37,1.0030} , {70,1.0023} , {73,0.9442} , {76,1.0102} ,
{78,0.9543} , {80,1.0119}}

ListPlot[veri]
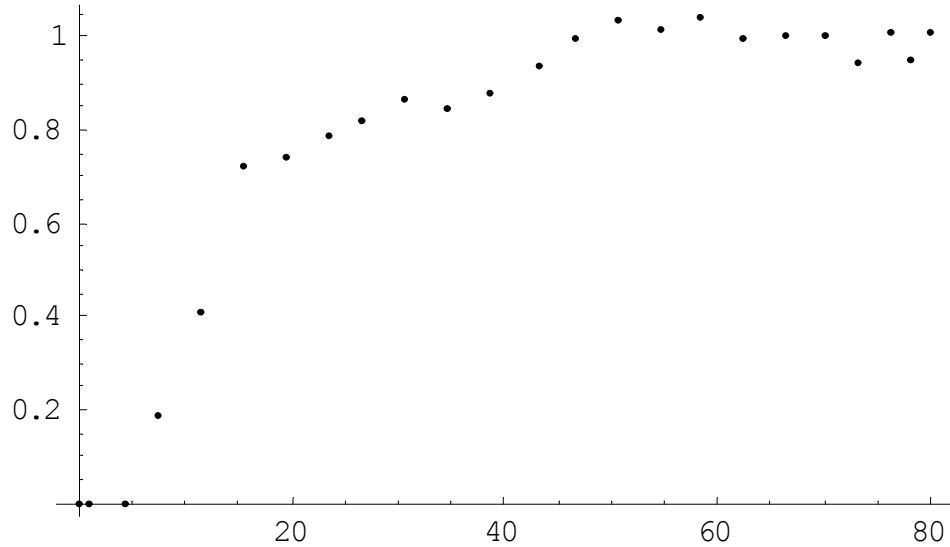
    Graphics

    <<Statistics`NonlinearFit`

NonlinearRegress[veri,Exp[a1*Exp[b1*t]], {t},{a1,b1}]

{a1→4.14785,b1→0.13196}

NonlinearRegress[veri,Exp[(1-Exp[a2*(1-Exp[b2*t])])*Exp[b2*t]/(1-

Exp[b2*t])],{t},{a2,b2]

{a2→2.43238,b2→0.187552}

EstimatedVariance→ 0.00544052

	DF	SumOFSq	MeanSq
ANOVATable → Error	22	**0.119691**	0.00544052

FitCurvatureTable → 95.% Confidence Region

f[t_]:=Exp[(1-Exp[2.43238*(1-Exp[-0.187552*t])])*

    Exp[-0.187552*t]/(1-Exp[-0.187552*t])]

f[80]

0.99999

XRD PATTERNS OF FRESH SORBENTS
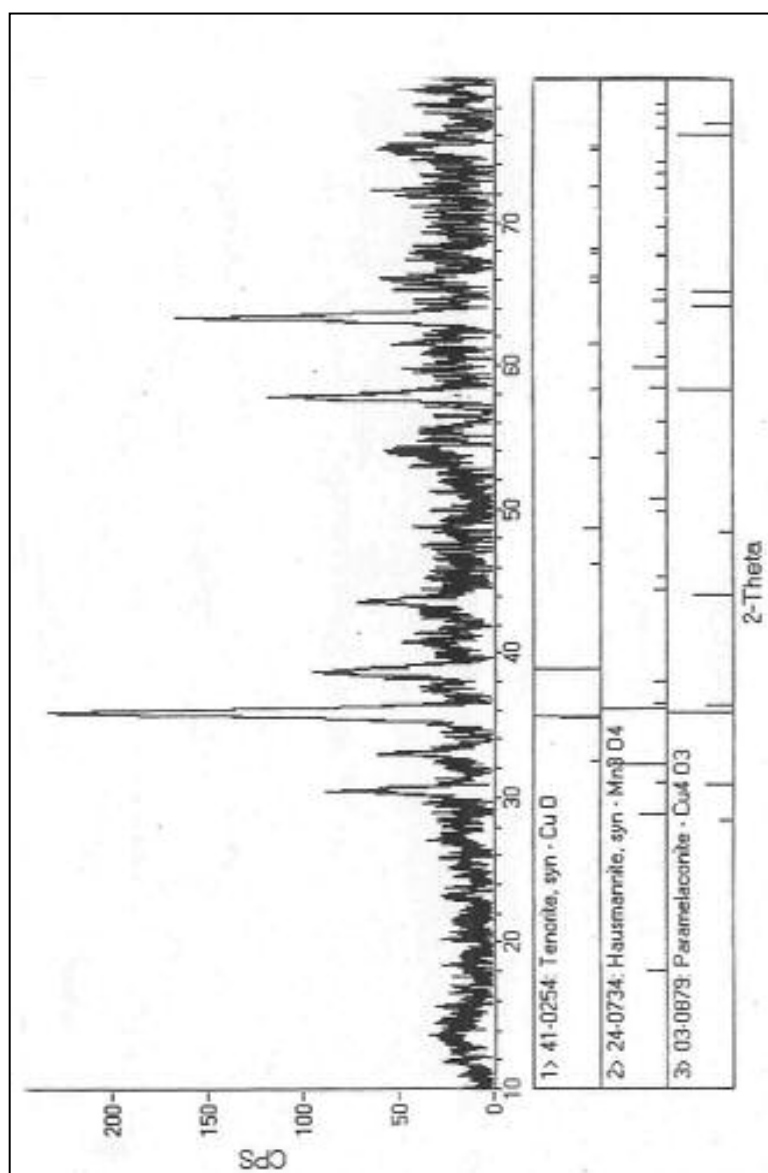
(b)Cu-Mn-O

Figure K.1. XRD patterns of the fresh sorbents
(a) Cu-Mn-O, (b) Cu-Mn-V-O, (c) Cu-V-O
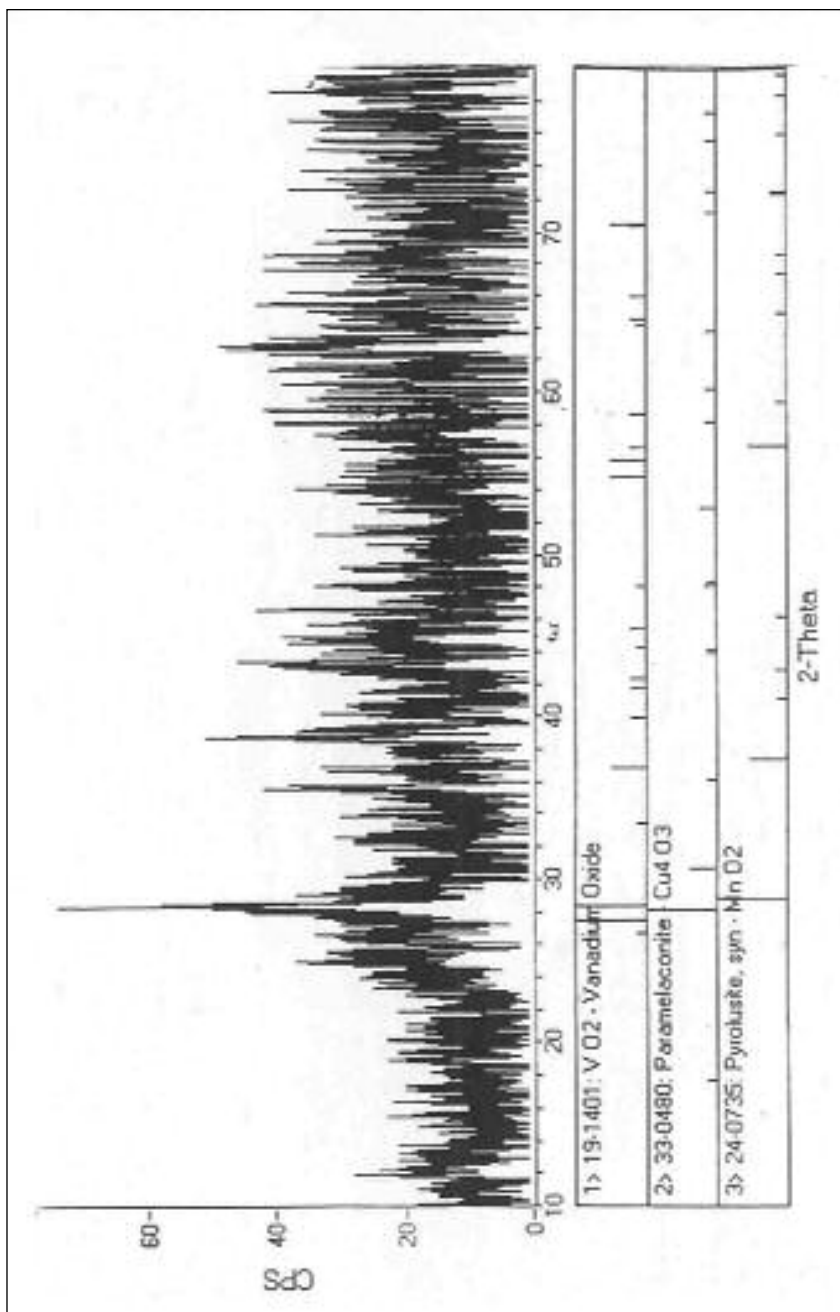
(b) Cu-Mn-V-O

Figure K.1. (continued)

165

(c) Cu-V-O

Figure K.1. (continued)